

1 **Title Page**

2
3 **LYMPHOID NEOPLASIA**

4
5 **LUBAC accelerates B-cell lymphomagenesis by conferring B cells resistance to**
6 **genotoxic stress**

7
8 Tomoyasu Jo,^{1,2} Momoko Nishikori,^{1,14,*} Yasunori Kogure,^{3,4} Hiroshi Arima,¹ Katsuhiko
9 Sasaki,² Yoshiteru Sasaki,² Tomoko Nakagawa,² Fumie Iwai,¹ Shuji Momose,⁵ Aki
10 Shiraishi,⁶ Hiroshi Kiyonari,^{6,7} Noritaka Kagaya,⁸ Tetsuo Onuki,⁹ Kazuo Shin-ya,^{8,10}
11 Minoru Yoshida,^{9,11,12} Keisuke Kataoka,^{3,4} Seishi Ogawa,^{3,13} Kazuhiro Iwai,^{2,*} and
12 Akifumi Takaori-Kondo¹

13
14 ¹Department of Hematology and Oncology, Graduate School of Medicine, Kyoto
15 University, Kyoto, Japan; ²Department of Molecular and Cellular Physiology, Graduate
16 School of Medicine, Kyoto University, Kyoto, Japan; ³Department of Pathology and
17 Tumor Biology, Graduate School of Medicine, Kyoto University, Kyoto, Japan;
18 ⁴Division of Molecular Oncology, National Cancer Center Research Institute, Tokyo,
19 Japan; ⁵Department of Pathology, Saitama Medical Center, Saitama Medical University,
20 Kawagoe, Japan; ⁶Laboratories for Animal Resource Development, RIKEN Center for
21 Biosystems Dynamics Research, Kobe, Japan; ⁷Laboratories for Genetic Engineering,
22 RIKEN Center for Biosystems Dynamics Research, Kobe, Japan; ⁸National Institute of
23 Advanced Industrial Science and Technology (AIST), Tokyo, Japan; ⁹Seed Compound
24 Exploratory Unit for Drug Discovery Platform, RIKEN Center for Sustainable Resource
25 Science, Wako, Japan; ¹⁰Biotechnology Research Center and Collaborative Research
26 Institute for Innovative Microbiology, The University of Tokyo, Tokyo, Japan;
27 ¹¹Chemical Genomics Research Group, RIKEN Center for Sustainable Resource
28 Science, Wako, Japan; ¹²Department of Biotechnology, Graduate School of Agriculture
29 and Life Sciences, The University of Tokyo, Tokyo, Japan; ¹³Department of Medicine,
30 Center for Hematology and Regenerative Medicine, Karolinska Institutet, Stockholm,
31 Sweden

32 ¹⁴ Lead Contact

33 *Correspondence:

34 Momoko Nishikori, Department of Hematology and Oncology, Graduate School of
35 Medicine, Kyoto University, 54 Shogoin Kawahara-cho, Sakyo-ku, Kyoto 606-8507,
36 Japan; e-mail: nishikor@kuhp.kyoto-u.ac.jp; Tel: +81-75-751-4964; Fax:
37 +81-75-751-4963

39 Kazuhiro Iwai, Department of Molecular and Cellular Physiology, Graduate School of
40 Medicine, Kyoto University, Yoshida-konoe-cho, Sakyo-ku, Kyoto 606-8501, Japan;
41 e-mail: kiwai@mcp.med.kyoto-u.ac.jp; Tel: +81-75-753-4671; Fax: +81-75-753-4676

42

43 **Note:** Presented in abstract form at the 60th annual meeting of the American Society of
44 Hematology, San Diego, CA, 3 December 2018.

45

46 **Running head:** Roles of LUBAC in B-cell lymphomagenesis

47

48 Abstract word count: 220 words

49 Text word count: 3,974 words

50 Number of Figures: 5

51 Number of Tables: 1

52 Number of References: 63

53 Number of supplemental Figures: 6

54 Number of supplemental Tables: 11

55

56 **Key Points**

- 57 1. LUBAC accelerates B-cell lymphomagenesis through protection of DNA
58 damage-induced apoptosis, thereby promoting AID-mediated mutations.
- 59 2. Inhibition of LUBAC by small molecules is a promising therapeutic strategy for
60 B-cell lymphomas with NF- κ B activation.

61 **Abstract**

62 Linear ubiquitin chain assembly complex (LUBAC) is a key regulator of NF- κ B
63 signaling. Activating single-nucleotide polymorphisms of HOIP, the catalytic subunit of
64 LUBAC, are enriched in patients with activated B cell-like diffuse large B-cell
65 lymphoma (ABC-DLBCL), and expression of HOIP which parallels LUBAC activity is
66 elevated in ABC-DLBCL samples. Thus, to clarify the precise roles of LUBAC in
67 lymphomagenesis, we generated a mouse model with augmented expression of HOIP in
68 B cells. Interestingly, augmented HOIP expression facilitated DLBCL-like B-cell
69 lymphomagenesis driven by MYD88-activating mutation. The developed lymphoma
70 cells partly shared somatic gene mutations with human DLBCLs, with increased
71 frequency of a typical AID mutation pattern. *In vitro* analysis revealed that HOIP
72 overexpression protected B cells from DNA damage-induced cell death through NF- κ B
73 activation, and the analysis of human DLBCL database showed that expression of HOIP
74 positively correlated with gene signatures representing regulation of apoptosis signaling,
75 as well as NF- κ B signaling. These results indicate that HOIP facilitates
76 lymphomagenesis by preventing cell death and augmenting NF- κ B signaling, leading to
77 accumulation of AID-mediated mutations. Furthermore, a natural compound that
78 specifically inhibits LUBAC was shown to suppress the tumor growth in a mouse
79 transplantation model. Collectively, our data indicates that LUBAC is crucially involved
80 in B-cell lymphomagenesis through protection against DNA damage-induced cell death,
81 and is a suitable therapeutic target for B-cell lymphomas.

82

83 **Keywords:** LUBAC, B-cell lymphoma, ABC-DLBCL, NF- κ B, AID, cell death

84 **Introduction**

85

86 Diffuse large B-cell lymphoma (DLBCL) is the most frequent lymphoma subtype in
87 adults,^{1,2} and it is classified into two major categories, germinal center B cell-like
88 (GCB)-DLBCL and activated B cell-like (ABC)-DLBCL, based on the gene expression
89 profiling.³⁻⁶ Since ABC-DLBCL has been shown to have a worse prognosis compared to
90 GCB-DLBCL, new therapeutic strategies against ABC-DLBCL are warranted.⁷⁻⁹

91 ABC-DLBCL is characterized by constitutive NF- κ B activation mediated by
92 the B-cell receptor (BCR) and Toll-like receptor (TLR) signaling pathways, and many
93 oncogenic mutations within these pathways have been identified. Among them,
94 activating mutations of MYD88, a signaling molecule in the TLR pathway, including
95 L265P, are present in around 30% of ABC-DLBCL cases,¹⁰ and constitute the most
96 frequent genetic abnormalities leading to aberrant NF- κ B activation.

97 Protein ubiquitination is involved in multiple steps of the NF- κ B pathway.¹¹
98 The linear ubiquitin chain assembly complex (LUBAC), which consists of the catalytic
99 subunit HOIP (RNF31) and two accessory subunits, HOIL-1L and SHARPIN, promotes
100 NF- κ B activation and protects against cell death by synthesizing unique N-terminally
101 linked linear polyubiquitin chains.¹²⁻¹⁹ We previously reported that rare germline
102 single-nucleotide polymorphisms (SNPs) in *HOIP* that increase LUBAC ligase activity
103 are significantly enriched in ABC-DLBCL patients, suggesting that augmentation of
104 LUBAC activity contributes to ABC-DLBCL pathogenesis.²⁰ The majority of
105 ABC-DLBCLs in patients with these HOIP SNPs also harbor the MYD88 L265P
106 mutation. Given that LUBAC plays a pivotal role in the NF- κ B activation by linearly
107 polyubiquitinating substrates, including the key NF- κ B regulator NEMO,^{18,19,21-24} it is
108 speculated that LUBAC collaborates with MYD88 signaling in B-cell lymphomagenesis
109 by further amplifying NF- κ B activation.

110 By analyzing published clinical RNA sequencing (RNA-seq) gene expression
111 data,²⁵ we found that expression of *HOIP* is elevated in human ABC-DLBCL (Figure
112 1A). As we previously reported that enforced expression of the catalytic subunit HOIP
113 augments LUBAC functions,¹⁷ we assumed that LUBAC activation is frequently
114 involved in the pathogenesis of ABC-DLBCL, independent of SNPs in *HOIP*. To clarify
115 the roles of LUBAC played in the pathogenesis of B-cell lymphoma, we established a
116 gene-engineered mouse with enforced expression of HOIP in B cells. We found that
117 increased expression of HOIP enhanced LUBAC activity, and it facilitated generation of
118 MYD88-mediated DLBCL, whereas it could not lead to B-cell lymphoma development
119 per se. Elevated expression of LUBAC was suggested to accelerate B-cell
120 lymphomagenesis, not only by activating NF- κ B in concert with MYD88-mediated
121 signals, but also by protecting cells from DNA damage-induced apoptosis. Importantly,
122 the mutations in B-cell lymphomas that arose in mice expressing an oncogenic MYD88
123 mutant and high levels of HOIP partially overlap with those reported in human DLBCLs,
124 indicating the biological similarity between these tumors. Finally, by using a mouse
125 lymphoma model with secondary transplantation of a newly established lymphoma cell
126 line, we demonstrated that LUBAC inhibition represents a novel and promising
127 therapeutic strategy against B-cell lymphomas.

128 **Methods**

129

130 **Mice**

131 Tissue-specific HOIP transgenic mice (ROSA26-STOP-Hoip-ires-eGFP-pA) and
132 MYD88 L252P transgenic mice (ROSA26-STOP-Myd88_L252P-ires-eGFP-pA)
133 (Accession No. CDB 1320K:
134 <http://www2.clst.riken.jp/arg/mutant%20mice%20list.html>) were established as
135 described in supplemental Methods. ROSA26-STOP-Hoip-ires-eGFP-pA or
136 ROSA26-STOP-Myd88_L252P-ires-eGFP-pA transgenic mice were crossed with
137 CD19-cre mice to express transgenic HOIP or MYD88 protein specifically in B cells
138 from the pre-B cell stage.²⁶ All mice were maintained under specific pathogen-free
139 conditions. All animal protocols were approved by Kyoto University and RIKEN Center
140 for Biosystems Dynamics Research.

141

142 **Analysis of European Genome-phenome Archive and The Cancer Genome Atlas**
143 **datasets**

144 Clinical and RNA sequencing (RNA-seq) gene expression data derived from the core
145 set of 624 human DLBCL samples were obtained from the European Genome-phenome
146 Archive (EGA) (dataset identifier [ID]: EGAD00001003600),²⁵ and the Cancer Genome
147 Atlas (TCGA) whole exome sequencing and RNA-seq data of 48 DLBCL samples
148 (project ID: TCGA-DLBC) were obtained from the Broad Institute Firehose
149 (<http://gdac.broadinstitute.org/>),^{27,28} and were analyzed as described in supplemental
150 Methods and supplemental Tables 1–4.

151

152 **Whole-exome sequencing**

153 Lymphoma tissues obtained from the transgenic mouse model were analyzed by
154 whole-exome sequencing using the SureSelect XT Mouse All Exon V2 kit (Agilent).
155 Mouse tail DNA was used as a germline control. Sequence alignment to
156 GRCm38/mm10 and mutation calling were performed using the Genomon pipeline
157 (<https://github.com/Genomon-Project>) as previously described²⁹ with minor
158 modifications. Candidate mutations with (i) $p < 0.01$ (Fisher's exact test), (ii) > 4
159 variant reads in tumor samples, and (iii) variant allele frequency (VAF) in tumor
160 samples > 0.05 or > 0.2 were selected and manually reviewed. Human orthologues of
161 mouse genes were assigned with the Ensembl 92 database. For each sample, the
162 number of mutations, SNVs at C:G base pairs, transitions, and SNVs within the
163 WRCY/RGYW motifs were calculated and compared using the Brunner–Munzel test.
164 Enrichment of SNVs at C/G within the WRCY/RGYW motifs in genes were
165 performed by binomial test. Gene enrichment analyses were performed with Fisher's
166 exact test using the gene sets derived from supplemental Tables 5–8.^{30,31}

167

168 **AlphaScreen binding assay for LUBAC inhibitors**

169 To search for inhibitors of linear polyubiquitination, an AlphaScreen-based HTS system
170 was established using N-terminally FLAG-His-tagged ubiquitin (FLAG-Ub),
171 C-terminally glutathione S-transferase (GST)-tagged ubiquitin (Ub-GST),
172 ubiquitin-activating enzyme E1, UbcH7 as the E2 ubiquitin–conjugating enzyme, and
173 Petit-LUBAC or Petit-SHARPIN as the E3 ubiquitin ligase, as described in
174 supplemental Methods.

175

176 **Generation of a preclinical model for validation of LUBAC inhibitor**

177 The cell line HM876 was established as described in supplemental Methods.
178 Transplantation of HM876 tumor cells was performed by subcutaneously injecting $5 \times$

179 10^6 cells into 6-week-old C57BL/6 females, that were sublethally irradiated (4.5 Gy) 6
180 hours before transplantation. The animals were divided into three groups: the control
181 group (n = 7) received intraperitoneal injection of DMSO diluted in 5% glucose; the
182 other two groups were injected intraperitoneally with thiolutin diluted in 5% glucose at
183 2.5 or 5.0 mg/kg/day (n = 7). Thiolutin was administered from days 2 to 6 and days 9 to
184 13. On day 14, the animals were euthanized, and tumor weight was assessed.
185

186 **Results**

187

188 **Augmented HOIP expression accelerates MYD88-mediated B-cell** 189 **lymphomagenesis in mice**

190 Based on the analysis of a publicly available database of gene expression in human B
191 cells,³² *HOIP* is physiologically expressed throughout B-cell development
192 (supplemental Figure 1A). However, we previously reported that two rare SNPs of
193 *HOIP* that augment LUBAC activity were enriched specifically in patients with
194 ABC-DLBCL.²⁰ Because the protein expression level of HOIP determines the amount
195 of other LUBAC subunits and activity of LUBAC,¹⁷ we hypothesized that *HOIP* plays a
196 key role in the activation of NF- κ B pathway in ABC-DLBCL,^{21,33,34} irrespective of the
197 SNP status. We examined expression of *HOIP* in RNA sequencing (RNA-seq) data from
198 624 DLBCL samples in the European Genome-phenome Archive (EGA; dataset
199 identifier [ID]: EGAD00001003600)²⁵ and found that its expression level was
200 significantly higher in ABC-DLBCL than in GCB-DLBCL, as well as *HOIL-1L* and
201 *SHARPIN*, that encode other subunits of LUBAC, although statistical significance was
202 not observed in *SHARPIN* (Figure 1A; supplemental Figure 1B; supplemental Table 1).
203 On the other hand, expression level of *OTULIN*, encoding a linear ubiquitin-specific
204 deubiquitinase that negatively regulates LUBAC signaling,^{35,36} was lower in
205 ABC-DLBCL (supplemental Figure 1B; supplemental Table 1). These results are
206 compatible to the increased LUBAC activity in ABC-DLBCL.

207 Therefore, to investigate the role of LUBAC played in B-cell
208 lymphomagenesis, we generated mice expressing high levels of HOIP specifically in B
209 cells from the pre-B cell stage (CD19-cre-HOIP) (Figure 1B). Bicistronic expression of
210 eGFP allowed us to confirm that transgenic HOIP was specifically expressed in CD19⁺
211 B cells (supplemental Figure 1C). In CD19-cre-HOIP mice, elevated expression of

212 HOIP increased expression of the other LUBAC subunits, thereby increasing the
213 amount of trimeric LUBAC in B cells (supplemental Figure 1D). As expected, high
214 levels of LUBAC increased expression of NF- κ B target genes in splenic B cells despite
215 mildly (Figure 1C; supplemental Figure 1E). Although some of the CD19-cre-HOIP
216 mice aged over 14 months showed splenomegaly, no lymphoma development was
217 observed (supplemental Figure 1F).

218 The majority of ABC-DLBCLs with the LUBAC-activating *HOIP* SNPs also
219 carry the oncogenic MYD88 L265P mutation.²⁰ Consistent with this, we found that B
220 cells with enforced HOIP expression proliferated more efficiently by TLR stimulation
221 (CpG-DNA and Pam3CSK4) (Figure 1D), which suggested the synergistic effect of
222 LUBAC and MYD88 signaling. To evaluate the combinatorial effect of LUBAC and
223 MYD88 L265P, we generated mice in which *Myd88 L252P*, the equivalent to human
224 *L265P*, was expressed specifically in B cells from the pre-B cell stage
225 (CD19-cre-MYD88LP) (supplemental Figure 1G-I). MYD88 L252P increased
226 proliferation and NF- κ B activity of splenic B cells (supplemental Figure 1J-K). Hence,
227 we assessed the synergistic effects of HOIP and MYD88 L252P on B-cell tumorigenesis
228 in these mice. We evaluated the linear ubiquitin chains in B cells by using linear
229 ubiquitin-specific tandem ubiquitin binding entity (M1-specific TUBE) (supplemental
230 Figure 1L),^{37,38} and found that the amount of linear ubiquitin chains was higher in
231 splenic B cells of CD19-cre-HOIP/MYD88LP mice than in those of
232 CD19-cre-MYD88LP mice (Figure 1E). As reported previously, B cell-specific
233 expression of MYD88 L252P led to decreased survival.³⁹ We found that introduction of
234 a HOIP transgenic allele significantly shortened the survival of CD19-cre-MYD88LP
235 mice (Figure 1F).

236 Next, we examined pathological changes in CD19-cre-HOIP/MYD88LP and
237 CD19-cre-MYD88LP mice. Mice with both genotypes developed marked

238 lymphosplenomegaly, and histological examination of spleens and lymph nodes
239 revealed infiltrates of lymphoid cells in these organs (Figure 1G–H). In addition, human
240 DLBCL-like eGFP and CD19-positive large abnormal B cells diffusely infiltrated into
241 the affected organs in mice with both genotypes (Figure 1H; supplemental Figure 2A).
242 Assessment of V(D)J recombination of immunoglobulin heavy chain loci using a
243 PCR-based method confirmed the presence of monoclonal B-cell populations in all
244 involved tissues derived from 14 mice (4 CD19-cre-MYD88LP and 10
245 CD19-cre-HOIP/MYD88LP) (Figure 1I; supplemental Figure 2B; Table 1). Lymphomas
246 developed in 4 CD19-cre-MYD88LP mice and those in 8 of the 10
247 CD19-cre-HOIP/MYD88LP mice were positive for CD19, B220, and IgM and negative
248 for CD138 by flow cytometric analysis (DLBCL-like lymphomas). These tumors were
249 Irf4 positive and Bcl6 negative by immunohistochemical staining (Figure 1H).
250 Moreover, sequence analysis of the variable regions of the clonally rearranged IgH gene
251 revealed the presence of somatic hypermutations in most of the DLBCL-like
252 lymphomas (supplemental Table 9). These results suggested that these tumors are
253 mostly derived from post-germinal center B cells and are compatible with human
254 ABC-DLBCL.⁴⁰ Tumor cells of the remaining two CD19-cre-HOIP/MYD88LP mice
255 exhibited a plasma cell-like phenotype of CD19 and B220-negative and
256 CD138-positive expression (Table 1). These results indicated that elevated expression of
257 LUBAC potentially has a function to facilitate MYD88-mediated B-cell tumorigenesis.

258

259 **High LUBAC expression is associated with increased accumulation of**
260 **AID-mediated somatic mutations**

261 We did not find any significant macroscopic, histological, and immunophenotypic
262 differences between DLBCL-like lymphomas developed in CD19-cre-MYD88LP and
263 CD19-cre-HOIP/MYD88LP mice (Figure 1G–H; Table 1). To understand the biological

264 background of the accelerated MYD88-mediated lymphomagenesis in the condition of
265 augmented LUBAC activity, we performed whole-exome sequencing analyses of
266 genomic DNA isolated from 12 lymphomas derived from 12 different mice (eight from
267 CD19-cre-HOIP/MYD88LP and four from CD19-cre-MYD88LP mice). Significantly
268 more mutations were detected in the whole exons of lymphoma cells derived from
269 CD19-cre-HOIP/MYD88LP mice than in those from CD19-cre-MYD88LP mice
270 (Figure 2A; supplemental Figure 3A), indicating that elevated LUBAC expression
271 increased the number of somatic mutations. Twenty-six genes were found to be
272 recurrently mutated non-synonymously in two or more samples among 12 mice.
273 Twenty-three of them were recurrently mutated among those from eight
274 CD19-cre-HOIP/MYD88LP mice. Moreover, 6 of them, including *Irf2bp2* and *Pim1*,
275 were reported to be frequently mutated in human DLBCLs, especially in ABC-DLBCL
276 (Figure 2B–C; supplemental Table 5).³⁰ These results suggested that B-cell lymphomas
277 generated in mice expressing HOIP with MYD88 mutant transgene share some genome
278 mutations with human DLBCLs.^{25,30}

279 Notably, a significant proportion of recurrently mutated genes in lymphomas
280 from CD19-cre-HOIP/MYD88LP mice were identified as known or predicted targets of
281 aberrant somatic hypermutation induced by activation-induced cytidine deaminase
282 (AID) (Figures 2C and 3A; supplemental Table 6).^{25,30,31,41,42} AID plays essential roles
283 in class-switch recombination and somatic hypermutation of the immunoglobulin genes
284 during physiological B-cell maturation,⁴³ and is also involved in the pathogenesis of
285 human DLBCL by introducing aberrant somatic hypermutations in
286 non-immunoglobulin genes.^{34,44-46} We found that somatic single-nucleotide variations
287 (SNVs) within WRCY/RGYW motifs, or at C:G sites and transition mutations
288 accumulated at higher levels in tumors derived from CD19-cre-HOIP/MYD88LP mice
289 than in those from CD19-cre-MYD88LP mice (Figure 3B; supplemental Figure 3B–D;

290 supplemental Tables 7–8). Additionally, most of these mutations were located within 2
291 kb downstream of the transcription start site (TSS) of each target gene (Figure 3C;
292 supplemental Figure 3E). Since all of these characteristics are known as hallmarks of
293 AID-mediated somatic mutations, it is indicated that AID-mediated mutagenesis is
294 involved in B-cell lymphoma development in CD19-cre-HOIP/MYD88LP mice.⁴⁷⁻⁴⁹
295 Meanwhile, in the analyses of the whole-exome sequencing and RNA-seq data from 48
296 human DLBCL samples (Project ID: TCGA-DLBC),^{27,28} we found that the frequency of
297 AID-induced mutations positively correlated with the expression level of *HOIP* (Figure
298 3D–E; supplemental Table 4). Taken together, these results indicated that elevated
299 expression of HOIP is associated with increased accumulation of somatic mutations of
300 AID pattern, and augmented LUBAC activity is suspected to explain the facilitation of
301 MYD88-mediated B-cell lymphomagenesis.

302

303 **Augmented LUBAC activity overcomes cell death induced by DNA damage**
304 **thereby accelerating accumulation of somatic mutations**

305 Although AID has a strong preference for immunoglobulin genes, it produces off-target
306 DNA damages as well, resulting in aberrant somatic mutations.^{34,44,46,50} As shown above,
307 AID-mediated mutations accumulated more prominently in CD19-cre-HOIP/MYD88LP
308 mice compared to CD19-cre-MYD88LP mice. However, the expression levels of AID
309 and the percentages of germinal center B cells in mesenteric lymph nodes were
310 comparable between CD19-cre-HOIP/MYD88LP and CD19-cre-MYD88LP mice
311 (Figure 4A). In addition, no correlation was found in the expression level of AID and
312 HOIP in human DLBCLs (data not shown). Therefore, the altered expression level of
313 AID did not seem to be the main reason for increased somatic mutations in lymphomas
314 derived from CD19-cre-HOIP/MYD88LP mice.

315 Previous studies showed that LUBAC has functions in protecting cells from

316 genotoxic damage–induced apoptosis, as well as mediating NF- κ B activation via
317 plasma membrane receptors.^{51,52} Therefore, we examined the cell protective effect of
318 LUBAC against genotoxic stress. Enforced expression of HOIP protected HBL1, a
319 human ABC-DLBCL–derived cell line,⁷ and murine splenic B cells from
320 cisplatin-induced cell death (Figure 4B–D; supplemental Figure 4A–B). We also found
321 that enforced expression of LUBAC protected Jurkat cells from cisplatin-induced cell
322 death by suppressing apoptosis (Figure 4E–H). It has been indicated that
323 LUBAC-mediated linear ubiquitination of NEMO is involved in genotoxic NF- κ B
324 activation and protects cells from DNA damage–induced cell death.^{52–55} Indeed,
325 expression of NF- κ B target genes, including anti-apoptotic genes, was modestly but
326 significantly higher in splenic B cells of the CD19-cre-HOIP/MYD88LP mice than in
327 those of the CD19-cre-MYD88LP mice (supplemental Figure 5). Elevated levels of
328 HOIP not only augmented activation of NF- κ B and expression of several anti-apoptotic
329 genes, but also enhanced linear ubiquitination of NEMO induced by cisplatin (Figure
330 4I–K; supplemental Figure 4C). In accordance with these results, RNA-seq analyses of
331 human DLBCLs revealed that expression of *HOIP* positively correlated with expression
332 of the genes involved in negative regulation of intrinsic apoptotic signaling, as well as
333 those involved in the NF- κ B pathway (Figure 4L). These results suggested that
334 enhanced HOIP expression increases LUBAC activity and confers tumor cells
335 resistance to cisplatin-induced DNA damage by modulating expression of genes
336 associated with cell death.

337 On the other hand, AID-induced DNA alterations are repaired by the DNA
338 double-strand break repair machinery, which also functions in repairing
339 cisplatin-induced DNA damage.^{41,56} Based on the observation that somatic mutations of
340 AID signature are increased in mouse lymphoma cells, it can be speculated that
341 increased LUBAC activity would also promote the accumulation of oncogenic somatic

342 mutations caused by AID, and in turn, facilitate the MYD88-mediated B-cell lymphoma
343 development.

344

345 **LUBAC is an effective target for the treatment of DLBCL**

346 Analysis of publicly available RNA-seq gene expression data^{25,30} suggested that the
347 prognosis of primary refractory or relapsed DLBCL patients with high *HOIP* expression
348 is worse than those with low *HOIP* expression (supplemental Figure 6A). Indeed, we
349 showed that LUBAC is involved in B-cell lymphomagenesis by protecting cells from
350 DNA damage-induced apoptosis (Figure 4D,G; supplemental Figure 4B), which may
351 lead to resistance to cytotoxic chemotherapies.⁵¹ We have previously described that
352 LUBAC represents a novel therapeutic target against this cancer because reduction of
353 LUBAC suppresses NF- κ B activation and proliferation of ABC-DLBCL cells *in vitro*
354 cell culture.^{20,57} We then tried to establish a preclinical model for B-cell lymphomas
355 using CD19-cre-HOIP/MYD88LP mice to evaluate whether LUBAC is a promising
356 drug target for B-cell lymphomas *in vivo*.

357 A cell line HM876, derived from a B-cell lymphoma with plasma cell-like
358 surface phenotype in a CD19-cre-HOIP/MYD88LP mouse, exhibited elevated
359 expression of trimeric LUBAC and constitutive activation of NF- κ B, manifested by
360 phosphorylation and reduced expression of I κ B α (Figure 5A; supplemental Figure 6B;
361 Table 1). Using HM876 cells, we established a mouse lymphoma model by secondary
362 transplantation of HM876 cells for *in vivo* drug evaluation (Figure 5B).

363 We next sought for small compounds that can inhibit the activity of LUBAC.
364 High-throughput screening (HTS) of 41,760 compounds in total using an
365 AlphaScreen-based method (supplemental Figure 6C) identified aureothricin as a
366 candidate LUBAC inhibitor (Figure 5C–D; supplemental Figure 6D–E). Because
367 thiolutin is a molecular derivative of aureothricin, we examined both compounds in

368 subsequent experiments (Figure 5C–E; supplemental Figure 6E).

369 Ubiquitin ligases are classified into three groups, RING, HECT, and
370 RING-IBR-RING (RBR). LUBAC is an RBR ligase,⁵⁸ and thiolutin inhibited catalytic
371 RBR domain of HOIP in LUBAC (Figure 5F). Thiolutin did not noticeably inhibit the
372 activities of a HECT ligase (Nedd4) or a RING ligase (cIAP2) *in vitro*, and only slightly
373 inhibited another RBR ligase (Parkin), when used in higher concentrations
374 (supplemental Figure 6F), suggesting that its inhibitory function is specific for LUBAC.
375 Thiolutin effectively suppressed CD40 ligand-mediated NF-κB activation, and
376 decreased the protein expression levels of LUBAC subunits at concentration as low as
377 0.07 μM in ABC-DLBCL-derived DLBCL2 cells and HM876 cells (Figure 5G–H).
378 Thiolutin did not decrease the amount of LUBAC components in the *in vitro*
379 ubiquitination assay, nor obviously altered the gene expression of LUBAC subunits in
380 DLBCL cells (supplemental Figure 6G–H). Thiolutin decreased the amount of linear
381 ubiquitin chains without affecting the amount of K48- or K63-ubiquitin chains in cells
382 (Figure 5I; supplemental Figure 6I), and appeared to decrease survival of
383 ABC-DLBCL-derived cell lines more effectively than GCB-DLBCL-derived cell lines
384 (Figure 5J). Likewise, thiolutin suppressed NF-κB activation and exerted significant
385 cytotoxicity in HM876 cells *in vitro* (Figure 5A,K). These results suggested that the
386 cytotoxic effect of thiolutin is mainly caused by the inhibition of LUBAC and the
387 blockade of NF-κB signaling. To validate whether LUBAC is an effective therapeutic
388 target for B-cell lymphomas, we intraperitoneally administered thiolutin to mice
389 inoculated with HM876 cells, and found that thiolutin significantly decreased the tumor
390 burden (Figure 5L–M), indicating that inhibition of LUBAC represents an effective
391 treatment for B-cell lymphomas with NF-κB activation. Moreover, our results
392 demonstrate that our mouse model provides a valuable preclinical platform for the
393 development of novel therapeutic approaches for B-cell lymphomas.

394 **Discussion**

395

396 Constitutive activation of NF- κ B signaling is required for survival and proliferation of
397 B cells and plays a crucial role in pathogenesis of ABC-DLBCL. Previously, we
398 reported that rare germline SNPs in the gene encoding HOIP, which activates LUBAC
399 ligase activity are accumulated in individuals with ABC-DLBCL.²⁰ We also found that
400 expression of HOIP is elevated in ABC-DLBCL compared to GCB-DLBCL (Figure 1A).
401 According to these observations, it is suspected that HOIP plays important roles broadly
402 in ABC-DLBCL, whereas the precise contribution of HOIP and its functional protein
403 complex LUBAC to lymphomagenesis has been poorly understood. Hence, we
404 established mice models that allow enhanced expression of HOIP in B cells and
405 assessed the roles of LUBAC in the pathogenesis of ABC-DLBCL. Because the
406 LUBAC activating SNPs of HOIP accumulate in patients with ABC-DLBCL with
407 oncogenic MYD88 L265P mutation,²⁰ we investigated the functional synergism of
408 LUBAC and MYD88 in B-cell lymphomagenesis in mice. The results revealed that
409 elevated expression of LUBAC accelerates MYD88-driven lymphomagenesis.

410 Our data showed that overexpression of HOIP increased NF- κ B activation and
411 enhanced proliferation of B cells upon MYD88 dependent signal activation (Figure 1C–
412 D; supplemental Figure 1E), although it could not induce lymphomas in mice by itself
413 (Figure 1F). However, enforced HOIP expression with oncogenic MYD88 L252P
414 signaling facilitates tumor formation in mice, of which phenotype is DLBCL-like. More
415 importantly, whole-exome sequence analysis of lymphomas developed in mice revealed
416 higher somatic mutations in lymphomas with co-expression of HOIP, many of which are
417 of AID signature and partially resemble those often seen in DLBCL patient samples
418 (Figures 2B–C and 3A–C; supplemental Figure 3A–E). This suggests that the mouse
419 model expressing HOIP and MYD88 L252P shares biological features with human

420 DLBCL.

421 NF- κ B is known to be activated by genotoxic damages, including those
422 triggered by AID, and it helps cell survival by inducing a variety of anti-apoptotic
423 genes.⁵³ We previously reported that LUBAC-mediated linear ubiquitination of NEMO
424 plays a key role in transducing nuclear genotoxic signals to the cytoplasm, and in turn
425 inducing genotoxic stress-induced NF- κ B activation.⁵² As no significant difference in
426 the expression levels of AID could be observed in B cells between
427 CD19-cre-HOIP/MYD88LP and CD19-cre-MYD88LP mice (Figure 4A), we assume
428 that increased mutation burden in the tumors of CD19-cre-HOIP/MYD88LP mice is
429 rather a result of higher tolerability to genotoxic stress in the condition of higher
430 catalytic activity of LUBAC (Figure 4D,G,J; supplemental Figure 4B). Therefore,
431 elevated expression of LUBAC is considered to facilitate MYD88-mediated B-cell
432 lymphomagenesis by conferring B cells resistance to genotoxic stress and, in turn,
433 augmenting the accumulation of oncogenic mutations. Our findings are compatible with
434 the previous report that apoptotic pathway countered MYD88-driven B-cell
435 proliferation⁵⁹ and aberrant expression of anti-apoptotic protein Bcl-2 facilitated
436 generation of oncogenic MYD88-driven DLBCL.^{39,60,61}

437 In accordance with our mouse experiment, the expression level of HOIP
438 appears to positively correlate with the number of somatic mutations of AID signature
439 in human DLBCL (Figure 3E). Since no correlation was found in the expression level of
440 AID and HOIP in human DLBCLs (data not shown), augmented protection of DNA
441 damage-induced cell death by enhanced LUBAC expression might rather be a main
442 cause for high mutation rates in human DLBCLs with high HOIP expression. Gene
443 mutations recurrently found in human DLBCLs could barely be detected in lymphomas
444 generated in mice with oncogenic MYD88 transgene alone. This could be simply due to
445 the limited number of tumors that could be analyzed in CD19-cre-MYD88LP mice, or

446 the potential differences in B-cell developmental stage in which oncogenic MYD88
447 transgene are acquired between our model and human DLBCL.

448 We observed a population of mice with tumors of a more differentiated
449 phenotype with CD138 and IgM expression (Table 1) and the presence of serum M
450 proteins (data not shown). These tumors may possibly be the equivalent of
451 lymphoplasmacytic lymphoma (LPL) in humans, another B-cell malignancy in which
452 MYD88 L265P is closely involved.^{62,63} Considering that these tumors were observed
453 only in CD19-cre-HOIP/MYD88LP mice (Table 1), augmented LUBAC activity may
454 have played some roles in their development, whereas there is presently no data of the
455 involvement of LUBAC in the pathogenesis of LPL.

456 Finally, we established a preclinical tumor transplantation model for human
457 B-cell lymphomas using a cell line derived from a CD19-cre-HOIP/MYD88LP mouse.
458 In this model, we showed that thiolutin, a specific inhibitor of LUBAC, suppressed the
459 growth of lymphoma cells. Reduction or deletion of LUBAC counteracts resistance to
460 cytotoxic chemotherapy, possibly by decreasing the expression of anti-apoptotic genes
461 that are induced by NF- κ B activation.⁵¹

462 In summary, our results suggest that LUBAC has a function to accelerate B-cell
463 lymphomagenesis by conferring B cells resistance to genotoxic stress. We have also
464 shown that, as a direct regulator of NF- κ B pathway, LUBAC is an effective treatment
465 target for lymphoma. Considering that resistance to genotoxic cell death is the common
466 feature of chemorefractory cancers, the inhibition of LUBAC would represent a
467 promising strategy for the treatment of multiple types of cancers.

468

469 **Acknowledgements**

470 We thank Y. Fuseya and H. Fujita for insightful discussions, Y. Sugahara for assistance
471 with animal cares, and I. Kuwahara for assistance with HTS for small-molecule
472 inhibitors of LUBAC. We also thank A. Reddy and S.S. Dave (Duke University,
473 Durham, NC) for providing DLBCL sequencing data. The results published here are in
474 whole or part based upon data generated by the TCGA Research Network:
475 <https://www.cancer.gov/tcga>. Preparation of paraffin-embedded sections was supported
476 by the Anatomic Pathology Center of the Graduate School of Medicine of Kyoto
477 University. This work was supported in part by P-DIRECT, a Grant-in-Aid to K.I. from
478 the Ministry of Education, Culture, Sports, Science, and Technology of Japan; grants
479 from AMED to S.O. (Grant Number 18cm0106501h0003) and A.T.-K. (Grant Numbers
480 18ck0106250h0002 and 17fk0108040h0002); and grants from KAKENHI from Japan
481 Society for the Promotion of Science or MEXT to M.N. (Grant Number 15K09474),
482 A.T.-K. (Grant Number 18H03992), M.Y. (Grant Number 18H05503), and K.I. (Grant
483 Numbers 24112002, 25253019, 26670154, 17H06174, and 18H05499).

484

485 **Authorship Contributions**

486 T.J., M.N., Y.S., K.I., and A.T.-K. conceived and designed the project. T.J. performed
487 most of the experiments. S.M. provided essential experimental support. A.S. and H.K.
488 supported generation of transgenic mice. Y.K., K.K., and S.O. performed whole-exome
489 sequencing analyses of the lymphomas derived from transgenic mice. H.A. performed
490 analyses of clinical RNA-seq data. N.K., T.O., K.S., M.Y. developed and performed the
491 HTS for small-molecule inhibitors for LUBAC. T.N., and F.I. performed experiments on
492 aureothricin and thiolutin. K.S. advised on experimental design. T.J., M.N., K.I., and
493 A.T.-K. wrote the manuscript with contributions from all other authors.

494

495 **Disclosure of Conflicts of Interest**

496 The authors declare that they have no conflict of interest.

497 **References**

- 498 1. Swerdlow SH, Campo E, Harris NL, et al. WHO Classification of Tumours of
499 Haematopoietic and Lymphoid Tissues (Revised 4th edition). Lyon: International
500 Agency for Research on Cancer (IARC). 2017.
- 501 2. Lenz G, Staudt LM. Aggressive lymphomas. *N Engl J Med*.
502 2010;362(15):1417-1429.
- 503 3. Alizadeh AA, Eisen MB, Davis RE, et al. Distinct types of diffuse large B-cell
504 lymphoma identified by gene expression profiling. *Nature*. 2000;403(6769):503-511.
- 505 4. Monti S, Savage KJ, Kutok JL, et al. Molecular profiling of diffuse large B-cell
506 lymphoma identifies robust subtypes including one characterized by host inflammatory
507 response. *Blood*. 2005;105(5):1851-1861.
- 508 5. Shaffer AL, 3rd, Young RM, Staudt LM. Pathogenesis of human B cell
509 lymphomas. *Annu Rev Immunol*. 2012;30:565-610.
- 510 6. Wright G, Tan B, Rosenwald A, Hurt EH, Wiestner A, Staudt LM. A gene
511 expression-based method to diagnose clinically distinct subgroups of diffuse large B cell
512 lymphoma. *Proc Natl Acad Sci USA*. 2003;100(17):9991-9996.
- 513 7. Kelly PN, Romero DL, Yang Y, et al. Selective interleukin-1
514 receptor-associated kinase 4 inhibitors for the treatment of autoimmune disorders and
515 lymphoid malignancy. *J Exp Med*. 2015;212(13):2189-2201.
- 516 8. Nowakowski GS, LaPlant B, Macon WR, et al. Lenalidomide combined with
517 R-CHOP overcomes negative prognostic impact of non-germinal center B-cell
518 phenotype in newly diagnosed diffuse large B-Cell lymphoma: a phase II study. *J Clin*
519 *Oncol*. 2015;33(3):251-257.
- 520 9. Tilly H, Gomes da Silva M, Vitolo U, et al. Diffuse large B-cell lymphoma
521 (DLBCL): ESMO Clinical Practice Guidelines for diagnosis, treatment and follow-up.
522 *Ann Oncol*. 2015;26 Suppl 5:v116-125.
- 523 10. Ngo VN, Young RM, Schmitz R, et al. Oncogenically active MYD88 mutations
524 in human lymphoma. *Nature*. 2011;470(7332):115-119.
- 525 11. Chen ZJ. Ubiquitination in signaling to and activation of IKK. *Immunol Rev*.
526 2012;246(1):95-106.
- 527 12. Fujita H, Rahighi S, Akita M, et al. Mechanism underlying IκB kinase
528 activation mediated by the linear ubiquitin chain assembly complex. *Mol Cell Biol*.
529 2014;34(7):1322-1335.
- 530 13. Ikeda F, Deribe YL, Skanland SS, et al. SHARPIN forms a linear ubiquitin
531 ligase complex regulating NF-κB activity and apoptosis. *Nature*.
532 2011;471(7340):637-641.
- 533 14. Kensche T, Tokunaga F, Ikeda F, Goto E, Iwai K, Dikic I. Analysis of nuclear
534 factor-κB (NF-κB) essential modulator (NEMO) binding to linear and lysine-linked
535 ubiquitin chains and its role in the activation of NF-κB. *J Biol Chem*.

536 2012;287(28):23626-23634.

537 15. Kirisako T, Kamei K, Murata S, et al. A ubiquitin ligase complex assembles
538 linear polyubiquitin chains. *EMBO J*. 2006;25(20):4877-4887.

539 16. Kumari S, Redouane Y, Lopez-Mosqueda J, et al. Sharpin prevents skin
540 inflammation by inhibiting TNFR1-induced keratinocyte apoptosis. *Elife*.
541 2014;3:e03422.

542 17. Tokunaga F, Nakagawa T, Nakahara M, et al. SHARPIN is a component of the
543 NF- κ B-activating linear ubiquitin chain assembly complex. *Nature*.
544 2011;471(7340):633-636.

545 18. Tokunaga F, Sakata S, Saeki Y, et al. Involvement of linear polyubiquitylation
546 of NEMO in NF- κ B activation. *Nat Cell Biol*. 2009;11(2):123-132.

547 19. Gerlach B, Cordier SM, Schmukle AC, et al. Linear ubiquitination prevents
548 inflammation and regulates immune signalling. *Nature*. 2011;471(7340):591-596.

549 20. Yang Y, Schmitz R, Mitala J, et al. Essential role of the linear ubiquitin chain
550 assembly complex in lymphoma revealed by rare germline polymorphisms. *Cancer*
551 *Discov*. 2014;4(4):480-493.

552 21. Sasaki Y, Sano S, Nakahara M, et al. Defective immune responses in mice
553 lacking LUBAC-mediated linear ubiquitination in B cells. *EMBO J*.
554 2013;32(18):2463-2476.

555 22. Satpathy S, Wagner SA, Beli P, et al. Systems-wide analysis of BCR
556 signalosomes and downstream phosphorylation and ubiquitylation. *Mol Syst Biol*.
557 2015;11(6):810.

558 23. Yang Y, Kelly P, Shaffer AL, 3rd, et al. Targeting Non-proteolytic Protein
559 Ubiquitination for the Treatment of Diffuse Large B Cell Lymphoma. *Cancer Cell*.
560 2016;29(4):494-507.

561 24. Yang YK, Yang C, Chan W, Wang Z, Deibel KE, Pomerantz JL. Molecular
562 Determinants of Scaffold-induced Linear Ubiquitylation of B Cell
563 Lymphoma/Leukemia 10 (Bcl10) during T Cell Receptor and Oncogenic Caspase
564 Recruitment Domain-containing Protein 11 (CARD11) Signaling. *J Biol Chem*.
565 2016;291(50):25921-25936.

566 25. Reddy A, Zhang J, Davis NS, et al. Genetic and Functional Drivers of Diffuse
567 Large B Cell Lymphoma. *Cell*. 2017;171(2):481-494 e415.

568 26. Rickert RC, Roes J, Rajewsky K. B lymphocyte-specific, Cre-mediated
569 mutagenesis in mice. *Nucleic Acids Res*. 1997;25(6):1317-1318.

570 27. Grossman RL, Heath AP, Ferretti V, et al. Toward a Shared Vision for Cancer
571 Genomic Data. *N Engl J Med*. 2016;375(12):1109-1112.

572 28. Lohr JG, Stojanov P, Lawrence MS, et al. Discovery and prioritization of
573 somatic mutations in diffuse large B-cell lymphoma (DLBCL) by whole-exome
574 sequencing. *Proc Natl Acad Sci USA*. 2012;109(10):3879-3884.

- 575 29. Kataoka K, Nagata Y, Kitanaka A, et al. Integrated molecular analysis of adult
576 T cell leukemia/lymphoma. *Nat Genet.* 2015;47(11):1304-1315.
- 577 30. Schmitz R, Wright GW, Huang DW, et al. Genetics and Pathogenesis of
578 Diffuse Large B-Cell Lymphoma. *N Engl J Med.* 2018;378(15):1396-1407.
- 579 31. Alvarez-Prado AF, Perez-Duran P, Perez-Garcia A, et al. A broad atlas of
580 somatic hypermutation allows prediction of activation-induced deaminase targets. *J Exp*
581 *Med.* 2018;215(3):761-771.
- 582 32. Petri A, Dybkaer K, Bogsted M, et al. Long Noncoding RNA Expression
583 during Human B-Cell Development. *PLoS One.* 2015;10(9):e0138236.
- 584 33. Dubois SM, Alexia C, Wu Y, et al. A catalytic-independent role for the LUBAC
585 in NF- κ B activation upon antigen receptor engagement and in lymphoma cells. *Blood.*
586 2014;123(14):2199-2203.
- 587 34. Pasqualucci L, Dalla-Favera R. Genetics of diffuse large B-cell lymphoma.
588 *Blood.* 2018;131(21):2307-2319.
- 589 35. Keusekotten K, Elliott PR, Glockner L, et al. OTULIN antagonizes LUBAC
590 signaling by specifically hydrolyzing Met1-linked polyubiquitin. *Cell.*
591 2013;153(6):1312-1326.
- 592 36. Rivkin E, Almeida SM, Ceccarelli DF, et al. The linear ubiquitin-specific
593 deubiquitinase gumby regulates angiogenesis. *Nature.* 2013;498(7454):318-324.
- 594 37. Hjerpe R, Aillet F, Lopitz-Otsoa F, Lang V, England P, Rodriguez MS. Efficient
595 protection and isolation of ubiquitylated proteins using tandem ubiquitin-binding
596 entities. *EMBO Rep.* 2009;10(11):1250-1258.
- 597 38. van Wijk SJ, Fiskin E, Dikic I. Selective monitoring of ubiquitin signals with
598 genetically encoded ubiquitin chain-specific sensors. *Nat Protoc.* 2013;8(7):1449-1458.
- 599 39. Knittel G, Liedgens P, Korovkina D, et al. B-cell-specific conditional
600 expression of Myd88p.L252P leads to the development of diffuse large B-cell
601 lymphoma in mice. *Blood.* 2016;127(22):2732-2741.
- 602 40. Hans CP, Weisenburger DD, Greiner TC, et al. Confirmation of the molecular
603 classification of diffuse large B-cell lymphoma by immunohistochemistry using a tissue
604 microarray. *Blood.* 2004;103(1):275-282.
- 605 41. Chapuy B, Stewart C, Dunford AJ, et al. Molecular subtypes of diffuse large B
606 cell lymphoma are associated with distinct pathogenic mechanisms and outcomes. *Nat*
607 *Med.* 2018;24(5):679-690.
- 608 42. Liu M, Duke JL, Richter DJ, et al. Two levels of protection for the B cell
609 genome during somatic hypermutation. *Nature.* 2008;451(7180):841-845.
- 610 43. Muramatsu M, Kinoshita K, Fagarasan S, Yamada S, Shinkai Y, Honjo T. Class
611 switch recombination and hypermutation require activation-induced cytidine deaminase
612 (AID), a potential RNA editing enzyme. *Cell.* 2000;102(5):553-563.
- 613 44. Lossos IS, Levy R, Alizadeh AA. AID is expressed in germinal center

- 614 B-cell-like and activated B-cell-like diffuse large-cell lymphomas and is not correlated
615 with intracloal heterogeneity. *Leukemia*. 2004;18(11):1775-1779.
- 616 45. Mlynarczyk C, Fontan L, Melnick A. Germinal center-derived lymphomas: The
617 darkest side of humoral immunity. *Immunol Rev*. 2019;288(1):214-239.
- 618 46. Pasqualucci L, Neumeister P, Goossens T, et al. Hypermutation of multiple
619 proto-oncogenes in B-cell diffuse large-cell lymphomas. *Nature*.
620 2001;412(6844):341-346.
- 621 47. Khodabakhshi AH, Morin RD, Fejes AP, et al. Recurrent targets of aberrant
622 somatic hypermutation in lymphoma. *Oncotarget*. 2012;3(11):1308-1319.
- 623 48. Rada C, Milstein C. The intrinsic hypermutability of antibody heavy and light
624 chain genes decays exponentially. *EMBO J*. 2001;20(16):4570-4576.
- 625 49. Storb U, Peters A, Klotz E, et al. Cis-acting sequences that affect somatic
626 hypermutation of Ig genes. *Immunol Rev*. 1998;162:153-160.
- 627 50. Bahjat M, Guikema JEJ. The Complex Interplay between DNA Injury and
628 Repair in Enzymatically Induced Mutagenesis and DNA Damage in B Lymphocytes. *Int*
629 *J Mol Sci*. 2017;18(9).
- 630 51. MacKay C, Carroll E, Ibrahim AFM, et al. E3 ubiquitin ligase HOIP attenuates
631 apoptotic cell death induced by cisplatin. *Cancer Res*. 2014;74(8):2246-2257.
- 632 52. Niu J, Shi Y, Iwai K, Wu ZH. LUBAC regulates NF- κ B activation upon
633 genotoxic stress by promoting linear ubiquitination of NEMO. *EMBO J*.
634 2011;30(18):3741-3753.
- 635 53. McCool KW, Miyamoto S. DNA damage-dependent NF- κ B activation: NEMO
636 turns nuclear signaling inside out. *Immunol Rev*. 2012;246(1):311-326.
- 637 54. Wang CY, Mayo MW, Baldwin AS, Jr. TNF- and cancer therapy-induced
638 apoptosis: potentiation by inhibition of NF- κ B. *Science*. 1996;274(5288):784-787.
- 639 55. Wu ZH, Miyamoto S. Induction of a pro-apoptotic ATM-NF- κ B pathway and
640 its repression by ATR in response to replication stress. *EMBO J*.
641 2008;27(14):1963-1973.
- 642 56. Di Noia JM, Neuberger MS. Molecular mechanisms of antibody somatic
643 hypermutation. *Annu Rev Biochem*. 2007;76:1-22.
- 644 57. Fujita H, Tokunaga A, Shimizu S, et al. Cooperative Domain Formation by
645 Homologous Motifs in HOIL-1L and SHARPIN Plays A Crucial Role in LUBAC
646 Stabilization. *Cell Rep*. 2018;23(4):1192-1204.
- 647 58. Smit JJ, Monteferrario D, Noordermeer SM, van Dijk WJ, van der Reijden BA,
648 Sixma TK. The E3 ligase HOIP specifies linear ubiquitin chain assembly through its
649 RING-IBR-RING domain and the unique LDD extension. *EMBO J*.
650 2012;31(19):3833-3844.
- 651 59. Wang JQ, Jeelall YS, Beutler B, Horikawa K, Goodnow CC. Consequences of
652 the recurrent MYD88(L265P) somatic mutation for B cell tolerance. *J Exp Med*.

653 2014;211(3):413-426.
654 60. Lenz G, Wright GW, Emre NC, et al. Molecular subtypes of diffuse large
655 B-cell lymphoma arise by distinct genetic pathways. *Proc Natl Acad Sci USA*.
656 2008;105(36):13520-13525.
657 61. Monni O, Joensuu H, Franssila K, Klefstrom J, Alitalo K, Knuutila S. BCL2
658 overexpression associated with chromosomal amplification in diffuse large B-cell
659 lymphoma. *Blood*. 1997;90(3):1168-1174.
660 62. Treon SP, Xu L, Yang G, et al. MYD88 L265P somatic mutation in
661 Waldenström's macroglobulinemia. *N Engl J Med*. 2012;367(9):826-833.
662 63. Kapoor P, Paludo J, Vallumsetla N, Greipp PR. Waldenström
663 macroglobulinemia: What a hematologist needs to know. *Blood Rev*.
664 2015;29(5):301-319.
665
666

Table 1. Surface phenotypes of lymphomas in transgenic mice

Tumor ID	Genotype	Surface phenotypes											Major site of involvement
		CD19	B220	IgM	IgD	CD5	CD21	CD23	CD38	CD138	Igκ	Igλ	
786	CD19-cre-HOIP/MYD88LP	+	+	+	-	-	-	-	+	-	+	-	Spleen
950	CD19-cre-HOIP/MYD88LP	+	+	+	-	-	-	-	+	-	+	-	Spleen
1032	CD19-cre-HOIP/MYD88LP	+	+	+	-	-	-	-	+	-	+	-	Extranodal (subcutaneous)
1074	CD19-cre-HOIP/MYD88LP	+	+	+	-	-	-	-	+	-	+	-	Mesenteric lymph nodes
1078	CD19-cre-HOIP/MYD88LP	+	+	+	-	-	-	-	+	-	-	+	Peripheral lymph nodes
1083	CD19-cre-HOIP/MYD88LP	+	+	+	-	-	-	-	+	-	+	-	Peripheral lymph nodes
1084	CD19-cre-HOIP/MYD88LP	+	+	+	-	-	-	-	+	-	+	-	Peripheral lymph nodes
1182	CD19-cre-HOIP/MYD88LP	+	+	+	-	-	NA	NA	NA	-	+	-	Mesenteric lymph nodes
1236	CD19-cre-MYD88LP	+	+	+	-	-	-	-	+	-	+	-	Mesenteric lymph nodes
1237	CD19-cre-MYD88LP	+	+	+	-	-	-	-	+	-	+	-	Extranodal (subcutaneous)
1289	CD19-cre-MYD88LP	+	+	+	-	-	-	-	+	-	+	-	Peritoneal
1385	CD19-cre-MYD88LP	+	+	+	-	-	-	-	+	-	+	-	Peripheral lymph nodes
876	CD19-cre-HOIP/MYD88LP	-	-	+	-	-	-	-	+	+	+	-	Peritoneal
1027	CD19-cre-HOIP/MYD88LP	-	-	+	-	-	-	-	-	+	+	-	Peritoneal

667 **Figure Legends**

668

669 **Figure 1. Augmented LUBAC expression accelerates oncogenic MYD88-mediated**

670 **B-cell lymphomagenesis in mice.** (A) Association of *HOIP* (*RNF31*) expression with

671 cell-of-origin in human DLBCL. Boxes represent the median and the first and third

672 quartiles, and whiskers represent the minimum and maximum of all data points. (B)

673 Schematic representation of conditional expression of HOIP in mice. (C) Transcript

674 levels of NF- κ B target genes in unstimulated splenic B cells from mice (10 weeks old),

675 normalized against *Actb* mRNA; n = 3 per genotype. Data are means \pm SD. (D) Cell

676 Trace Violet-labeled splenic B cells were cultured with or without stimuli. (E) Cell

677 lysates of splenic B cells derived from CD19-cre, CD19-cre-MYD88LP, and

678 CD19-cre-HOIP/MYD88LP mice were subjected to Halo-tagged linear

679 ubiquitin-specific tandem ubiquitin binding entity (M1-specific TUBE) binding and

680 Halo Tag based purification, and analyzed by immunoblotting. (F) Kaplan–Meier plots

681 of survival of transgenic mice (n = 18, CD19-cre; n = 36, CD19-cre-HOIP; n = 26,

682 CD19-cre-MYD88LP; and n = 33, CD19-cre-HOIP/MYD88LP). (G–I) Representative

683 tumor involvement of lymphoid organs isolated from 9-month-old

684 CD19-cre-HOIP/MYD88LP mice. (G) Macroscopic appearance of spleens (left) and

685 lymph nodes (right). (H) Representative H&E and immunohistochemical staining for

686 *Irf4* and *Bcl6* of spleens (CD19-cre mice) or tumors (CD19 cre-MYD88LP and

687 CD19-cre-HOIP/MYD88LP mice). Scale bars: 200 μ m; inset 20 μ m. (I) Representative

688 analyses of clonality. Tumor 1084-specific primers specifically amplified tumor 1084–

689 specific V(D)J, but did not amplify V(D)J from genomic DNA of normal splenic B cells

690 or tumor 786. (C and F) * p < 0.05, ** p < 0.01, *** p < 0.001. (A and C), two-tailed

691 unpaired Student's *t*-test; (F) log–rank test.

692 See also supplemental Figures 1–2 and supplemental Table 1.

693 **Figure 2. LUBAC facilitates somatic mutations in genes frequently mutated in**
694 **human DLBCL.** (A-C) Mutations with variant allele frequency (VAF) > 0.05 in tumor
695 samples were selected and analyzed. (A) Numbers of total mutations including both
696 synonymous and non-synonymous mutations in each tumor sample. Boxes represent the
697 median and the first and third quartiles, and whiskers represent the minimum and
698 maximum of all data points. (B) Venn diagram depicting the overlap between genes
699 recurrently mutated non-synonymously in lymphoma cells derived from
700 CD19-cre-HOIP/MYD88LP mice and those frequently detected in human DLBCL.³⁰
701 (C) Mutational heatmap showing recurrently mutated genes across sequenced samples,
702 color-coded according to five types of genetic alteration. Above the mutational heatmap,
703 the bar graph indicates the number of non-synonymous mutations in each sample. To
704 the right of the mutational heatmap, the stacked bar graph indicates the percentage of
705 tumors that have each mutations, using the same five-color scheme. Target genes of
706 aberrant somatic hypermutation induced by AID in human DLBCL are labeled in red.
707 Black daggers indicates murine homologous genes frequently mutated in human
708 DLBCL.³⁰ Red and blue daggers indicate murine homologue of previously reported
709 altered genes significantly enriched in human ABC-DLBCL and GCB-DLBCL,
710 respectively.³⁰

711 (A) *** $p < 0.001$. (A) Brunner–Munzel test; (B) Fisher’s exact test.

712 See also supplemental Figure 3 and supplemental Table 5.

713

714 **Figure 3. LUBAC facilitates aberrant somatic hypermutations mediated by AID.**

715 (A-C) Mutations with VAF > 0.05 in tumor samples were selected and analyzed. (A)
716 Venn diagram depicting the overlap between genes recurrently mutated in lymphoma
717 cells derived from CD19-cre-HOIP/MYD88LP mice and murine homologue of known
718 or predicted targets of aberrant somatic hypermutation mediated by AID.³⁰ (B) Numbers

719 of SNVs at C/G within the WRCY/RGYW motifs (left), and numbers of C:G (center)
720 and transition mutations (right) in each tumor sample. (C) Mutation distribution in
721 targeted genes observed in lymphoma cells derived from eight
722 CD19-cre-HOIP/MYD88LP mice. Shadows indicate the 2 kb region downstream of the
723 transcription start site (TSS). (D) Numbers of nonsynonymous mutations in each human
724 DLBCL sample. (E) Numbers of SNVs at C/G within the WRCY/RGYW motifs (left),
725 and numbers of C:G (center) and transition mutations (right) in each human DLBCL
726 sample. (D and E) Average fold change of FPKM (high vs. low) = 1.36. Boxes
727 represent the median and the first and third quartiles, and whiskers represent the
728 minimum and maximum of all data points.

729 (B, D, and E), * $p < 0.05$, ** $p < 0.01$, *** $p < 0.001$. (A) Fisher's exact test; (B)
730 Brunner–Munzel test; (D and E) two-tailed unpaired Student's *t*-test.

731 See also supplemental Figure 3 and supplemental Tables 6–8.

732

733 **Figure 4. Augmented LUBAC activity overcomes cell death induced by DNA**
734 **damage thereby accelerating accumulation of somatic mutations.** (A) Transcript
735 levels of *Aicda*, normalized to *Actb* (left panel) and percentages of germinal center B
736 cells (right panel) in mesenteric lymph nodes from 10-week-old mice; $n = 3$ per
737 genotype. Data are means \pm SD. (B) HOIP-overexpressing HBL1 cells were established,
738 and immunoblot analyses were performed using lysates from WT, mock-transfected, or
739 HOIP-overexpressing HBL1 cells. (C) Live cells were analyzed by FACS using
740 TO-PRO-3 staining. HBL1 cells were treated with or without 10 μ g/mL cisplatin for 0–
741 24 hours. (D) Percentage of live cells (\pm SD); $n = 6$ per group in three independent
742 experiments. (E) Immunoblot analyses were performed using lysates from WT,
743 HOIP-knockout, or HOIP-overexpressing Jurkat cells. (F) Live cells were analyzed by
744 FACS using FSC and TO-PRO-3 staining. Jurkat cells were treated with or without 0.5

745 $\mu\text{g/mL}$ cisplatin for 0–72 hours. (G) Percentage of live cells (\pm SD) in three independent
746 experiments. (H–J) Jurkat cells were treated with 3 $\mu\text{g/mL}$ cisplatin for the indicated
747 periods, followed by immunoblotting (H–I) or quantitative RT-PCR, normalized against
748 *Actb* mRNA (J). (K) Jurkat cells were treated with 5 $\mu\text{g/mL}$ cisplatin for the indicated
749 periods. Whole-cell lysates were analyzed by anti-NEMO immunoprecipitation,
750 followed by immunoblotting using antibodies against linear polyubiquitin and NEMO.
751 (L) Correlation of expression of *HOIP* (*RNF31*) and negative regulation of intrinsic
752 apoptotic signaling signature (left), and NF- κ B signaling signature (right).
753 (A, D, G and J), * $p < 0.05$, ** $p < 0.01$, *** $p < 0.001$. (A) one-way ANOVA with
754 Turkey's post hoc test; (D, G and J) two-way ANOVA with Bonferroni post hoc test; (L)
755 Pearson's correlation.

756 See also supplemental Figures 4 and 5, and supplemental Tables 1–4.

757

758 **Figure 5. LUBAC is an effective target for the treatment of DLBCL.** (A) Elevated
759 phosphorylation and degradation of $\text{I}\kappa\text{B}\alpha$ in unstimulated HM876 cells were suppressed
760 by thiolutin. (B) Diagram of allogeneic transplantation model. (C) Chemical structure of
761 aureothricin. (D) Inhibition of LUBAC ligase activity by aureothricin and thiolutin *in*
762 *vitro*. (E) Chemical structure of thiolutin. (F) Thiolutin inhibited linear
763 polyubiquitination mediated by HOIP (aa 699–1072). (G) Upon stimulation of DLBCL2
764 cells with CD40 ligand, thiolutin suppressed phosphorylation and degradation of $\text{I}\kappa\text{B}\alpha$
765 in a dose-dependent manner. DLBCL2 cells were exposed to thiolutin or DMSO for 2
766 hours, and then stimulated with CD40 ligand (30 ng/mL) for the indicated times. (H)
767 Levels of LUBAC components in DLBCL2 (upper panel) and HM876 (lower panel)
768 cells treated with thiolutin were reduced in a dose-dependent manner. (I) Cell lysates of
769 DLBCL2 (left panel) and HM876 (right panel) cells treated with or without thiolutin
770 (0.1 μM) for two hours were analyzed by immunoblotting. Samples were probed with

771 anti-linear ubiquitin specific antibody (LUB9). (J) Viability of DLBCL lines after 48
772 hours treatment with the indicated concentrations of thiolutin, normalized against that of
773 control (DMSO-treated) cells. Data are means \pm SD from three experiments. (K)
774 Viability of HM876 cells after 48 hours treatment with the indicated concentrations of
775 thiolutin, normalized against that of control (DMSO-treated) cells. Data are means \pm SD
776 from three experiments. (L and M) Thiolutin suppressed growth of lymphomas *in vivo*.
777 (L) Gross appearance of engrafted tumors. (M) Tumor weight. Data are means \pm SD.
778 (J, K and M) * $p < 0.05$, ** $p < 0.01$, *** $p < 0.001$. (J and K) two-tailed unpaired
779 Student's *t*-test; (M) one-way ANOVA with Turkey's post hoc tests.
780 See also supplemental Figure 6.

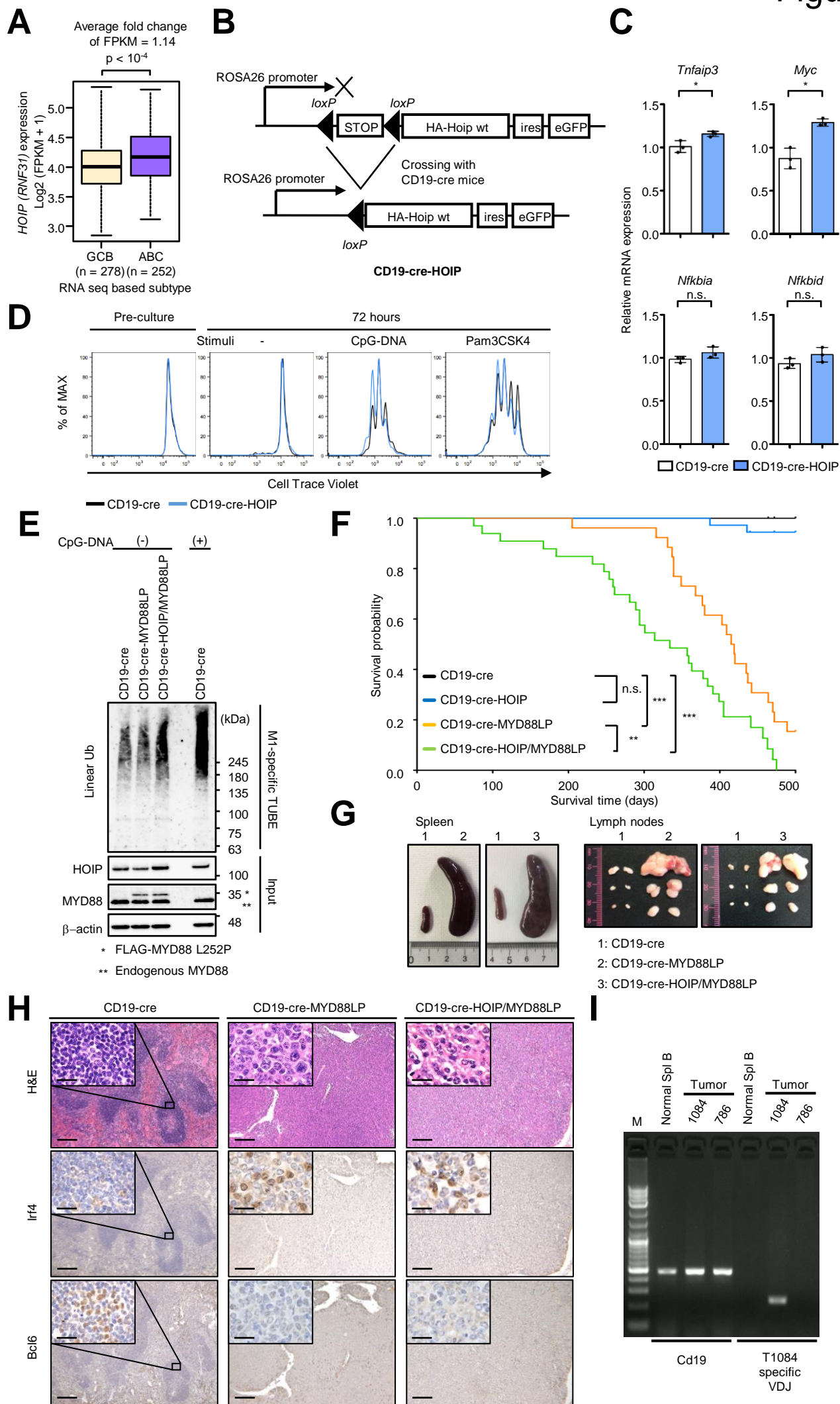


Figure 2

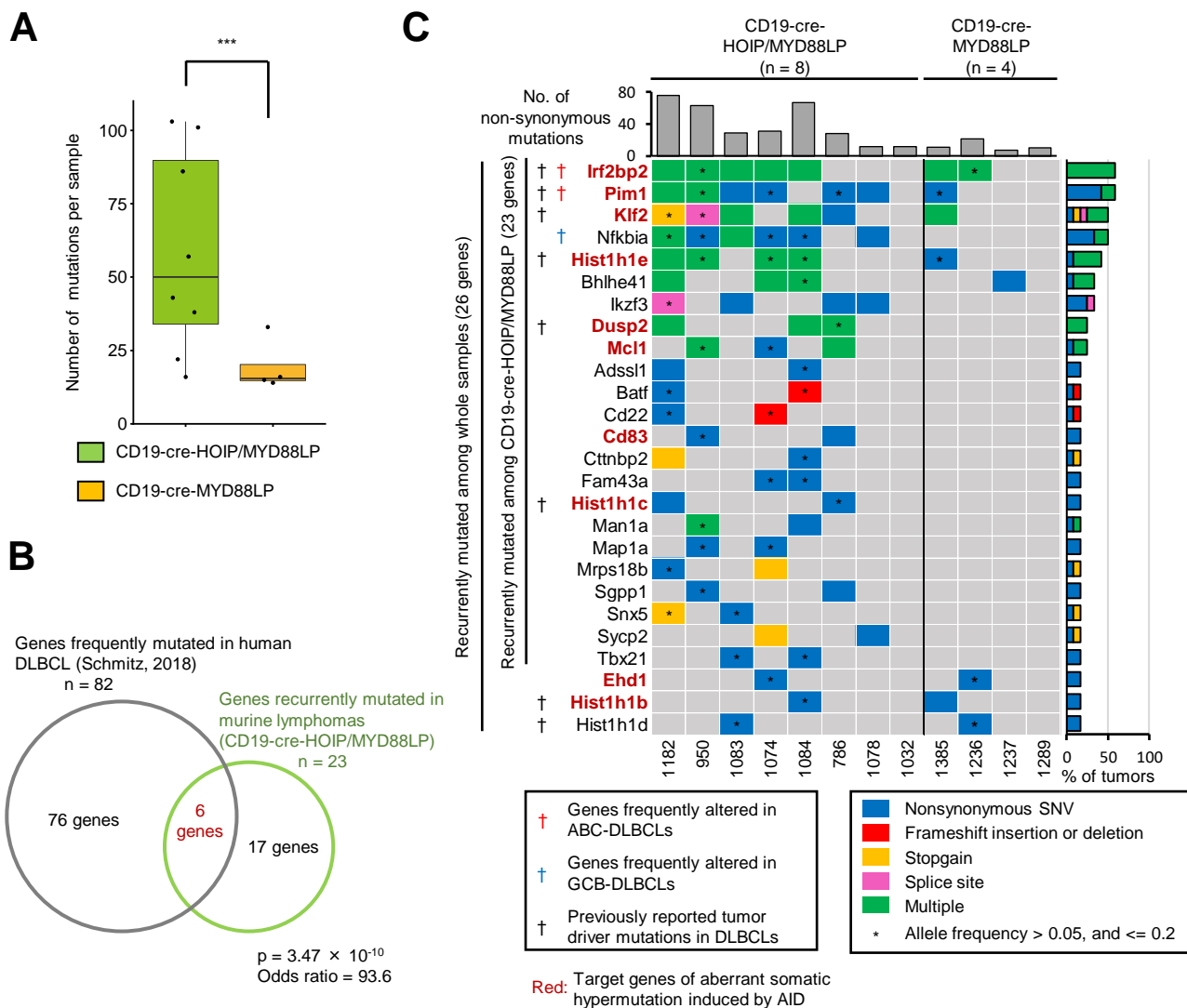
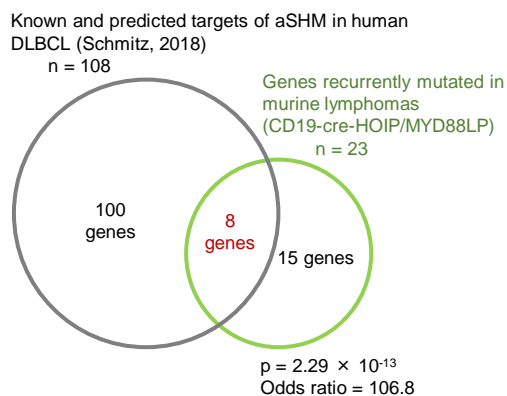
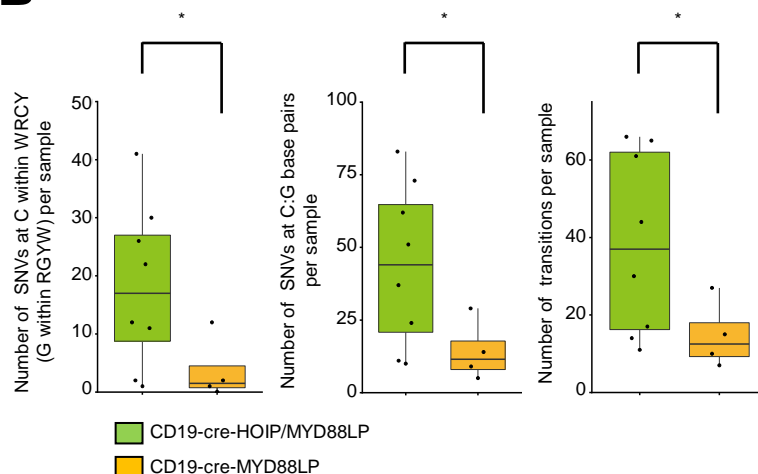


Figure 3

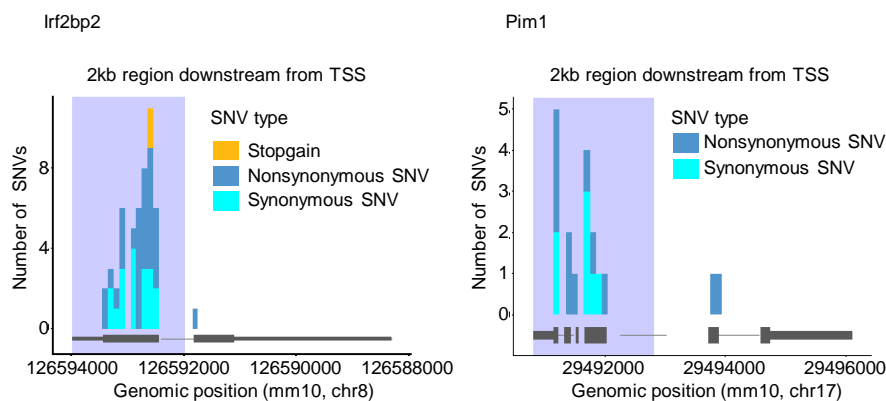
A



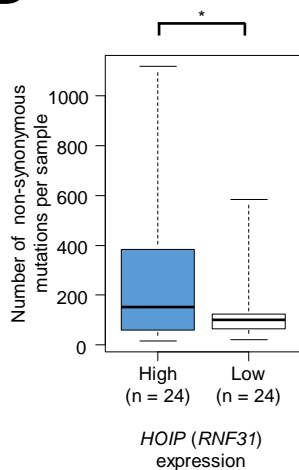
B



C



D



E

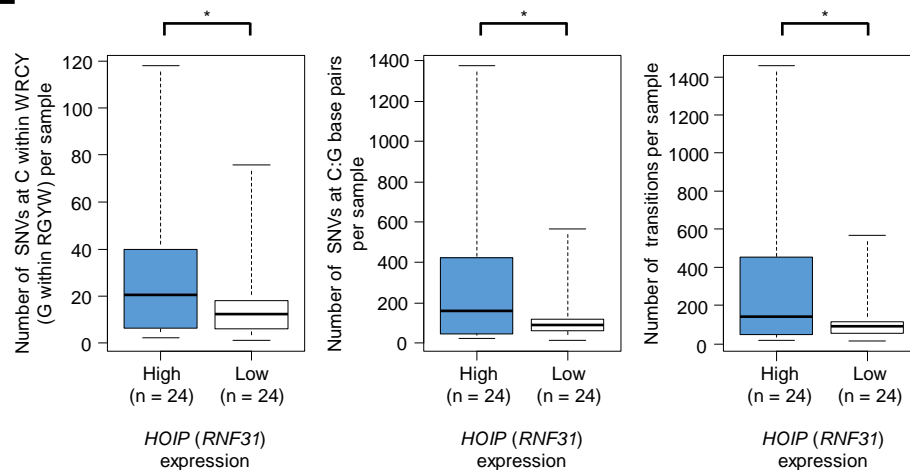


Figure 4

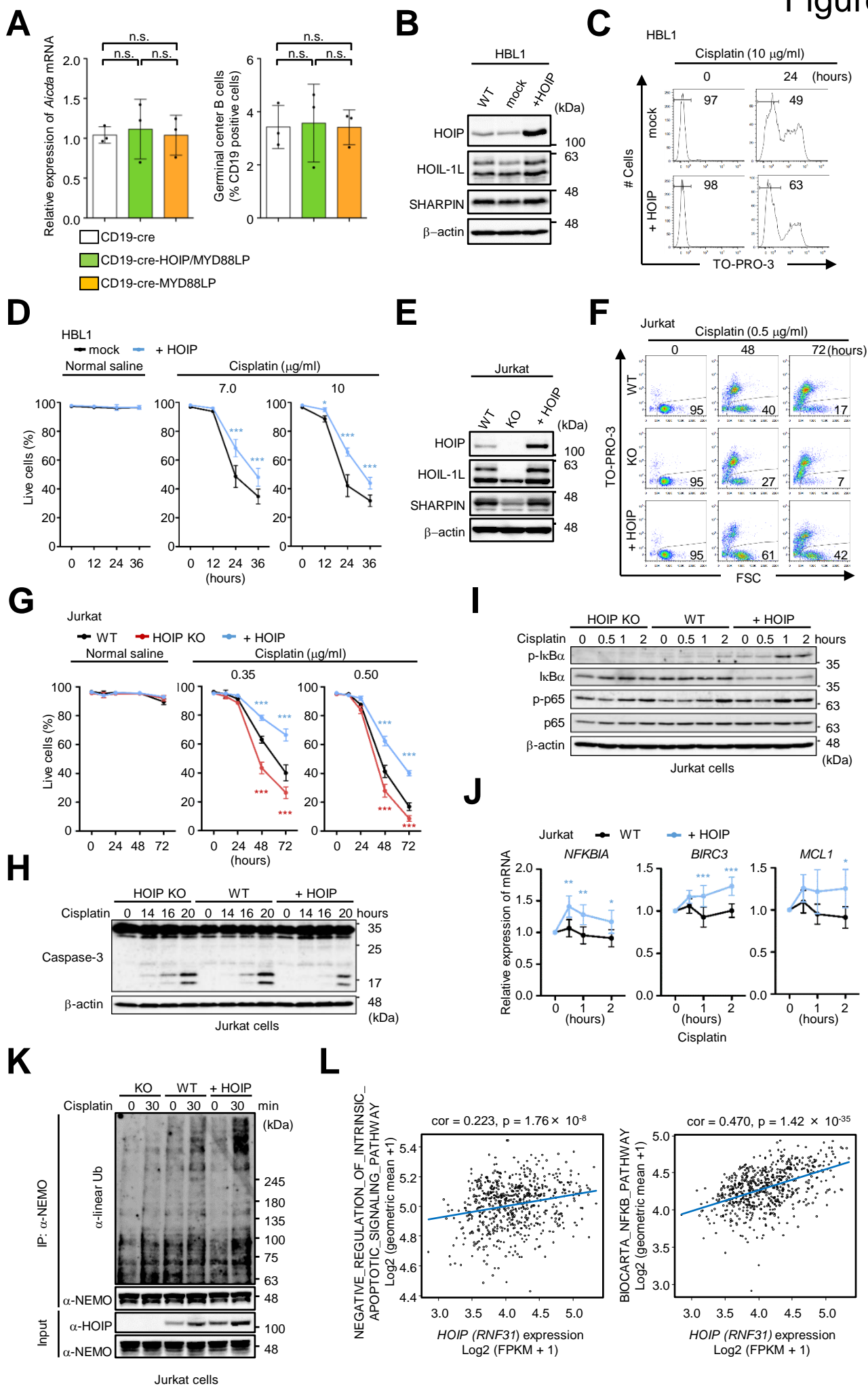
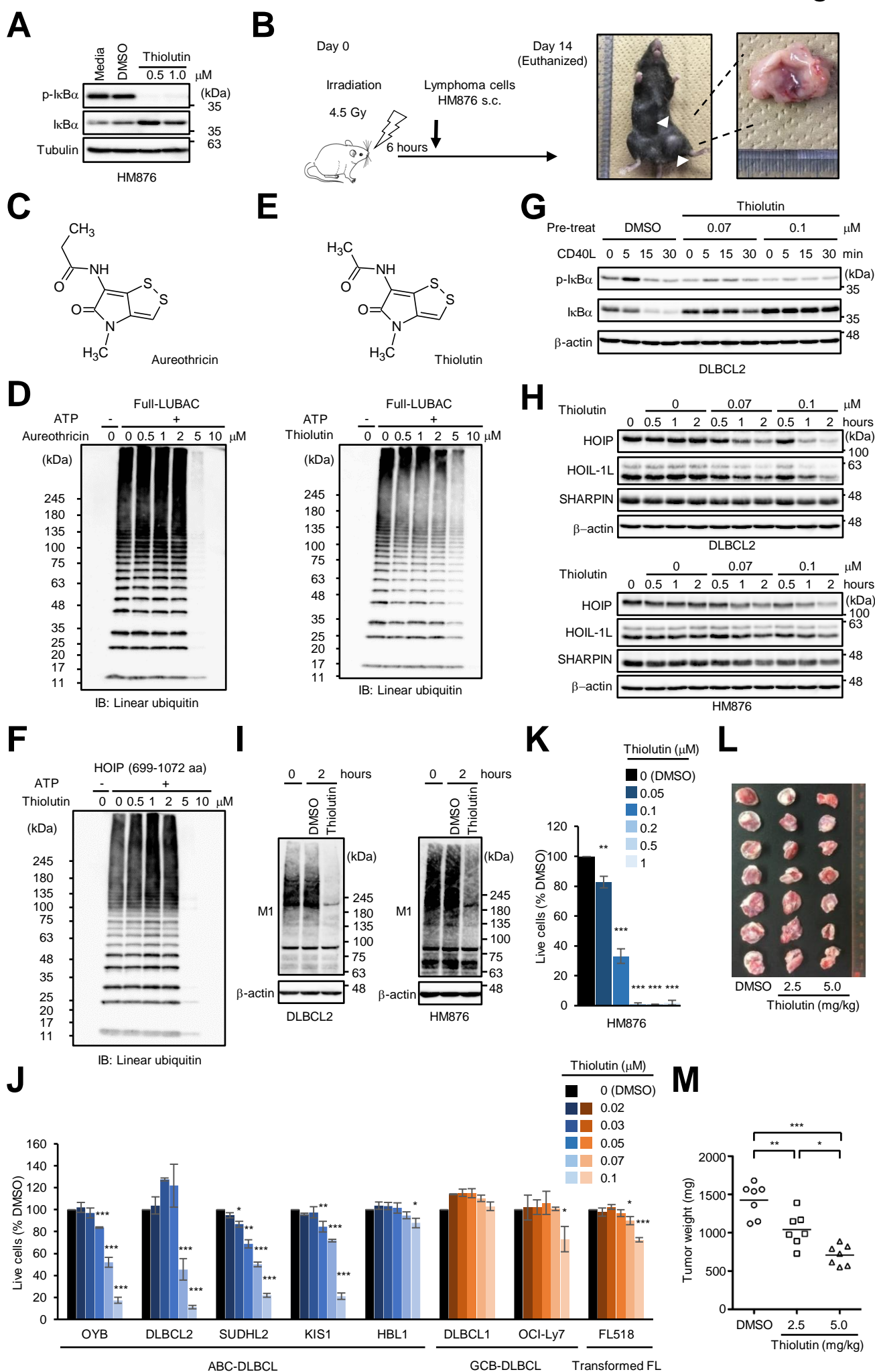


Figure 5



1 **Supplemental Information**

2

3 **LUBAC accelerates B-cell lymphomagenesis by conferring B cells resistance to**
4 **genotoxic stress**

5 Tomoyasu Jo, Momoko Nishikori, Yasunori Kogure, Hiroshi Arima, Katsuhiko Sasaki,
6 Yoshiteru Sasaki, Tomoko Nakagawa, Fumie Iwai, Shuji Momose, Aki Shiraishi, Hiroshi
7 Kiyonari, Noritaka Kagaya, Tetsuo Onuki, Kazuo Shin-ya, Minoru Yoshida, Keisuke
8 Kataoka, Seishi Ogawa, Kazuhiro Iwai, Akifumi Takaori-Kondo

9

10 **Supplemental Methods**

11

12 **Generation of tissue specific HOIP transgenic and MYD88 L252P transgenic mice**

13 Tissue-specific HOIP transgenic mice (ROSA26-STOP-Hoip-ires-eGFP-pA) and
14 MYD88 L252P transgenic mice (ROSA26-STOP-Myd88_L252P-ires-eGFP-pA)
15 (Accession No. CDB 1320K:

16 <http://www2.clst.riken.jp/arg/mutant%20mice%20list.html>) were established as follows:

17 The cDNA encoding N-terminally HA-tagged murine HOIP or FLAG-tagged murine
18 MYD88 L252P was subcloned into vector STOP-eGFP-ROSA26TV¹. Bruce-4 ES cells
19 derived from C57BL/6 embryos (for ROSA26-STOP-Hoip-ires-eGFP-pA) or TT2 ES
20 cells derived from C57BL/6 × CBA F1 embryos (for ROSA26-STOP-Myd88_L252P-
21 ires-eGFP-pA) transfected with the targeting vector were screened for homologous
22 recombination. Homologous recombination at the 5' and 3' ends and single integration
23 were confirmed by Southern blot analysis. The recombinant ES cells were injected into
24 eight cell-stage Crl:ICR embryos to generate germline chimeras, and subsequent

25 chimeric breeding yielded ROSA26-STOP-Hoip-ires-eGFP-pA or ROSA26-STOP-
26 Myd88_L252P-ires-eGFP-pA transgenic mice, which were then crossed with CD19-Cre
27 mice.² Offspring were routinely genotyped by PCR with primers 5'-ACT GGA CCC AGC
28 TAC CTT GTA TG-3' and 5'-GCA ATA TGG TGG AAA ATA AC-3' for the ROSA26-
29 STOP-Hoip-ires-eGFP-pA allele, yielding a 367 bp product, and with primers 5'-GAC
30 TAT ACC AAC CCT TGC AC-3' and 5'-CCT TGC TCA CCA TGG TTG TG-3' for the
31 ROSA26-STOP-Myd88_L252P-ires-eGFP-pA allele, yielding a 783 bp product.
32 Littermates were used in all subsequent experiments.

33

34 ***In vitro* B-cell culture**

35 Splenic B cells were positively selected using anti-CD19 microbeads and a MACS
36 Separation Column (Miltenyi Biotec); purity was > 90%. Purified splenic B cells were
37 cultured in Dulbecco's modified Eagle's medium (DMEM) supplemented with 10% fetal
38 bovine serum (FBS), 50 μ M 2-ME, 10 mM HEPES-KOH (pH 7.4), and
39 penicillin/streptomycin, and then stimulated with CpG-DNA (100 nM) (cat. no. tlr1-1826;
40 InvivoGen) or Pam3CSK4 (1 μ g/mL) (cat. no. tlr1-pms; InvivoGen) for the indicated
41 times. For *in vitro* labeling, cells were incubated at 37°C for 10 minutes in RPMI1640
42 medium containing 5 μ M Cell Trace Violet (Life Technologies), and then washed with
43 RPMI medium containing 10% FBS. Labeled cells were cultured and exposed to various
44 stimuli. After 72 hours, cell proliferation was measured by flow cytometry.

45

46 **Establishment of the HM876 cell line**

47 Lymphoma cells derived from the peritoneal cavity (T876) were seeded on 10 cm dishes
48 in DMEM supplemented with 10% FBS, 50 μ M 2-ME, 10 mM HEPES-KOH (pH 7.4),

49 and penicillin/streptomycin, and then incubated at 37°C in 5% CO₂. The medium was
50 changed every 3–4 days. Continuously growing cell cultures were further passaged;
51 frozen samples were prepared regularly from low passages.

52

53 **Cell lines**

54 HOIP KO Jurkat cells were established in our laboratory.³ HBL1, OYB, DLBCL2,
55 SUDHL2, KIS1,⁴⁻⁶ DLBCL1, FL518, and Jurkat cells were cultured at 37°C in humidified
56 air containing 5% CO₂ in RPMI medium (SIGMA) containing 10% FBS, 100 U/mL
57 penicillin G, and 100 µg/mL streptomycin. OCI-Ly7⁷ cells were cultured at 37°C in
58 humidified air containing 5% CO₂ in Iscove's modified Dulbecco's medium (SIGMA)
59 containing 10% FBS, 100 U/mL penicillin G, and 100 µg/mL streptomycin.

60

61 **Lentiviral transduction of HBL1 and Jurkat cells**

62 Lentiviral transduction of HBL1 and Jurkat cells were performed as described
63 previously.⁸ Wild-type human *HOIP* cDNA was ligated into pCSII-EF-MCS-IRES2-
64 Venus. The resultant plasmid was transfected into HEK293T cells along with pCMV-
65 VSV-G-RSV-Rev and pMDLg/pRRE. After 12 hours, the culture medium was replaced
66 with fresh DMEM containing 10 µM forskolin and incubated for 72 hours. Lentivirus in
67 the culture supernatant was concentrated using a Lenti-X concentrator (Takara), and
68 lentiviral titer was determined by measuring Venus expression. HBL1 or Jurkat cells were
69 infected with lentivirus (multiplicity of infection = 10) in the presence of Polybrene (10
70 µg/mL). Infected Venus+ HBL1 or Jurkat cells were enriched using a FACSAria III cell
71 sorter (BD Biosciences).

72

73 **Flow cytometry analysis**

74 Single-cell suspensions prepared from various lymphoid organs were stained with
75 fluorochrome-conjugated antibodies. Flow cytometry data were acquired on a
76 FACSCanto II (BD Biosciences), and the results were analyzed using the FlowJo software
77 (Tree Star, Inc.). Antibodies used for analysis are listed below.

78

79

80 **BrdU proliferation assay**

81 BrdU was administered intraperitoneally to animals at 50 mg/kg, 1.5 hours prior to
82 euthanasia. Splenocytes were stained with FxCycle Violet (Thermo Fisher) and
83 fluorochrome-conjugated antibodies against BrdU (clone 3DE, cat. no. 364104;
84 BioLegend), and then analyzed by FACSCanto II.

85

86 **Antibodies**

87 The following antibodies were used for flow cytometry analysis:

88 Biotinylated-anti-IgM (cat. no. 115-067-020; Jackson ImmunoResearch Laboratories),
89 biotinylated-anti-CD21 (clone 7E9, cat. no. 123405; BioLegend), biotinylated-anti-Igk
90 (clone RMK-12, cat. no. 407203; BioLegend), streptavidin-APC (cat. no. 17-4317-82;
91 eBioscience), streptavidin-PerCP (cat. no. 405213; BioLegend), PE-Cy7-anti-CD19
92 (clone 6D5, cat. no. 115520; BioLegend), PerCP-anti-B220 (clone RA3-6B2, cat. no.
93 103234 or 103224; BioLegend), PE-anti-IgD (clone 11-26, cat. no. 12-5993-81;
94 eBioscience), APC-anti-Ig λ (clone RML-42, cat. no. 407306; BioLegend), BV421-anti-
95 CD5 (clone 53-7.3, cat. no. 562739; BD Biosciences), PE-anti-CD23 (clone B3B4, cat.
96 no. 12-0232-82; eBioscience), PE-Cy7-anti-CD38 (clone 90, cat. no. 102718;
97 BioLegend), and PE-anti-CD138 (clone 281-2, cat. no. 553714; BD Biosciences).

98 The following antibodies were used for immunoblot analysis:

99 anti-mouse HOIP,⁹ anti-human HOIP,¹⁰ anti-HOIL-1L (clone 2E2, cat. no. MABC576;
100 Merck Millipore), anti-SHARPIN (cat. no. ABF128; Merck Millipore), anti-MYD88 (cat.
101 no. 4283; Cell Signaling Technology), anti-phospho-I κ B α (cat. no. 9246; Cell Signaling
102 Technology), anti-I κ B α (cat. no. 4812; Cell Signaling Technology), anti-caspase-3 (cat.
103 no. 9662; Cell Signaling Technology), anti-ubiquitin (clone P4D1, cat. no. sc-8017; Santa
104 Cruz Biotechnology), anti-K48 polyubiquitin (clone Apu2, cat. no. 05-1307; Merck
105 Millipore), anti-K63 polyubiquitin (clone Apu3, cat. no. 05-1308; Merck Millipore),
106 anti-linear polyubiquitin (LUB9),¹¹ anti-linear polyubiquitin (clone 1E3, cat. no.
107 MABS199; Merck Millipore), anti-phospho-NF- κ B p65 (cat. no. 3033; Cell Signaling
108 Technology), anti-NF- κ B p65 (cat. no. sc-109; Santa Cruz Biotechnology), anti- β -actin
109 (cat. no. A5316; Sigma-Aldrich), anti-NEMO (cat. no. KO159-3; MBL), anti- β -tubulin
110 (cat. no. CLT9002; CEDARLANE), and anti-HA (clone Tana2, cat. no. M180-3; MBL).

111 The following antibodies were used for immunohistochemical staining:

112 Anti-Irf4 (cat. no. 11247-2-AP; Proteintech), and anti-Bcl6 (clone D-8, cat. no. sc-7388;
113 Santa Cruz Biotechnology).

114

115 **Histology**

116 Tissues were fixed with 4% paraformaldehyde, followed by paraffin embedding. Sections
117 were prepared and stained with hematoxylin and eosin (H&E) and antibodies against Irf4,
118 and Bcl6, as described previously.¹²

119

120 **Molecular analysis of tumor clonality**

121 Clonally rearranged V(D)J sequences of immunoglobulin heavy chains were amplified

122 from genomic DNA extracted from tumor tissue by nested PCR, as previously
123 described.¹³ A total of 100 ng of genomic DNA was used as the starting template for the
124 first round of nested PCR. Initial reactions consisted of 2.5 µl of 10× *Taq* buffer (Qiagen),
125 2 mM MgCl₂, 100 nM dNTP mix, 0.5 nM VH-specific primer 1, 0.5 nM JH universal
126 primer¹³ (supplementary Table 10), 1.25 U of *Taq* DNA polymerase (Qiagen), 5 µl of 5×
127 Q-solution (Qiagen), and H₂O to a total volume of 25 µl. Thermal cycler conditions were
128 as follows: 5 minutes at 96°C; 30 cycles of 96°C for 30 sec, 60°C for 30 sec, and 72°C
129 for 1 minute; 5 minutes at 72°C; and 4°C hold. One microliter of the initial reaction was
130 used as the template for the second round of PCR, which was conducted as described¹³
131 except that VH-specific primer 1 was replaced by VH-specific primer 2, and one of four
132 JH-specific primers (supplementary Table 10) was used instead of the JH universal primer.
133 Thus, four independent second-round PCR amplifications, using each JH-specific primer
134 individually, were conducted to isolate V(D)J rearrangements. PCR products were
135 purified by gel purification and sequenced using the Big Dye Terminator Cycle
136 sequencing kit (Applied Biosystems). Sequence alignment was performed using
137 IgBLAST (<http://www.ncbi.nlm.nih.gov/igblast>). Primers were designed to anneal to
138 tumor-specific complement-determining region 3 (CDR3). If specific bands were
139 detected after PCR with 30 cycles, the V(D)J rearrangement was considered clonal.

140

141 **IgH somatic mutation analysis**

142 IgH-V gene rearrangements were PCR amplified using the PrimeSTAR Max DNA
143 Polymerase (Takara) and forward and reverse primers designed in the process of analysis
144 of tumor clonality described above. PCR products were purified by gel purification and
145 sequenced by the Big Dye Terminator Cycle sequencing kit (Applied Biosystems).

146 Sequence alignment was performed using IgBLAST
147 (<http://www.ncbi.nlm.nih.gov/igblast>) to determine V_HD_HJ_H usage. The sequences were
148 then aligned to their germline counterparts.

149

150 **Cell death and viability assays**

151 HBL1 cells and Jurkat cells were seeded at 5×10^4 cells per well in 24-well plates. Cells
152 were pre-incubated for a minimum of 8 hours, and then exposed to the indicated
153 concentration of cisplatin for 12, 24, or 36 hours (HBL1), or 12, 24, 48, or 72 hours
154 (Jurkat). Purified splenic B cells were seeded at 2×10^5 cells per well in 96-well plates,
155 and cultured in Dulbecco's modified Eagle's medium (DMEM) supplemented with 10%
156 fetal bovine serum (FBS), 50 μ M 2-ME, 10 mM HEPES-KOH (pH 7.4), and
157 penicillin/streptomycin, stimulated with an anti-CD40 antibody (10 μ g/ml) (HM40-3)
158 (eBioscience) for 24 hours, and then exposed to the indicated concentration of cisplatin
159 for 24 hours. Dead cells were labeled with TO-PRO-3 (Thermo Fisher), and the
160 proportion of live cells was calculated from the percentage of TO-PRO-3–negative cells,
161 as determined on a FACSCanto II.

162

163 **Quantitative RT-PCR (QPCR) analysis**

164 Total RNA was isolated using the RNeasy Micro or Mini Kit (Qiagen). DNase-treated
165 RNA (20–200 ng) was reverse-transcribed using the high-capacity RNA-to-cDNA Kit
166 (Applied Biosystems). Real-time PCR was performed using Power SYBR Green PCR
167 master mix (Applied Biosystems) on an ABI 7900 Real-time PCR system (Applied
168 Biosystems). All gene expression levels were normalized against the corresponding levels
169 of β -actin mRNA. qPCR primer sequences were shown in supplemental Table 8.

170

171 **Immunoblotting**

172 Cells were lysed in lysis buffer containing 50 mM Tris-HCl (pH 7.5), 150 mM NaCl, 1%
173 Triton X-100, 2 mM phenylmethylsulfonyl fluoride (PMSF), protease inhibitor cocktail
174 (Sigma-Aldrich), and phosphatase inhibitor cocktail (Nacalai Tesque). Lysates were
175 centrifuged at 15,000 rpm for 20 minutes at 4°C, and the supernatant was used in
176 subsequent steps. Samples were resolved by sodium dodecyl sulfate–polyacrylamide gel
177 electrophoresis (SDS-PAGE) and transferred to polyvinylidene difluoride membranes.
178 After blocking in Tris-buffered saline containing 0.1% Tween 20 and 5% (w/v) nonfat
179 dry milk, the membranes were immunoblotted with the appropriate primary antibodies,
180 followed by the corresponding secondary antibodies. The membranes were visualized by
181 enhanced chemiluminescence and analyzed on LAS3000 or LAS4000mini instrument
182 (GE Healthcare). The following antibodies were used in immunoblotting assays:

183

184 **Tandem Ubiquitin Binding Entity (TUBE) assay**

185 Halo-tagged linear ubiquitin chain specific Tandem Ubiquitin Binding Entity (M1-
186 specific TUBE) was purified as described previously.^{14,15} To measure linear
187 ubiquitination in splenic B cells or Jurkat cells, 200 µg of cell lysates were subjected to
188 incubation with 2 µg of M1-specific TUBE coupled with 20 µl of equilibrated Magne
189 Halo Tag beads (Promega) at 4°C for 4 hours in 300 µl of buffer 50 mM Tris-HCl (pH
190 7.5), 150 mM NaCl, 1% Triton X-100. The precipitates were washed three times with the
191 same buffer, boiled in sodium dodecyl sulfate sample buffer, and analyzed by
192 immunoblotting.

193

194 **Immunoprecipitation of NEMO**

195 Jurkat cells were treated with cisplatin (5 $\mu\text{g}/\text{mL}$) at 37°C for the periods indicated in
196 Figure 3J and lysed on ice for 20 minutes in lysis buffer containing 50 mM Tris-HCl (pH
197 7.5), 150 mM NaCl, 1% Triton X-100, 2 mM PMSF, protease inhibitor cocktail (Sigma-
198 Aldrich), phosphatase inhibitor cocktail (Nacalai Tesque), and 10 mM *N*-ethylmaleimide.
199 Cysteine was added to a final concentration of 15 mM to neutralize the *N*-ethylmaleimide.
200 The lysates were centrifuged at 15,000 rpm for 20 minutes at 4°C, and the supernatant
201 was used in subsequent steps. Lysates were incubated with anti-NEMO antibody (Santa
202 Cruz Biotechnology, sc-8330) for 60 minutes at 4°C, and then immobilized on rmp-
203 Protein A–Sepharose beads (GE Healthcare). The beads were washed five times with lysis
204 buffer. NEMO was eluted with sample buffer and analyzed by immunoblotting.

205

206 **Analysis of European Genome–phenome Archive and The Cancer Genome Atlas**
207 **datasets**

208 Clinical and RNA sequencing (RNA-seq) gene expression data derived from the core set
209 of 624 human DLBCL samples were obtained from EGA (dataset ID:
210 EGAD00001003600).¹⁶ Gene expression was measured in terms of fragments per
211 kilobase of exon per million fragments mapped (FPKM) and normalized using the
212 Cufflinks package (version 2.2.1). Quantile normalization was performed, and the data
213 were \log_2 normalized. The Cancer Genome Atlas (TCGA) whole exome sequencing and
214 RNA-seq data of 48 DLBCL samples (project ID: TCGA-DLBC) were obtained from the
215 Broad Institute Firehose (<http://gdac.broadinstitute.org/>).^{17,18} Mutation consequences
216 were annotated using Oncotator (version 1.8.0), and single nucleotide polymorphisms
217 (SNPs) that had minor allele frequency of 0.01 in the 1000 Genomes Phase 3 data were

218 removed.

219

220 **Defining correlated gene signatures**

221 Gene signatures were defined using a collection of widely used annotated gene set
222 databases (BioCarta, Gene Ontology). To obtain better signal-to-noise estimates, genes
223 whose expression data included FPKM value < 0.01 in any samples were excluded.

224 Subsequently, `BIOCARTA_NFKB_PATHWAY` signature, and
225 `NEGATIVE_REGULATION_OF_INTRINSIC_APOPTOTIC_SIGNALING_PATHWA`
226 `Y` signature were calculated as the geometric mean (log-average) of the expression of 22,
227 and 66, as shown in supplemental Tables 2–4. Classification of DLBCL into ABC and
228 GCB subtypes by RNA-seq were based on a previous report.¹⁶

229

230 **Survival analysis**

231 To assess the effects of *HOIP* expression on the survival of patients with DLBCL, we
232 analyzed data from two independent cohorts of DLBCL patients with available clinical
233 information and RNA-seq data on *HOIP* expression; Reddy, 2017 (n = 604),¹⁶ and
234 Schmitz, 2018 (n = 234).¹⁹ If two Kaplan-Meier curves crossed early (≤ 18 months),
235 differences between survival functions were examined by the log-rank test based on
236 observations after the crossing point. For the cohort of Reddy, 2017, we analyzed overall
237 survival following diagnosis of n = 102 patients who did not achieve complete response
238 to the initial chemotherapy, and for the cohort of Schmitz, 2018, we analyzed survival
239 after disease progression or relapse of n = 62 patients.

240

241 **B cell gene expression profiling**

242 Gene expression profiling data of flow-sorted B-cell subsets in human bone marrow was
243 obtained at the Gene Expression Omnibus at the National Center for Biotechnology
244 Information, Bethesda, USA (<https://www.ncbi.nlm.nih.gov>, GEO profiles/DATA sets)
245 (dataset ID: GSE68878),²⁰ and analyzed using the integrated GEO2R tool
246 (<https://www.ncbi.nlm.nih.gov/geo/geo2r/>).

247

248 **Preparation of purified recombinant proteins**

249 Because it was difficult to obtain a sufficient quantity of LUBAC for high-throughput
250 screening (HTS), two truncated subcomplexes of LUBAC were generated: Petit-LUBAC,
251 which consists of residues 1–191 of human HOIL-1L and residues 474–1072 of human
252 HOIP; and Petit-SHARPIN, which consists of residues 474–1072 of human HOIP (aa)
253 and residues 172–346 of human SHARPIN.^{3,10,21} Both Petit-LUBAC and Petit-SHARPIN
254 can be expressed in a bacterial expression system and purified, and both proteins exhibit
255 potent linear polyubiquitination activity. Recombinant Petit-LUBAC, Petit-SHARPIN,
256 full-LUBAC (consisting of HOIP, HOIL-1L, SHARPIN, and HOIP [aa 699–1072]), E1,
257 UbcH5c, UbcH7, and ubiquitin were prepared as described previously.^{3,10,21} Briefly, pT7-
258 7 was used to purify recombinant N-terminally FLAG-His-tagged ubiquitin, C-terminally
259 glutathione S-transferase (GST)-tagged ubiquitin, UbcH5c, and UbcH7. pET Duet1 was
260 used to purify Petit-LUBAC and Petit-SHARPIN. pVL1393 was used to purify full-
261 LUBAC. FAST Bac vector was used to purify recombinant E1.

262

263 **Compound libraries**

264 The following libraries were screened: NPDepo (19,449 compounds, RIKEN, Japan); the
265 MyriaScreen chemical library (10,000 compounds, Sigma-Aldrich, St. Louis, MO, USA);

266 LOPAC library (713 compounds, Sigma-Aldrich), the SPECS synthetic compound library
267 (10,000 compounds, Specs, Netherlands), the NAMIKI synthetic compound library (318
268 compounds, NAMIKI, Japan), and the Isolated Natural Compound Library (1280
269 compounds, AIST, Japan).

270

271 **AlphaScreen binding assay for LUBAC inhibitors**

272 To search for inhibitors of linear polyubiquitination, an AlphaScreen-based HTS system
273 was established using N-terminally FLAG-His-tagged ubiquitin (FLAG-Ub), C-
274 terminally glutathione S-transferase (GST)-tagged ubiquitin (Ub-GST), ubiquitin-
275 activating enzyme E1, UbcH7 as the E2 ubiquitin-conjugating enzyme, and Petit-
276 LUBAC or Petit-SHARPIN as the E3 ubiquitin ligase. The candidate compounds were
277 transferred to an AlphaPlate-384 (Perkin Elmer) with the following final concentrations:
278 10 µg/mL for NPDepo, 20 µM for MyriaScreen and LOPAC, 50 µM for SPECS, and 20
279 µg/mL for NAMIKI and the isolated natural compound library.

280 Ubiquitination reactions contained 100 ng of E1, 200 ng of E2/UbcH7, 1 µg of
281 E3 (Petit-LUBAC or Petit-SHARPIN), 1 µg of FLAG-Ub, 250 ng of Ub-GST, and 2 mM
282 ATP in 15 µl of buffer containing 20 mM Tris-HCl (pH 7.5), 5 mM MgCl₂, 1 mM DTT,
283 and 0.01% (v/v) Tween20. ATP was added last to minimize autocatalytic ubiquitination
284 by the ubiquitination enzymes. Reactions were allowed to proceed at 30°C for 0.5 hours
285 (Petit-LUBAC) or 2–6 hours (Petit-SHARPIN).

286 After the ubiquitination reactions, AlphaScreen Glutathione Donor Beads
287 (Perkin Elmer) and FLAG Detection Kit (Perkin Elmer) (both at a final concentration of
288 16 µg/mL for petit-LUBAC and 20 µg/mL for petit-SHARPIN) in 10 µl of 1× PBS buffer
289 containing 5 mM EDTA-4Na were added. Plates were incubated at 23°C for 1 hour, laser

290 excitations were carried out at 680 nm, and readings were performed at 520–620 nm using
291 the EnSpire Alpha plate reader (Perkin Elmer). Primary screening data from the
292 AlphaScreen HTS assays were processed as follows: (1) Z' , signal/background ratio (S/B),
293 and coefficient of variation (CV) were calculated and compared with the minimum pass
294 criteria ($Z' > 0.5$, S/B ratio > 2 , CV $< 20\%$); (2) the primary hits for the AlphaScreen
295 assays were classified as compounds that led to a decrease in the normalized assay signal:
296 $> 60\%$ (for Petit-LUBAC) or $> 70\%$ (for Petit-SHARPIN) for compounds from the
297 NPDepo library; $> 50\%$ (for Petit-LUBAC) or $> 60\%$ (for Petit-SHARPIN) for
298 compounds from the MyriaScreen library, and $> 80\%$ (for Petit-LUBAC) or $> 80\%$ (for
299 Petit-SHARPIN) for compounds from other libraries. Based on these criteria, 568 hit
300 compounds (NPDepo: 291; MyriaScreen: 223; LOPAC: 1; SPECS: 34; NAMIKI: 0;
301 isolated natural compounds: 19) were identified. These compounds were tested for false-
302 positive hits using the AlphaScreen TruHits kit (Perkin Elmer). Compounds with $IC_{50} >$
303 $20 \mu\text{M}$ were excluded. Finally, compounds that were immediately available were tested
304 for inhibition of linear ubiquitination using *in vitro* ubiquitination assay.

305

306 ***In vitro* ubiquitination assay**

307 E1 (5 $\mu\text{g}/\text{mL}$), E2/UbcH5 (10 $\mu\text{g}/\text{mL}$), each E3 (5 $\mu\text{g}/\text{mL}$ for full-LUBAC; 50 $\mu\text{g}/\text{mL}$ for
308 Parkin, Nedd4, and cIAP2; and 60 $\mu\text{g}/\text{mL}$ for HOIP [aa 699–1072]), and 250 $\mu\text{g}/\text{mL}$
309 ubiquitin (SIGMA) were incubated at 37°C for 1 hour (full-LUBAC, HOIP [aa 699–1072],
310 and cIAP2) or 3 hours (Parkin and Nedd4) in buffer containing Tris-HCl (pH 7.5) (50
311 mM for full-LUBAC, Parkin, Nedd4, and cIAP1/2; and 20 mM for HOIP [aa 699–1072]),
312 5 mM MgCl_2 , 1 mM DTT, and 2 mM ATP. Ubiquitination reaction products were probed
313 with anti-ubiquitin antibody or anti-linear polyubiquitin monoclonal antibody.

314

315 **Cell viability assay**

316 Cells were seeded in 96-well flat-bottom plates at 5×10^4 cells/mL and treated with serial
317 dilutions of the LUBAC inhibitor thiolutin or DMSO (as a solvent control). After
318 incubation for 48 hours, cell viability was determined using the Cell Counting Kit-8
319 (Dojindo Laboratories). Cell treatment and viability analyses were performed in triplicate.

320

321 **Statistical analysis**

322 Statistical analyses were performed using Prism 5 and R (<https://www.r-project.org>).
323 Statistical tests included two-tailed unpaired Student's *t*-test, one-way ANOVA with
324 Turkey's post hoc test, two-way ANOVA with Bonferroni post hoc test, the log-rank test,
325 Fisher's exact test, binomial test, and the Brunner–Munzel test. Specific tests are
326 identified in the respective figures. Differences are indicated as n.s. (not significant; $p >$
327 0.05), * $p < 0.05$, ** $p < 0.01$, or *** $p < 0.001$, unless indicated otherwise in the figures.

328

329 **References**

- 330 1. Sasaki Y, Derudder E, Hobeika E, et al. Canonical NF- κ B activity, dispensable
331 for B cell development, replaces BAFF-receptor signals and promotes B cell proliferation
332 upon activation. *Immunity*. 2006;24(6):729-739.
- 333 2. Rickert RC, Roes J, Rajewsky K. B lymphocyte-specific, Cre-mediated
334 mutagenesis in mice. *Nucleic Acids Res*. 1997;25(6):1317-1318.
- 335 3. Sakamoto H, Egashira S, Saito N, et al. Gliotoxin suppresses NF- κ B activation
336 by selectively inhibiting linear ubiquitin chain assembly complex (LUBAC). *ACS Chem*
337 *Biol*. 2015;10(3):675-681.
- 338 4. Kamesaki H, Miwa H, Ohno Y, et al. A novel B cell line established from Ki-1-
339 positive diffuse large cell lymphoma. *Jpn J Cancer Res*. 1988;79(11):1193-1200.
- 340 5. Ohno H, Furukawa T, Fukuhara S, et al. Molecular analysis of a chromosomal
341 translocation, t(9;14)(p13;q32), in a diffuse large-cell lymphoma cell line expressing the
342 Ki-1 antigen. *Proc Natl Acad Sci USA*. 1990;87(2):628-632.
- 343 6. Ohno H, Nakagawa M, Kishimori C, et al. Diffuse large B-cell lymphoma
344 carrying t(9;14)(p13;q32)/PAX5-immunoglobulin heavy chain gene is characterized by
345 nuclear positivity of MUM1 and PAX5 by immunohistochemistry. *Hematol Oncol*. 2020.
- 346 7. Mehra S, Messner H, Minden M, Chaganti RS. Molecular cytogenetic
347 characterization of non-Hodgkin lymphoma cell lines. *Genes Chromosomes Cancer*.
348 2002;33(3):225-234.
- 349 8. Sasaki K, Himeno A, Nakagawa T, Sasaki Y, Kiyonari H, Iwai K. Modulation of
350 autoimmune pathogenesis by T cell-triggered inflammatory cell death. *Nat Commun*.
351 2019;10(1):3878.
- 352 9. Tokunaga F, Sakata S, Saeki Y, et al. Involvement of linear polyubiquitylation of

- 353 NEMO in NF- κ B activation. *Nat Cell Biol.* 2009;11(2):123-132.
- 354 10. Kirisako T, Kamei K, Murata S, et al. A ubiquitin ligase complex assembles
355 linear polyubiquitin chains. *EMBO J.* 2006;25(20):4877-4887.
- 356 11. Sasaki Y, Sano S, Nakahara M, et al. Defective immune responses in mice
357 lacking LUBAC-mediated linear ubiquitination in B cells. *EMBO J.* 2013;32(18):2463-
358 2476.
- 359 12. Toda Y, Kono K, Abiru H, et al. Application of tyramide signal amplification
360 system to immunohistochemistry: a potent method to localize antigens that are not
361 detectable by ordinary method. *Pathol Int.* 1999;49(5):479-483.
- 362 13. Kline GH, Hayden TA, Riegert P. The initiation of B cell clonal expansion occurs
363 independently of pre-B cell receptor formation. *J Immunol.* 2001;167(9):5136-5142.
- 364 14. Hjerpe R, Aillet F, Lopitz-Otsoa F, Lang V, England P, Rodriguez MS. Efficient
365 protection and isolation of ubiquitylated proteins using tandem ubiquitin-binding entities.
366 *EMBO Rep.* 2009;10(11):1250-1258.
- 367 15. van Wijk SJ, Fiskin E, Dikic I. Selective monitoring of ubiquitin signals with
368 genetically encoded ubiquitin chain-specific sensors. *Nat Protoc.* 2013;8(7):1449-1458.
- 369 16. Reddy A, Zhang J, Davis NS, et al. Genetic and Functional Drivers of Diffuse
370 Large B Cell Lymphoma. *Cell.* 2017;171(2):481-494 e415.
- 371 17. Grossman RL, Heath AP, Ferretti V, et al. Toward a Shared Vision for Cancer
372 Genomic Data. *N Engl J Med.* 2016;375(12):1109-1112.
- 373 18. Lohr JG, Stojanov P, Lawrence MS, et al. Discovery and prioritization of somatic
374 mutations in diffuse large B-cell lymphoma (DLBCL) by whole-exome sequencing. *Proc*
375 *Natl Acad Sci USA.* 2012;109(10):3879-3884.
- 376 19. Schmitz R, Wright GW, Huang DW, et al. Genetics and Pathogenesis of Diffuse

377 Large B-Cell Lymphoma. *N Engl J Med*. 2018;378(15):1396-1407.

378 20. Petri A, Dybkaer K, Bogsted M, et al. Long Noncoding RNA Expression during
379 Human B-Cell Development. *PLoS One*. 2015;10(9):e0138236.

380 21. Tokunaga F, Nakagawa T, Nakahara M, et al. SHARPIN is a component of the
381 NF- κ B-activating linear ubiquitin chain assembly complex. *Nature*. 2011;471(7340):633-
382 636.

383

384

385

386

387

388

389

390

391

392

393

394

395

396

397

398

399

400

401 **Supplemental Tables**

402

403 **Supplemental Table 1.** RNA-seq data derived from EGAD00001003600

404 **Supplemental Table 2.** Source of gene sets

405 **Supplemental Table 3.** Gene of BIOCARTA_NFKB_PATHWAY and

406 NEGATIVE_REGULATION_OF_INTRINSIC_APOPTOTIC_SIGNALING_PATHWA

407 Y

408 **Supplemental Table 4.** Whole-exome sequencing data and RNA-seq data derived from

409 TCGA-DLBC

410 **Supplemental Table 5.** Murine homologue of previously reported driver genes in human

411 DLBCL

412 **Supplemental Table 6.** Murine homologue of previously known and predicted

413 hypermutated genes in human DLBCL

414 **Supplemental Table 7.** Previously reported AID target genes in mice

415 **Supplemental Table 8.** Enrichment of WRCY mutations in genes mutated in lymphomas

416 derived from transgenic mice

417 **Supplemental Table 9.** Analysis of somatic mutations in clonal IgH rearrangements of

418 DLBCL-like lymphomas derived from transgenic mice

419 **Supplemental Table 10.** Primers for testing clonality of IgH V(D)J

420 **Supplemental Table 11.** Primer sequences used for real-time PCR

421

Supplemental Table 1

LUBAC accelerates B-cell lymphomagenesis by conferring B cells resistance to genotoxic stress

T Jo et al.

Supplemental Table 1. RNA-seq data derived from EGAD00001003600

For each DLBCL patient sequenced, clinical features are shown. The “Signatures” section shows the geometric mean of the expression of genes involved in each pathway (see also supplemental Tables 2 and 3). Blank fields indicate that a measurement was not taken or was irrelevant to the patient.

Sample ID	Cell Of Origin by RNA-Seq	HOIP (RNF31) expression (log2[fpkm+1])	HOIL1L (RBCK1) expression (log2[fpkm+1])	SHARPIN expression (log2[fpkm+1])	OTULIN expression (log2[fpkm+1])	BIOCARTA_NFKB_PATHWAY	Signatures		COO
							NEGATIVE_REGULATION_OF_INTRINSIC_APOPTOTIC_SIGNALING_PATHWAY		
648	Unclassified	4.195717649	4.31519581	3.277641923	4.956514297	4.614161432		5.087244089	2
658	GCB	4.092387126	3.898355631	3.100934845	5.342089921	4.443884255		5.147378636	0
683	ABC	5.004024657	4.921808994	3.46800145	4.57766278	4.395643052		5.073229173	1
684	GCB	3.763522925	3.707060358	2.787447028	5.519449818	4.318039406		5.16707185	0
689	ABC	4.384255027	4.252816353	2.735319439	5.513209754	4.4557751		5.002923748	1
690	Unclassified	4.005425217	3.898355631	2.92274059	5.883301336	4.070451909		5.05442557	2
695	GCB	4.739987864	5.08722852	2.997202359	5.222936525	4.516688257		4.897774993	0
702	GCB	3.469948533	3.690909115	2.867809935	4.968035071	4.06139149		5.010415253	0
704	ABC	3.704276839	3.770049876	3.109557367	5.136238378	4.368531662		5.041074611	1
705	GCB	3.676195688	4.118120389	3.250321036	6.266936066	3.922399202		4.630682268	0
759	ABC	4.724882154	4.992352289	3.818200628	3.724416657	4.539771007		5.193364216	1
787	ABC	3.858287194	3.932834051	3.327465928	4.854269929	4.111559511		5.070042274	1
793	ABC	3.201302555	3.601592665	3.012642894	4.731683197	4.291487947		4.976847885	1
799	Unclassified	3.361162098	2.922018394	3.304065558	4.943040856	3.688718846		4.856810953	2
800	ABC	3.791105901	3.886273142	2.817437442	5.043681848	4.408336728		4.884653479	1
813	ABC	3.909467611	4.386568773	2.829095917	4.412480107	4.561161571		5.02626163	1
816	ABC	5.026608081	4.944309794	4.599632141	4.226338935	4.630389193		5.142343577	1
823	ABC	4.803982209	4.572335379	4.267855087	5.271658475	4.593382271		5.219421893	1
829	ABC	4.424910334	4.515693734	3.562500405	5.612903283	3.825286912		4.871292938	1
830	ABC	4.077833144	4.61063381	3.308286428	4.735105773	4.534273467		5.071999236	1
831	GCB	3.564386475	3.580399279	3.043617231	4.744531962	4.269243128		5.040704604	0
1008	GCB	3.400851219	3.475116413	2.837774914	6.061943906	4.116286614		4.989077553	0
1016	GCB	3.451793152	3.835169616	2.802980803	5.14881689	4.370900222		5.170748226	0
2043	GCB	5.052482388	4.788924404	4.212810172	5.79812658	4.276528485		4.872723623	1
2044	ABC	5.01380854	4.955677489	4.586447377	5.857875643	4.068806649		5.053505628	1
2045	GCB	4.224045569	4.820167832	3.496950094	5.203682858	4.310011749		4.853711449	0
2046	Unclassified	4.420214608	4.676476017	3.790473173	5.487265113	4.414159889		5.065319985	2
2047	GCB	4.288595033	4.546087557	3.941239784	5.984761383	4.373861161		4.801339811	0
2048	GCB	4.873401354	4.797385513	3.786090824	5.9770724	4.434605644		5.067935478	0
2057	GCB	4.781318677	5.064831481	3.808528441	5.074649601	4.535576642		5.352719476	0
2060	GCB	4.872152713	4.960800222	3.778063863	6.778105628	4.221656273		5.107111867	0
2072	Unclassified	4.840459425	5.808458312	3.838297801	5.972307807	4.57493274		4.936889033	2
2074	ABC	4.270693637	4.10831842	3.200650522	6.618631543	4.117870754		4.986115237	1
2075	GCB	4.682662876	5.482388672	5.146528312	4.330507022	4.562921307		4.921871084	0
2076	GCB	4.827167061	5.592195874	4.367302062	5.92430143	4.648262495		5.162684013	0
2078	Unclassified	4.095183016	4.786635557	3.855179987	4.137964507	4.234166871		4.947964946	2
2079	GCB	4.061624264	4.197258663	3.004287375	5.246849507	4.535740571		5.20118903	0
2080	GCB	4.360340965	4.708384743	3.772532367	4.49726199	4.348586048		5.067459855	0
2081	ABC	3.492202499	3.881289201	3.302089252	5.363927327	3.85914941		4.917344833	1
2084	GCB	3.984409398	3.445409	2.737599776	6.368712923	4.50009492		5.046654019	0
2085	ABC	3.241119	3.991879203	2.282110364	5.979924179	3.878403093		4.616291747	1
2087	ABC	4.305376149	5.165925437	3.806987067	5.020316576	4.108682704		4.921288973	1
2088	ABC	3.166365158	4.263565685	3.317701231	4.934042802	3.995994794		4.664630489	1
2089	Unclassified	4.882975353	4.70978644	3.65477259	6.094017109	5.11460595		5.112486785	2
2091	GCB	4.078604791	4.041997226	3.368602846	5.957217133	4.318144805		5.043265305	0
2092	GCB	3.73300487	3.94991838	3.052886148	5.720174737	4.11430249		5.087951525	0
2093	ABC	3.648250318	4.241074585	2.894748459	5.189012409	4.395900744		4.954370233	1
2095	Unclassified	3.630010348	3.759158788	2.905950836	5.442321234	4.052617699		5.122827141	2
2097	GCB	3.71051805	4.104241445	2.918107457	5.981880481	4.245796801		5.080369296	0
2110	GCB	4.526718447	4.648788793	3.73727173	6.274733118	4.601314054		5.082345587	0
2112	ABC	4.746083244	4.32267373	3.573756472	5.258534024	4.590030272		5.220053807	1
2115	ABC	4.511175399	4.191219895	3.724416657	6.226341193	4.074984502		4.730955257	1
2122	ABC	3.428095667	3.978185584	3.034967696	6.290208883	4.191567621		4.936708015	1
2125	GCB	4.459943869	4.579059532	3.663858652	5.630217963	4.25523799		4.779373821	0
2126	ABC	4.27162497	4.56147475	4.331152529	5.201259568	4.318184549		5.029297736	1
2127	Unclassified	4.281446986	4.413146788	4.185881167	6.061943906	4.54772804		5.060628585	2
2128	GCB	5.134316748	4.787413284	4.367617312	5.137212562	4.241101193		4.914477494	0
2130	GCB	3.639180094	3.541263026	2.781471543	6.333516965	4.337611261		5.141039346	1
2141	Unclassified	4.42624329	4.759966339	3.09888476	4.622377455	4.648903636		4.939897509	2
2142	GCB	3.592034285	3.887869226	3.086599656	5.504666836	4.386661944		5.118110493	0
2147	GCB	4.333059477	4.849936944	3.626283426	5.601994529	4.728293014		5.071908877	0
2148	ABC	3.915418308	4.286353339	3.478321834	4.911183902	4.524358298		5.193710006	1
2149	ABC	3.866406497	4.588539878	3.275347265	4.670793182	4.299921218		5.164643059	1
2150	ABC	4.732067115	4.523976149	3.408235623	4.853463978	4.514378867		4.947765012	1
2153	ABC	4.26618951	3.943379427	3.184268699	5.252376895	4.114658524		5.046788368	1
2155	ABC	3.680181959	3.458236209	2.776588845	5.193444197	4.182282928		4.968581078	1
2156	ABC	3.497912317	3.388017347	2.415514368	6.708262699	3.997463784		4.832996513	1
2160	ABC	4.591017582	4.830633415	3.689025851	4.948062995	4.107513537		5.033980494	1
2191	Unclassified	4.546087557	4.710144652	4.087308038	5.119069315	4.549134414		5.135472264	2
2192	ABC	5.090344067	5.060883367	4.217271139	4.524663199	4.838161184		5.074063813	1
2193	GCB	4.276841004	4.831415658	3.255988684	6.088820979	4.309796314		4.872515965	0
2194	ABC	4.825186019	5.178328473	3.894621858	4.277168269	4.678047718		4.95406674	1
2195	Unclassified	4.966788376	5.612220989	4.512494324	4.519804673	4.596622837		5.208835238	2
2196	GCB	4.228917949	4.439976544	3.632240913	5.962846013	4.396469309		5.157322913	0
2199	GCB	4.300540073	4.054740766	3.244079307	4.995409873	3.827119194		4.941544193	0
2204	ABC	4.388904968	4.90957799	4.34088847	4.444041841	4.500530066		5.071401301	1
2205	GCB	4.214074615	4.628765016	3.380986739	5.619738867	4.472319262		5.134225566	0
2206	ABC	4.543990739	4.921808994	3.674934739	4.848380505	4.688335684		5.14345233	1
2209	GCB	4.307667577	2.96078718	3.876574227	6.537494635	4.104039011		5.025009939	0
2210	ABC	4.844028747	4.966346952	3.967291964	4.600660539	4.650999512		5.091176828	1
2211	GCB	4.351793714	4.434324282	4.15365604	5.034785816	4.182227022		5.080235675	0
2212	ABC	3.601592665	4.140106628	3.074100116	4.430290828	4.431782405		5.171829416	1
2213	GCB	4.730560109	5.176324895	4.783652516	5.580772162	4.529873697		5.090032966	0
2214	ABC	5.011641946	5.60399668	4.688916293	4.711209707	4.718743335		5.368719608	1
2215	ABC	4.740381169	4.970979726	4.162665783	5.589501341	4.361314164		4.919285936	1
2217	GCB	3.926314422	4.773763753	2.79634776	6.399766232	4.708544342		5.220224458	0
2219	Unclassified	4.481883564	4.630148904	3.719457032	6.534006812	4.61748658		5.074449136	2
2221	ABC	5.020744672	4.781318677	3.511659678	6.858805548	4.545684875		5.038220942	1
2224	GCB	4.568564369	4.54225418	3.745430063	6.303125109	4.62258162		5.072073488	0
2225	ABC	4.217590661	3.878793581	3.214294992	6.14734604	3.958093189		5.043934754	1
2226	ABC	4.495212983	4.472020492	3.59840924	4.336094867	4.452091235		5.123426885	1
2228	Unclassified	4.432299145	4.508803493	4.031296235	4.707645174	4.555330821		5.217066281	2
2229	GCB	4.065733257	4.963352138	4.945532397	4.908744762	3.658995093		4.800840102	0
2230	ABC	4.353560909	3.91006968	2.986373447	6.166566865	4.266278155		5.039940962	1
2231	GCB	4.097077255	3.99467065						

2233	GCB	4.797749456	4.805490394	4.891732918	5.29376686	4.32054909	4.917211356	0
2234	ABC	4.299881917	4.529827542	3.346261803	5.735905743	4.458950386	5.115199154	1
2235	GCB	4.695880117	4.619838187	3.500071526	4.854669563	4.604825443	4.996400106	0
2236	GCB	4.352448081	4.560750036	3.281905125	5.879779652	4.659196065	4.949500373	0
2237	Unclassified	3.861738741	4.74532918	3.881289201	5.961954199	4.383328206	5.096239776	2
2240	ABC	4.259675445	4.495212983	3.208999113	5.093033038	4.609716431	5.13879843	1
2241	ABC	4.421570992	5.468474787	4.018850077	4.401807313	4.168252179	5.007029235	1
2242	Unclassified	4.062926116	4.460618695	3.272426428	4.79003569	4.244506095	5.121210184	2
2243	ABC	4.385240665	4.246633472	3.065844157	6.026416112	4.539529419	5.137399181	1
2244	GCB	3.926959615	3.899296346	3.333335973	6.141033021	3.733349852	4.763041098	0
2246	ABC	4.42624329	4.3613209	3.798897491	5.634383441	4.199483596	4.931686688	1
2247	ABC	4.724503586	5.36662781	4.611663466	4.583267659	4.612015524	5.092090479	1
2248	GCB	3.921632574	4.682310723	3.395774936	4.99191136	4.017229321	4.859373411	0
2249	ABC	3.986609496	4.927157955	3.88789955	5.225925908	4.332748451	4.850200794	1
2250	ABC	4.32043073	4.807769984	3.802005015	4.216954665	4.541599418	5.083001595	1
2254	ABC	3.948359469	5.22936525	4.102027307	5.394569539	4.263746043	4.837636147	1
2257	GCB	4.015714163	3.860509889	3.232840438	7.608797991	4.529536303	5.093249507	0
2260	ABC	4.816324799	4.755857673	4.063523832	5.315430426	4.512203386	4.950764482	1
2262	Unclassified	4.297602769	4.657215821	4.107070554	5.060883367	4.381890435	4.982899942	2
2263	GCB	3.674616036	3.311524663	2.399633593	6.28118692	3.803967525	4.725732894	0
2269	Unclassified	4.943862684	5.069824639	4.281766765	4.625242001	4.537403252	5.10088347	2
2270	GCB	4.477772949	4.233568898	3.323552727	5.682036326	4.554486645	4.883901162	0
2290	ABC	4.847975849	4.948475433	4.737374398	5.29642338	4.167078439	4.891417386	1
2291	GCB	4.329207482	4.379266364	3.704276839	4.948062995	4.686371233	5.115180716	0
2300	ABC	5.027601877	4.553066036	3.443230082	5.138613414	4.265664785	4.88911158	1
2306	ABC	4.474693784	5.152116827	3.948359469	4.386568773	4.175259377	4.959681343	1
2450	Unclassified	3.436196897	3.389624273	2.684927819	5.151643532	3.915450279	5.014244085	2
2451	ABC	3.141104723	4.132543674	3.392575893	6.139724179	4.081341098	5.010479382	1
2453	ABC	3.859894511	4.10831842	2.344013424	6.14734604	4.205227154	4.730411932	1
2455	GCB	3.954596248	4.09798529	2.96007024	5.789173731	4.363472807	5.073409932	0
2459	GCB	3.950550641	4.592830275	3.36667034	5.778933682	4.47897892	5.064720693	0
2462	GCB	4.103609042	4.127269914	3.773777519	4.773388491	4.292715851	4.928699478	0
2468	GCB	4.255403565	4.161072128	3.271452579	6.174502524	4.057990038	4.998495573	0
2470	GCB	4.087960412	4.164844655	3.248995462	5.711340338	4.533835567	5.107572025	0
2482	ABC	3.907629937	3.580722371	2.93922517	6.754705024	3.955001479	4.982195051	1
2483	GCB	3.556842356	3.46800145	3.298548432	7.188955957	4.200907876	5.026599532	0
2522	ABC	4.23046571	4.238137121	3.32033336	5.068935779	4.168737912	4.990536404	1
2524	ABC	5.310136401	5.020744672	4.364985179	4.780174712	4.831839415	5.265785208	1
2525	ABC	4.750219741	4.570546097	3.54157521	4.915696221	4.403980285	4.997927519	1
2530	ABC	4.353882336	4.470281656	3.639180094	6.345704514	4.21751865	4.849799356	1
2539	Unclassified	4.339948999	4.572335379	3.233170979	6.578109873	4.095717996	4.805938501	2
2542	GCB	3.694045376	3.623118569	2.800753891	6.957057741	4.312623088	5.161011443	0
2548	ABC	4.410118737	4.448051058	3.901747778	5.85368771	4.491359835	5.006372438	1
2550	Unclassified	4.272292563	4.441007421	3.032253569	5.130214609	4.907774761	5.249245232	2
2552	GCB	4.767700019	4.557240416	4.173687694	5.844423989	4.482997297	4.88376408	0
2553	GCB	4.640823224	4.637276818	3.422335004	5.664896823	4.544928507	5.106042156	0
2554	Unclassified	4.499215319	4.890912792	3.699956859	4.668589271	4.284800995	5.069204793	2
2561	GCB	5.345882506	5.264078774	4.538117881	4.739987864	4.697861857	5.018732118	0
2565	ABC	3.826528842	3.702101959	3.018878261	4.789675329	4.034089822	4.918374602	1
2566	GCB	3.996207862	3.865478171	3.208672052	4.982108115	4.229966694	5.017835297	0
2570	GCB	4.049459489	4.175586116	3.391278674	5.236358749	3.621608409	4.692582336	0
2571	GCB	4.853063362	4.404150507	4.009179685	5.36662781	4.669240779	5.117507919	0
2573	GCB	4.495212983	4.526036148	3.76257925	5.336790202	4.726315423	5.077628691	0
2575	Unclassified	4.582913886	5.240805823	3.639796623	5.891902988	4.61189039	5.175383322	2
2576	GCB	3.859591281	3.713946377	3.37223222	5.709900189	4.0731452	5.06457089	0
2577	ABC	4.584675947	3.360522849	3.21826972	4.715313905	3.775410194	4.66196419	1
2578	GCB	3.665094535	3.924459994	3.232840438	5.210082552	4.463605658	4.997443692	0
2585	Unclassified	3.835473547	4.303481151	3.325829649	4.872950431	4.377987227	5.074224111	2
2588	ABC	4.316490495	4.42624329	3.08961835	5.33248901	4.932702307	5.304418166	1
2591	ABC	4.03263517	3.86912421	2.660019801	4.524311436	4.244312985	4.910272574	1
2596	GCB	4.473338663	4.386897921	3.423897497	5.578762961	4.565504241	4.885731786	0
2597	GCB	4.12505771	4.480497589	3.034628096	5.426980075	4.235017375	4.929426752	0
2603	GCB	4.284392679	4.519464395	2.952361824	5.088561668	4.662494606	5.212586993	0
2605	GCB	4.083585116	3.878163699	2.81223166	4.53081904	3.959654106	4.958501156	0
2606	GCB	3.76879898	4.185881167	4.003259703	5.373251875	3.992158059	5.053078018	0
2608	GCB	4.380290108	4.487645868	3.468980479	6.269496395	4.344240231	4.879640233	0
2612	ABC	4.525023111	4.559681811	3.886273142	5.109397972	3.916129617	4.817854407	1
2613	GCB	4.072685155	3.917615953	3.428095667	5.662826564	4.251358656	4.726860026	0
2616	GCB	4.184932762	4.107070554	3.1092161	7.138441122	3.95385876	4.885723721	0
2617	GCB	3.584477801	4.151027281	3.137344028	5.421830343	3.792747332	4.841999295	0
2619	Unclassified	4.05834683	4.4455061	3.093403116	5.187592172	4.471218712	5.214959375	2
2620	ABC	3.932211743	3.927574232	3.271452579	6.686977493	4.374854543	5.059847806	1
2622	ABC	3.826528842	3.940301717	3.18629839	4.919756559	3.993889557	5.055249624	1
2624	ABC	3.894915441	4.231773274	2.776188177	5.073326746	4.589015711	5.025212837	1
2626	GCB	4.142749613	3.99373492	3.333980842	5.093033038	4.087985976	4.69761716	0
2628	GCB	4.438967912	4.601029431	3.188334464	5.267601292	4.570427438	5.204097108	0
2629	ABC	4.782903672	4.953166703	3.961612292	4.653177993	4.497086677	5.249113673	1
2634	ABC	4.360676556	4.255403565	3.584477801	6.46353184	4.297428818	5.171726484	1
2635	ABC	4.094874504	4.187109072	3.760077584	5.07868456	4.576377703	5.101595412	1
2636	GCB	3.83302953	3.854223094	3.089966597	5.821580526	3.568389287	4.584002217	0
2637	GCB	3.573756472	3.626587094	2.837427849	5.464367234	4.093449468	4.980457264	0
2640	GCB	3.9496117276	3.837361041	3.04669545	6.253287137	4.355974519	4.85422393	0
2642	ABC	3.915721142	3.744820972	2.893007219	6.269496395	4.405231754	5.226098065	1
2643	ABC	4.442021426	4.383607434	3.980375842	5.262038314	4.660321346	5.326293448	1
2644	ABC	3.965754492	3.93346037	3.207284076	6.542518914	4.203372408	4.93365867	1
2646	ABC	4.562161254	4.28078678	3.59297822	3.721638814	4.275547143	4.891313956	1
2647	ABC	4.324348185	4.429950454	3.451175954	5.288644512	4.311376912	5.258179522	1
2649	ABC	4.03658651	4.150407845	3.275347265	5.20067712	4.080777066	4.95622579	1
2650	GCB	4.112097007	4.194748863	3.405342108	5.841993034	4.356871566	4.851352641	0
2651	ABC	4.127585537	4.115231431	2.992981109	4.542950891	4.472628028	4.876462286	1
2652	ABC	3.853386653	3.622126617	2.727156786	5.214510166	4.265193297	4.932932141	1
2654	GCB	4.491440451	4.473014939	3.91006968	5.318655647	4.201254178	4.725711334	0
2655	Unclassified	4.472348992	4.569126211	3.698402993	4.853063362	4.479436227	5.053978913	2
2656	GCB	3.896140594	4.24010624	3.284842542	5.543206451	4.28421263	5.036575522	0
2657	Unclassified	5.251856356	5.629504997	4.440634091	4.287649687	4.828531299	5.115210775	2
2659	ABC	5.237747966	5.55724939	5.457175008	5.258534024	4.272677706	4.793121211	1
2660	Unclassified	3.713340749	4.055683109	2.757139482	6.647759598	3.879509809	4.731421431	2
2663	ABC	4.812076687	5.387235672	3.979109776	4.659377602	4.593369804	5.158640582	1
2664	GCB	4.129426101	4.149132732	3.101269293	4.730914219	4.328940218	4.85598851	0
2666	ABC	4.589927565	5.126948276	3.127958372	4.642617261	4.443737203	4.949084197	0
2669	GCB	4.237190726	4.86330649	3.322247291	5.403480661	4.011213157	4.658100021	1
2673	Unclassified	4.10265711	4.45752803	3.05353141	5.016			

2700	GCB	4.173030209	4.60426055	3.390298664	5.236814179	4.123270135	5.015453063	0
2704	GCB	4.217271139	4.692228219	3.808229302	5.495729176	4.73919898	4.811749785	0
2706	ABC	4.796201458	4.882596377	3.126291356	4.684862928	4.637278411	5.163527109	1
2707	ABC	4.032837193	4.344513599	3.656894654	5.075083879	4.108569282	4.952877638	1
2709	GCB	3.65817677	4.059148876	2.795252025	5.100246511	4.206274753	4.81160591	0
2713	Unclassified	3.647035161	3.826237925	3.184680602	5.181657639	4.475981713	5.048122869	2
2714	GCB	4.184285114	4.684862928	2.784122944	4.096458697	4.133438295	4.824702404	0
2715	GCB	4.608842672	4.727511171	4.254005415	4.344829498	4.122294593	4.974592607	0
2716	ABC	4.448051058	4.187760465	3.77712123	5.068048893	4.317136889	5.076353994	1
2718	Unclassified	3.699596859	4.630148904	3.679271319	5.198290333	4.35125788	5.051039333	2
2719	Unclassified	4.436980882	4.543647286	3.45240714	5.019456253	4.57610806	5.085755624	2
2720	ABC	4.286018138	4.472020492	3.645147684	4.122518832	4.140515246	4.893256125	1
2725	ABC	4.346128008	4.286018138	3.609702513	4.88495832	4.718535557	5.108411832	1
2727	ABC	4.46331344	4.994977817	4.286353339	2.950596804	4.575450747	4.917082024	1
2728	ABC	4.914046459	4.890115373	5.096614107	3.68239435	4.601857429	5.003590851	1
2758	ABC	4.701370518	4.813571217	3.471884575	4.958236452	4.8461332	5.212481558	1
2764	Unclassified	4.352124869	4.769197283	3.965471326	5.184088352	4.443719893	4.963880646	2
2765	ABC	5.104798027	5.470250119	3.87165041	4.855054459	4.928009547	5.096181213	1
2767	ABC	3.89002531	3.916340598	2.965039591	5.067101503	4.431322582	5.136161444	1
2769	GCB	4.213763434	4.411143333	3.331376875	5.483662184	4.294564975	5.04329984	0
2772	GCB	4.200443992	4.432983094	3.185291291	5.646881385	4.549883901	5.129743752	0
2773	ABC	4.647006128	4.741487479	3.671535173	5.115880945	4.631548873	5.217823287	1
2776	GCB	3.736763469	4.705114147	3.820386739	5.83955891	4.568724323	5.075368349	0
2777	ABC	3.679563997	3.850787639	2.970654486	4.934456122	4.182089962	5.087493547	1
2778	Unclassified	3.810985753	3.463230667	3.194015138	5.069382274	4.144372989	5.159628546	2
2779	GCB	3.914127572	3.905779982	2.940271855	6.345704514	4.278047576	4.958219729	0
2781	GCB	3.789198933	3.885335511	3.070646145	5.621825046	4.474948134	5.140632061	0
2783	GCB	3.607241114	3.663858652	2.852808201	5.442321234	4.276140677	5.070352332	0
2784	ABC	3.725036151	3.758828495	2.607070063	5.21303896	4.35154381	5.189464436	1
2785	GCB	3.786748266	4.070768888	3.215898848	5.290173928	4.586375886	5.09506872	0
2786	GCB	3.834874084	3.626587094	3.085246456	6.079532148	3.93879525	4.859754565	0
2788	GCB	3.580399279	3.848946683	2.791875708	4.943862684	3.847277812	4.758097053	0
2789	GCB	3.630010348	3.611273592	3.193699789	6.784643028	4.096828658	5.194081989	0
2790	Unclassified	3.825942725	3.852687348	3.070646145	5.508910326	4.141759173	4.954186956	2
2791	Unclassified	3.556842356	4.016954388	2.971349062	5.442943113	4.412696743	5.050136384	2
2792	ABC	3.554006759	3.843627299	2.854987351	5.865360993	4.088893444	4.745798843	1
2805	GCB	4.574515048	4.80971274	3.481139783	6.166566865	4.702507229	5.201473858	0
2808	ABC	4.543647286	3.941533872	3.676195688	5.31598178	4.571226723	5.346605015	1
2809	GCB	4.237498759	4.580081477	3.647035161	5.1793391	4.408875332	4.926086929	0
2810	ABC	4.01836535	4.005425217	3.216563999	5.447710452	4.729238813	5.444016809	1
2812	ABC	4.26685871	4.667470936	3.91866244	4.289852242	4.436054021	5.275443334	1
2813	GCB	4.183657443	4.590656014	3.52290036	4.75623522	4.38386191	5.026222401	0
2815	ABC	5.220060591	5.151643532	4.122830169	4.587517793	4.279771551	5.124796401	1
2816	GCB	4.355720214	4.238477166	3.159690651	5.809296151	4.283836314	5.083413914	0
2819	ABC	4.553409539	4.696090751	3.686769674	5.835473044	4.26907674	4.836401099	1
2820	GCB	3.830800205	4.034693908	3.499422158	4.639423582	4.568343502	5.283857694	0
2821	GCB	4.505335156	4.610263504	3.381641517	7.278299999	4.239485429	4.92941001	0
2823	GCB	4.083893278	4.024182469	3.628457424	4.908744762	4.044103582	4.973550842	0
2824	ABC	3.46198982	3.461679133	2.78454078	6.181441238	4.207248953	4.949850193	1
2826	GCB	3.868835672	4.504651171	3.494715923	5.124096809	4.323147093	5.158572642	0
2827	GCB	4.121542538	3.934718254	3.2659476	6.666336858	4.056454974	5.048433338	0
2828	GCB	3.498224484	3.295585661	2.773987205	7.820994105	4.212264806	5.157229165	0
2829	GCB	3.393207942	3.765752537	3.529204589	5.040996446	4.21422112	4.783675828	0
2830	ABC	3.903587298	3.76319231	3.199630596	5.349088148	3.928132973	5.22437973	1
2832	GCB	3.729020906	4.508442193	4.196037818	5.280489858	3.655795362	4.671477887	0
2834	GCB	3.412432547	3.086274019	2.862662952	5.83955891	4.140798213	4.973455172	0
2837	GCB	3.619391109	4.299546827	2.719248993	5.280489858	4.234968121	4.941856678	0
2838	Unclassified	3.863631065	3.84767831	3.193017039	6.624010061	4.267274876	5.125576829	2
2839	GCB	4.265863038	4.000473372	3.580099261	5.694569573	4.138057124	4.996262472	0
2840	GCB	4.806629875	4.868126768	4.08986884	5.635769495	4.097827626	4.874414909	0
2841	ABC	3.994348602	4.041374823	3.34079103	6.845197276	4.391644225	5.076184829	1
2843	ABC	5.110306064	5.691654866	4.414473316	3.945524063	4.753413905	5.112620445	1
2844	GCB	3.87535347	3.948054353	3.470602313	5.08051101	4.061162183	4.864242766	0
2865	ABC	4.866196729	4.1670629	3.388971631	4.788924404	3.914631163	4.851410016	1
2867	ABC	3.763522925	4.064812344	2.135852408	5.906659388	4.162542657	4.815176734	1
2871	ABC	4.440285627	4.59028635	3.455018008	5.199287902	4.263781276	5.088837297	1
2872	GCB	3.902673886	4.181078602	2.953808165	6.297962991	4.052358509	4.968956595	0
2873	GCB	4.220210132	4.353721074	3.385451137	7.10808287	4.442299473	5.132870089	0
2874	GCB	3.580722371	3.88221866	2.450810539	6.985234214	4.279188885	4.991486113	0
2878	Unclassified	4.452479576	4.641925358	2.721886574	5.05694752	4.429857862	4.888160219	2
2879	ABC	4.174312428	3.66859351	3.122486312	5.92702648	3.960310047	5.068775793	1
2881	Unclassified	4.294004686	4.691109655	3.394192518	5.324966264	4.807746972	5.199756187	2
2882	GCB	4.757362356	4.919353728	4.496557103	4.742253046	4.662622929	4.969557604	0
2884	Unclassified	4.211495213	4.179141694	2.670398365	5.601994529	4.435952599	5.052438509	2
2886	Unclassified	4.332092096	4.470947869	3.367628666	4.844787768	4.45599857	4.921774922	2
2887	GCB	3.82069345	4.185573589	2.991258641	6.166566865	4.460373196	5.121949478	0
2888	ABC	3.854223094	3.940012548	3.008816949	4.999227495	4.091927289	4.93127926	1
2889	GCB	4.146896137	3.625980599	3.268845905	6.218114333	4.412122033	4.983883133	0
2891	GCB	3.808849928	4.338312113	3.437794367	4.061940677	3.831094074	4.978544288	0
2892	GCB	3.606908648	3.836080488	2.782602337	5.781311413	4.277755587	5.124624264	0
2893	ABC	4.587149392	5.074649601	3.683025761	4.606023766	4.864595328	5.136305645	1
2894	Unclassified	4.522219662	4.440634091	4.300215357	4.31519581	4.403417007	5.040798219	2
2897	ABC	4.741876729	4.830259428	3.661027323	4.260320214	4.084438158	4.95479104	1
2898	GCB	4.769591208	4.957811864	4.140751066	5.61702708	4.176588672	5.177315754	0
2899	GCB	4.172082344	4.655736085	3.232840438	5.610877469	3.944513048	4.678363716	0
2900	GCB	3.597739578	3.868529645	3.810985753	4.450930171	4.276624035	5.183016198	0
2901	GCB	3.620017863	3.730877225	2.903720881	5.300735832	4.286409972	5.168737091	0
2902	GCB	4.113057101	4.415843783	2.882954916	6.055816807	4.508435979	5.02948521	0
2903	GCB	3.880352322	3.791410678	3.014078895	6.724341263	4.359476054	5.232699977	0
2905	GCB	3.831109584	3.840190791	2.932811629	5.626687399	4.065407147	5.052840234	0
2908	ABC	3.870881462	4.350141244	2.910296462	4.606707554	4.204848622	5.22942688	1
2909	GCB	3.971034898	3.456630409	3.167384831	4.629795312	6.30670824	4.758333356	0
2910	ABC	4.166413271	4.450068743	3.926652575	3.354613712	4.005058012	5.076286365	1
2912	Unclassified	4.306354782	4.380290108	2.834900838	6.77377967	4.416718064	4.777866656	2
2917	GCB	3.809448591	3.99589791	3.41940637	6.014555076	4.429841665	4.835733648	0
2918	GCB	3.811938078	3.703347773	2.389958521	7.799159108	4.191332491	4.847472536	0
2919	ABC	4.437627931	4.896193418	3.385131515	4.629410416	4.446937299	5.130967912	1
2921	ABC	3.87476195	4.286994399	2.818499965	5.727642891	3.864982906	4.764772934	1
2923	GCB	2.849519808	3.759158788	2.400457423	7.441563828	3.935046493	4.693819804	0
2925	GCB	4.012611144	4.144989189	3.677133617	6.256938886	3.884085639	4.490406882	0
2928	Unclassified	3.581995807	2.615537952	1.960442532	8.739285354	3.87788538	4.711180044	2
2933	Unclassified	3.734226906	4.002638639	2.8385031				

2955	GCB	4.129426101	4.075799952	3.055946345	6.208579348	4.46662402	4.808066145	0
2957	ABC	3.710829151	3.810052342	3.018548404	6.702547936	4.112000115	4.92749636	2
2958	Unclassified	3.64386691	4.04386691	2.404232902	6.718047674	4.318083515	4.782261992	2
3382	GCB	5.137212562	5.390663574	4.487645868	5.050720262	4.708541737	4.989704677	0
3385	GCB	4.90064288	5.012063323	3.758185629	6.07114394	4.591259371	5.29692922	0
3386	GCB	4.864577209	4.754732735	3.864553187	5.246328316	4.432372782	5.144840863	0
3389	Unclassified	4.9291883	5.179787106	4.186205114	4.393874789	4.803241712	5.161238601	2
3401	GCB	3.73362622	3.713340749	2.714384415	6.902765321	4.293242741	5.172800778	0
3403	ABC	3.590409022	3.796076056	2.298416314	6.077406262	4.321428312	4.867557389	1
3405	ABC	3.650374627	3.81378489	2.193556971	6.041534212	4.338782973	4.782111836	1
3408	ABC	3.463869502	3.458558877	2.971010355	5.860381006	3.927056302	5.107689493	1
3409	ABC	3.620925411	3.858625873	2.971058752	6.005695038	4.094760128	5.133564558	1
3411	ABC	4.053797722	4.082960191	2.995764105	5.50251791	4.366731705	5.042488574	1
3412	ABC	3.526976597	3.892796704	2.7105985	5.590841803	4.130730367	4.737312016	1
3418	ABC	3.599336675	4.36796053	3.194363254	5.869634311	4.462467935	4.847931505	1
3429	ABC	4.783652516	5.598728077	4.156123287	4.568049864	4.719459366	4.867399951	1
3430	ABC	3.861413096	4.272594521	2.845127234	4.510851983	4.173446312	5.286471158	1
3431	Unclassified	3.45051168	4.555510184	2.916019072	5.486669865	4.16339589	4.94186842	2
3433	ABC	3.993116034	4.155455014	2.353036655	5.726146226	4.342652796	4.972815946	1
3434	ABC	4.651720653	4.629103407	3.742939065	5.007894342	4.699757709	5.112763061	1
3439	ABC	3.666025744	3.970482828	3.554638224	6.454339832	4.214171852	4.87879305	1
3441	GCB	3.66936622	3.770049876	3.270476637	6.341815389	3.82362416	4.484776004	1
3444	Unclassified	4.100185579	3.816614494	2.830918682	6.103479096	4.26924325	4.877719018	2
3446	ABC	4.37706678	4.670061646	3.227897666	5.159725398	4.782526087	5.092090243	1
3447	ABC	4.732626451	4.718645477	2.735703631	6.072244848	4.290677059	5.113378227	1
3448	GCB	3.925065823	4.403483807	3.224907973	6.53074537	4.095650254	4.905672791	1
3449	GCB	3.824121332	3.644497828	2.602339189	6.022401123	4.437397788	4.896658625	0
3450	GCB	4.156123287	3.774083549	3.853924063	6.265699829	4.216316283	4.969397868	0
3451	GCB	4.483940905	5.144636949	3.187984644	5.178819993	4.613688936	5.003015227	0
3453	GCB	3.971342103	4.005425217	3.381641517	5.3448239	4.231475763	5.132583665	0
3454	Unclassified	4.418878002	4.538804806	3.703964889	5.439396047	4.622836041	5.170749452	2
3455	GCB	3.61189572	3.84951635	2.642747023	5.52552632	4.308739617	4.932994264	0
3456	ABC	3.987849552	4.261911765	3.028403338	4.704380419	4.574115586	5.028975645	1
3458	Unclassified	4.274183529	4.930392193	3.329099977	4.593529249	4.281128622	4.763076768	2
3459	ABC	3.565986318	3.979437301	2.920602405	5.072027153	4.439913642	5.06904499	1
3460	GCB	4.74532918	5.369850878	3.918515892	4.886898666	4.700743685	5.098158331	0
3461	ABC	4.359667319	4.524663199	2.987063877	5.190004701	4.259101304	5.250634637	1
3462	ABC	4.003877184	3.828644494	2.819253874	5.696777552	4.1474596	5.042459396	1
3463	GCB	4.547834902	4.35084306	3.417006922	5.708427218	4.401793502	5.121865886	0
3464	ABC	3.89803618	4.162044136	3.208338506	5.535005702	4.310870688	5.064736477	1
3465	ABC	4.710535871	4.657558505	3.623767439	4.913643764	4.372728273	5.072316639	1
3467	ABC	3.8918696	3.786090824	3.283209965	4.951057289	4.374205946	5.117464187	1
3470	GCB	3.890932316	4.048134905	5.804512313	4.557240416	2.912500368	4.583188253	0
3471	GCB	3.871982483	4.328220111	2.948449466	6.501090347	4.268420888	5.081758687	0
3472	Unclassified	3.924142706	4.111169776	3.126291356	5.450136015	4.051636662	5.037186077	2
3473	Unclassified	3.833616564	4.451443784	2.719248993	4.767303201	4.128324879	4.983106935	2
3474	GCB	4.14369488	4.118120389	3.376819482	6.121005661	4.159785022	4.979872693	0
3475	GCB	3.474785388	4.174008216	2.617113107	6.649631358	4.327701017	4.942485686	0
3476	ABC	3.817244386	4.140106628	2.968567855	4.710892749	3.950626579	4.820279201	1
3477	ABC	4.244689452	4.403483807	3.812855215	5.340550543	4.124397623	5.013811832	1
3478	Unclassified	4.716430268	4.253772057	3.638215463	4.05038546	4.246799549	5.012746907	2
3479	ABC	5.046732035	5.103910837	4.125385083	4.803566925	4.613727066	5.084203193	1
3480	Unclassified	3.807919038	4.011974612	2.192745968	5.508910326	3.615510667	4.535654398	2
3481	GCB	4.337404049	4.055363121	3.70147817	6.85644748	4.406096034	5.080166798	0
3482	GCB	3.939689918	4.157692111	3.046351577	5.3962205	4.051297764	5.073919675	0
3483	ABC	3.223927784	3.36667034	2.740961118	5.61553667	4.105680022	4.919354311	1
3484	GCB	3.823796829	3.467682669	3.072718452	5.745772594	4.500298257	5.072847058	0
3485	GCB	3.744165086	3.805078714	3.516057094	4.385630018	4.359142614	4.873666573	0
3487	ABC	3.543406	3.647035161	2.753038377	5.497645735	4.317386489	5.174049829	1
3488	GCB	3.619079288	3.951754735	2.873677673	7.505795169	4.246407562	4.930252654	0
3490	ABC	4.651720653	4.477263675	2.815936064	5.755734665	4.556139118	4.8316246	1
3493	ABC	3.722840495	3.968193564	2.856427853	6.197743379	4.354770493	4.808249226	1
3502	ABC	4.288892285	4.419214644	3.090641705	5.22493451	4.127413131	4.925039587	1
3504	Unclassified	4.490745002	5.064831481	3.636976148	4.969316299	4.697142113	5.30498669	2
3505	GCB	3.609702513	4.518770517	3.831109584	5.499442861	4.281551651	4.96097483	0
3506	GCB	4.193153799	3.911003804	3.574069835	6.365957209	4.344614102	5.136146315	0
3507	Unclassified	3.866700266	4.161407855	2.948780311	5.1116346527	4.577554739	5.144704098	2
3508	GCB	4.283744788	4.610263504	3.158354085	4.989365561	4.654733215	5.126223974	1
3546	ABC	3.775266522	3.641068725	2.605910842	5.801355267	4.037703465	5.126500197	1
3547	Unclassified	3.488059159	4.659007886	3.864553187	6.523973511	4.482453586	5.253405593	2
3549	GCB	5.115431386	5.520674266	4.489721533	4.488007045	4.447587599	4.992004384	0
3551	ABC	4.934456122	5.111233345	3.935643677	4.46393826	4.389116416	5.159415946	1
3552	ABC	5.007034687	4.754016844	4.420575208	5.146528312	4.235626834	5.095060538	1
3555	GCB	4.450068743	4.861010613	4.129740625	5.303409667	4.688390097	5.112281096	0
3557	ABC	5.101624293	5.033416951	4.061024066	4.56387274	4.785874207	5.135494672	1
3558	Unclassified	4.742253046	5.46018186	4.211495213	4.130370811	4.288461732	5.058670582	2
3559	ABC	4.182720561	4.03376207	2.773987205	5.790818549	4.179094861	5.103447907	1
3560	GCB	4.167379984	3.854536547	3.12013044	5.060883367	3.941434098	4.828632541	0
3562	ABC	4.100500098	4.420575208	3.534153126	5.076434877	4.404414373	4.913424976	1
3563	GCB	4.093627491	4.107991027	3.61000203	6.049688427	3.880017558	4.941580766	0
3565	ABC	4.154507392	4.732435693	3.222573676	5.474505631	4.365609233	5.217667162	1
3566	ABC	4.284723763	4.677093204	3.165337913	6.52565858	4.187531045	5.066706035	1
3579	ABC	4.028818423	3.927880798	3.189691614	7.692314593	4.01751546	4.869958833	1
3582	Unclassified	3.674934739	4.534976706	3.830800205	4.782711506	4.205147594	5.044831306	2
3584	ABC	4.706909218	4.975661393	3.566594589	6.912531757	4.06698144	4.756531471	1
3585	Unclassified	4.362641037	4.876105709	3.315137065	5.780514788	4.733791983	5.144164202	1
3586	GCB	4.202991956	3.759158788	2.740243797	6.189572689	3.767071943	4.658230785	0
3587	GCB	4.10929049	3.965754492	3.818823995	6.422759383	3.955972331	4.67229631	0
3590	ABC	4.956514297	5.070281423	4.168463507	5.310681259	4.515721773	5.144771288	1
3592	Unclassified	4.55377314	4.994563602	3.451175954	5.132436955	4.704322689	5.256869377	2
3593	GCB	4.126340411	5.284541479	3.24242602	6.399766232	4.459513591	5.32711801	0
3595	GCB	4.364643755	4.821283125	3.595491383	5.362795793	3.662205556	4.428743284	0
3596	ABC	4.330822809	4.588202919	3.079513439	6.297962991	4.48080494	5.089527227	1
3598	ABC	4.208666617	4.391189601	3.712065162	5.220066591	4.007830721	5.042411547	1
3600	GCB	3.823184361	3.672769807	3.439701009	7.517973759	3.899447531	4.737917991	0
3601	ABC	3.576659141	3.782646355	2.767215252	5.472127652	3.957318607	5.145754383	1
3602	ABC	4.31354537	4.346784075	3.133660471	5.894467655	4.232638098	5.034838766	1
3604	GCB	4.031296235	4.087960412	2.919194875	6.330817702	4.465982048	4.83691299	0
3606	ABC	5.005731448	5.145832045	3.524472091	5.4666727147	4.748915122	4.796206997	1
3608	GCB	3.935360329	3.703036298	2.824706637	7.965879314	4.44837126	5.081665814	0
3609	GCB	3.497587972	3.628778677	2.562049234	7.18235241	4.126533342	4.933714245	0
3611	Unclassified	4.968878364	5.283554367	3.85896				

3637	ABC	3.981606276	3.672158845	3.237761613	6.640401743	4.267996791	5.070263971	1
3638	ABC	3.811299561	4.169547352	3.466727852	5.29852904	4.400889132	5.099483169	1
3639	GCB	4.506380012	4.508442193	2.809610474	5.156940793	4.217429511	4.878937488	0
3640	GCB	4.147857541	3.671535173	2.69683039	7.356916542	4.326746711	5.08172305	0
3644	GCB	4.242735859	4.303140993	3.303411306	7.01189003	4.080586021	4.966299266	0
3645	GCB	4.321393089	4.523976149	3.402438737	5.065277902	4.411734152	4.908445142	0
3646	ABC	3.93346037	3.951457822	3.442910568	6.634911893	4.101375729	4.892697356	1
3647	GCB	3.528585786	3.460439751	2.84364066	7.241302706	4.057492088	4.757324068	0
3651	ABC	4.03376207	4.291774753	3.309254939	5.597464281	4.360898007	5.444316597	1
3653	ABC	4.045727521	4.205215705	3.481139783	5.691654686	4.497460337	5.153058509	1
3654	Unclassified	3.931890381	4.345138298	2.839220585	5.531190383	4.369621661	5.005619078	2
3655	GCB	3.998979833	3.60440937	3.191692766	4.860625472	3.257990585	4.664912287	0
3659	Unclassified	4.22857245	4.049459489	3.707825562	6.026416112	4.296740144	5.256584463	2
3660	ABC	3.814680843	4.114580845	3.109557367	5.704702193	4.562701272	5.116332568	1
3661	GCB	3.850787639	4.088590606	3.23876336	7.198878846	4.347992888	5.041518178	0
3664	ABC	4.971820924	5.530554788	4.111169776	3.926652575	4.652164325	5.239637779	1
3666	GCB	4.428946688	4.410801661	3.525067134	7.390802577	4.176650058	5.114551186	0
3667	GCB	4.05038546	4.742987989	3.124892542	6.480320808	4.518297041	5.070294443	0
3671	GCB	3.761639864	4.095183016	2.582507388	6.353837577	4.219634881	4.780948232	0
3672	ABC	4.314533502	4.261289517	3.752339096	5.40293477	4.062546386	5.008730302	1
3673	Unclassified	4.127585537	4.26224712	3.304065558	5.001843777	4.338496235	4.937867	2
3675	Unclassified	3.771944095	4.926759908	3.89002531	5.038779615	4.183820074	5.095526463	2
3677	GCB	3.572170642	4.074838231	3.413069076	6.350999345	4.125978569	5.163073594	0
3682	GCB	3.467682669	3.46198982	3.219910102	6.786716873	3.914792444	4.820731504	0
3684	ABC	3.711766971	4.620201625	2.713265163	6.239547697	4.554432652	5.196505053	1
3685	GCB	4.786264676	5.420146461	4.503578776	5.171536703	4.451146981	4.946947668	0
3687	Unclassified	4.071421352	4.26882914	2.596787659	5.701800286	3.88504911	4.878154791	2
3688	GCB	3.808849928	4.602471194	2.930336675	6.365957209	4.609733857	5.002712131	0
3689	GCB	4.038490379	4.0144719	2.800005739	5.016005227	4.012747391	4.94313741	0
3691	ABC	3.850163613	3.539703657	2.718534	5.934197003	4.520232005	5.172880495	1
3692	GCB	3.512276265	3.996518155	2.610150469	6.301814222	3.939303035	4.822608949	0
3693	Unclassified	4.029450026	4.123809484	3.748865785	5.973224135	4.291271111	5.075914032	2
3694	GCB	4.221150882	4.825994769	5.102512977	5.383777594	4.169911545	5.023434651	0
3696	ABC	4.611295647	4.517379144	3.91666244	4.637648216	4.64683222	5.311697636	1
3697	ABC	4.323685274	4.449053087	3.151162244	5.198802804	4.500138176	4.985293364	1
3700	GCB	3.653496386	3.625658108	3.255658401	7.030703127	4.11105729	5.103419502	0
3701	Unclassified	4.4589012573	5.2507593904	3.354613712	4.548900978	4.67417861	5.28279086	2
3703	ABC	4.144326325	4.191544455	2.687241459	5.035663305	4.516129985	5.125408729	1
3704	ABC	3.574398855	3.516387181	2.677225479	5.547626502	4.219839622	5.172925459	1
3707	GCB	3.748225103	4.230465715	2.424508945	5.65517555	4.401604109	5.348497592	0
3708	GCB	3.751391075	4.177868715	2.562850459	6.274733118	4.454300284	5.015022008	0
3709	ABC	3.911639033	4.161729086	2.861970658	5.37646108	4.104562424	5.008769103	1
3712	GCB	3.724416657	4.071095816	2.597574805	6.241997183	4.583175384	5.197606778	0
3713	GCB	3.847995529	4.154212181	3.165337913	6.136451116	4.553489613	5.327075607	0
3715	Unclassified	3.709545516	3.539119104	3.142757784	5.016428561	4.35187481	5.195057049	2
3716	ABC	3.598077613	3.670913343	2.852808201	4.564926185	4.07314827	4.992268303	1
3717	ABC	3.526050697	3.168383017	2.639300639	5.946999861	4.003285165	5.077471556	1
3718	GCB	3.74792009	3.699188002	3.162689513	5.872981072	4.223245628	5.082414772	0
3719	GCB	3.487092052	3.485205949	2.678357114	5.651149271	4.162698496	4.825652328	0
3721	GCB	4.147857541	4.240754425	3.236440139	4.92879602	4.064434819	5.133130425	0
3722	Unclassified	4.029132681	4.208354767	2.862310127	5.420674452	4.367770993	4.946592768	2
3724	GCB	3.465425983	4.033149633	2.70023682	4.865789262	4.18240702	5.122073274	0
3726	GCB	3.370568359	3.40858112	2.638528443	6.355138302	4.138852435	4.820846301	0
3727	GCB	3.88724941	3.25799517	2.952737586	5.385502796	3.891126383	4.768389633	0
3728	GCB	4.237807952	4.483260292	3.255321671	5.548892375	3.926805523	4.85367512	0
3729	Unclassified	3.761000145	3.922592003	2.389958521	5.497008906	4.574833145	5.006235141	2
3730	GCB	3.52290036	3.667204213	2.892284831	4.86255958	4.436033813	5.114075166	0
3731	ABC	4.316987002	3.962684139	3.481139783	5.101192059	4.509626493	5.199940043	1
3733	Unclassified	3.603453757	3.717960159	2.652328387	4.69918617	4.222859627	5.023283956	2
3737	GCB	3.872620712	4.112413266	3.058659396	6.150669737	4.200557406	4.990074847	0
3739	GCB	4.166104783	4.140751066	3.258324901	7.154281527	4.048293886	4.900268749	0
3740	GCB	3.716267755	4.149748373	2.779591056	5.837051666	4.341256581	4.854289297	0
3741	GCB	3.176177973	3.686444975	3.241437334	5.140897476	3.622255239	4.609179162	0
3742	ABC	4.09924531	4.003563522	3.815659204	5.17345113	4.575627783	5.213190437	1
3743	GCB	4.158628594	4.42624329	4.046975803	5.486006422	4.15046975	5.033690509	0
3744	ABC	4.105787332	4.423557981	3.671833901	3.73300487	3.792551034	4.956712374	1
3745	GCB	3.390944289	3.116363325	3.094759202	7.59830859	4.19147031	4.992196472	0
3746	GCB	3.600003512	4.244689452	2.40170935	5.075528997	3.856003598	4.765185537	0
3747	GCB	3.148134667	3.074433667	2.876211611	5.393999443	3.986797931	4.967997711	0
3749	ABC	4.039778769	4.420214608	2.943493957	5.550815777	4.272967319	4.987919814	0
3750	ABC	3.619079288	3.644497828	3.296255412	5.661384625	3.719255027	4.898327119	1
3753	ABC	3.785138207	5.096614107	4.79384945	4.936074695	3.825823206	5.1125150363	1
3754	GCB	4.815521257	5.282513417	3.959597007	6.645558601	4.584473128	5.024924525	0
3755	GCB	4.055043787	4.02357247	2.86262952	5.264573559	4.146318209	4.892976537	0
3756	GCB	3.500392471	3.082847402	3.642961699	5.054680839	3.426256809	4.666230435	0
3757	GCB	3.7547883	3.412106427	3.77501454	4.877364275	3.649619569	4.829651395	0
3758	GCB	4.093316608	4.1670629	3.181570332	5.456569944	4.372369568	4.947807387	0
3759	GCB	3.773140622	4.041374823	2.807049879	6.840697922	4.106531678	4.811088935	0
3762	Unclassified	3.793627314	3.870714895	2.818164803	5.721649859	4.535666574	5.117820079	2
3763	ABC	4.142093262	5.132436955	2.688818315	5.132942269	4.069088636	4.73483127	1
3764	GCB	3.65477259	3.909467611	2.597574805	6.137538982	4.431642929	4.958350513	0
3765	ABC	4.342547566	4.823633282	4.437480941	5.897062704	4.183736877	4.870623339	1
3766	ABC	3.575363873	3.740777168	2.952361824	5.446407977	4.187362275	5.134701314	1
3767	GCB	3.631925867	3.738926815	3.058659396	6.219303101	4.489792856	5.001155565	0
3770	GCB	4.380626618	4.636916383	4.260965732	5.034785816	4.120883307	4.996020772	1
3771	ABC	3.75851692	4.11461573	2.761268196	5.102512977	4.432603985	5.054229951	1
3776	Unclassified	3.298209781	3.755114137	3.086924986	6.402545379	3.992915686	4.971960552	2
3777	ABC	3.880352322	4.090526629	2.839220585	5.812508271	4.033775109	4.975534309	1
3778	ABC	4.238307154	3.908099607	3.65817677	5.398448091	4.075661711	5.106739208	1
3781	ABC	4.942242523	4.942242523	5.850273745	4.271010838	4.174034522	5.134947086	1
3783	ABC	3.521345921	4.275160341	3.432050027	5.6586192	4.125341749	5.065280559	1
3784	ABC	4.205527545	4.692772273	3.824121332	5.356660872	4.095930426	5.141611497	1
3785	ABC	3.984844951	3.911940703	2.60820275	5.3973175	4.101437991	5.027116094	1
3786	Unclassified	4.470281656	5.310136401	3.628131274	4.967236333	4.644419224	5.152190278	2
3787	ABC	4.151343108	4.51184883	3.187984644	5.303409667	4.364766073	5.144107472	1
3810	GCB	3.912562273	4.487645668	2.806304338	5.783695803	4.39233122	5.024577768	0
3811	GCB	3.443528489	4.670434733	3.298209781	5.616287137	4.291567434	4.963812322	0
3812	GCB	4.610953583	5.284541479	3.715172955	5.767221605	4.672150136	5.131244496	0
3813	Unclassified	4.380979284	4.862176578	3.993116034	4.685626322	4.811659348	5.345141402	2
3814	ABC	3.770049876	4.639770904	3.998333534	4.92513344	4.49163525	4.915465553	1
3815	GCB	4.136986327	4.533930398	3.091689469	5.757291535	4.423646908	5.120953049	0
3816	GCB	4.489058025	4.462649972	3.313525194	5.7			

3883	ABC	3.880971315	3.756642178	3.176856281	5.097062197	4.396210639	5.152325757	1
3886	Unclassified	4.213446016	4.522571422	3.681455765	6.415387588	4.642608902	5.181141744	2
3887	GCB	4.703642875	4.473338663	3.928479232	5.177811014	4.139180668	4.830625795	0
3888	ABC	4.418204384	4.679365699	3.522275287	4.812815092	4.562341923	5.192790741	1
3891	GCB	3.589796417	3.589796417	2.605910842	5.951491438	4.317084927	4.962680107	0
3892	Unclassified	4.179794818	4.069193684	3.511352507	5.6330052	4.736810496	5.131351833	2
3893	GCB	3.648250318	3.926652575	3.640757811	4.575901754	3.952484399	4.889262025	0
3894	ABC	4.465270782	4.751331283	3.794558604	4.509845323	4.550225367	5.109131401	1
3895	GCB	4.277805579	4.25839043	3.542498084	5.352395247	4.296457556	5.022739132	0
3896	GCB	4.099859078	3.952417921	4.009500529	4.523976149	3.805321193	4.885963204	0
3898	GCB	4.059777871	4.337079141	3.356920532	4.905104579	4.474140021	5.193104887	0
3900	Unclassified	3.536912539	4.671162195	4.170489057	2.751559553	4.306757487	5.034724775	2
3902	GCB	3.908854762	4.093627491	2.982555503	5.987520088	4.443200131	5.200063421	0
3903	ABC	3.658797203	4.329866538	3.33492745	6.758935343	4.15542868	5.051866226	1
3904	GCB	3.315451029	3.903282364	2.750416237	7.292089549	4.157729951	4.893404472	0
3905	ABC	3.950240011	3.961154307	2.778447715	5.849456869	4.214776541	5.140723073	1
3908	GCB	3.566842356	4.146562463	2.928862007	7.202122613	4.141914459	5.068475169	0
3910	ABC	3.78108047	4.595688028	3.216563999	4.554114605	4.258791372	5.05333258	1
3911	GCB	4.06513671	4.458912573	2.91991401	6.096109599	4.563656935	5.191885329	0
3914	ABC	3.437480941	3.835169616	2.263627849	5.641296762	4.270508597	4.906165237	1
3915	Unclassified	3.666913298	3.595806893	2.542909953	6.346964331	4.111363203	4.895130382	2
3918	ABC	4.516368635	4.200124283	2.992285909	5.033416951	4.229688625	5.040564425	1
3919	ABC	4.028209386	4.245016848	2.71887082	5.62254902	4.274800672	4.843853425	1
3922	ABC	4.242079247	4.106752731	3.318970755	4.026849105	3.944657774	4.780905677	1
3925	GCB	4.112716031	4.21952447	2.110658977	7.254644157	4.333888794	4.978752237	0
3928	ABC	4.274833051	4.366635325	3.374914956	5.034785816	4.500821824	5.230066397	1
3929	GCB	4.086380168	4.020415447	2.542909953	6.827025381	4.239298761	4.907587306	0
3930	GCB	4.199481319	3.697776704	3.272426428	6.675750511	4.107429735	4.895509317	0
3932	GCB	4.593895862	4.460956141	3.602243072	5.946127729	4.293542508	4.97242303	0
3933	ABC	3.450163381	3.641387913	3.18629839	5.949717129	4.2026754	5.054824304	1
3936	GCB	4.35309559	5.011232632	3.271452579	5.751850538	4.537377176	4.953949754	0
3937	Unclassified	3.888170844	3.89803618	2.612813311	5.105733581	4.357897662	5.172007691	2
3940	GCB	3.372551852	2.879464552	2.702235769	6.922084478	3.93714801	4.745024139	0
3944	ABC	4.512858235	4.148810961	3.504137376	5.135764408	4.018941862	5.07093939	1
3945	ABC	4.568735284	5.330444398	3.375877304	5.326578681	4.53848076	5.086550018	1
3948	GCB	3.709855176	4.284392679	3.12559996	4.849161554	4.343346561	5.055502919	0
3949	GCB	3.738779943	3.898668777	2.725605337	5.881546187	4.242403765	5.100059052	0
3950	ABC	3.738633057	4.075004712	2.837427849	5.455982766	4.303992475	4.817845913	1
3951	GCB	3.667516603	3.862682275	2.567263431	6.688892279	4.294598916	5.054145882	0
3952	Unclassified	3.791741968	4.579733613	2.92237668	5.212040703	4.393124526	5.092325959	2
3954	Unclassified	4.093627491	4.92879602	3.063764179	5.176848007	4.702077895	5.07038631	2
3956	GCB	3.860812799	4.575203088	3.728095949	7.43360276	4.240417895	4.939168885	0
3957	ABC	4.113057101	3.612205112	3.321598011	5.397878199	4.199483787	5.101009878	1
3958	ABC	3.831757463	3.983443907	2.610150469	5.566920152	4.06644462	4.834416078	1
3959	ABC	3.842711173	4.270043866	3.537235661	4.727124222	4.143295868	5.018581997	1
3960	GCB	3.263258232	3.482086247	2.885096234	6.12984053	3.819023791	4.785977533	0
3963	GCB	3.717960159	4.437963907	2.928862007	7.465573521	4.091541033	4.610146435	0
3964	ABC	4.668223081	4.553066036	3.34984433	5.045470204	4.113270365	5.056098591	1
3965	ABC	3.612854989	3.851713898	2.835981242	5.809296151	4.112157959	4.993313395	1
3966	GCB	3.779864356	4.03376207	2.821440182	5.648980304	4.208717472	5.08954604	0
3967	Unclassified	3.886607349	4.302177405	3.075477759	6.624010061	4.171285415	5.061776604	2
3968	Unclassified	3.935050703	4.357393798	3.332357622	6.732311968	4.182738418	5.064611533	2
3969	GCB	3.222573676	3.18629839	2.274090493	5.753354715	3.911227382	4.737652063	0
3971	GCB	3.455340999	3.795179674	2.426883273	8.095517141	4.226232803	4.9156315	0
3972	GCB	4.049770921	4.270693637	2.898711802	7.757309548	4.302683356	4.92014803	0
3974	GCB	3.78950792	4.348815968	3.361162098	5.856249304	4.140378804	5.060379396	0
3975	GCB	3.971034898	4.109929049	3.291363091	6.716032087	4.052584549	4.986225535	0
3976	ABC	4.198533996	4.702491733	2.913161045	5.83626283	4.44865637	4.986589592	1
3977	GCB	4.376004437	4.783652516	3.576659141	5.885004778	4.516840335	5.139289829	0
3980	GCB	3.678059856	4.163898839	2.799282764	5.071191366	4.221734552	5.08815788	0
3981	ABC	4.888509492	5.620439858	4.043548879	4.889730899	4.757577537	5.089092934	1
3983	GCB	3.904508978	4.348815968	3.120791188	5.677705897	4.058043055	4.715617974	0
3985	ABC	3.963294739	4.233356898	3.120791188	5.008304761	4.329455903	5.086926611	1
3987	Unclassified	3.811626951	3.638537584	2.564456763	6.692764837	4.486289232	5.22528798	2
3989	GCB	3.874459581	3.45209844	3.029790241	5.289661332	3.964155135	4.876499274	0
3990	ABC	4.117802001	4.34813777	2.87981132	4.917716995	4.365672399	5.077681001	1
3992	ABC	3.342691019	3.895532441	2.908110017	5.462563582	4.016654471	4.84903993	1
3997	Unclassified	3.759760351	3.947424166	2.466152853	5.489039813	4.156284189	4.962608688	2

Supplemental Table 2. Source of gene sets

Signature	Pathway Collection	Original Pathway Source	Accession
BIOCARTA_NFKB_PATHWAY	Biocarta	http://cgap.nci.nih.gov/Pathways/BioCarta/h_nfkbPathway	N/A
NEGATIVE_REGULATION_OF_INTRINSIC_APOPTOTIC_SIGNALING_PATHWAY	Gene Ontology	http://www.geneontology.org/	GO:2001243

Supplemental Table 3. Gene of BIOCARTA_NFKB_PATHWAY and
NEGATIVE_REGULATION_OF_INTRINSIC_APOPTOTIC_SIGNALING_PA
THWAY

BIOCARTA_NFKB_PATHWAY	NEGATIVE_REGULATION_OF_INTRINSIC_APOPTOTIC_SIGNALING_PATHWAY
CHUK	AKT1
FADD	ARHGEF2
IKBKB	BAG5
IKBKG	BCL2
IL1R1	BCL2L1
IRAK1	BCL2L12
MAP3K1	BCL2L2
MAP3K14	CD44
MAP3K7	CD74
MYD88	CLU
NFKB1	CREB3
NFKBIA	CXCL12
RELA	DDX3X
RIPK1	ELL3
TAB1	FIGNL1
TLR4	GPX1
TNF	GRINA
TNFAIP3	HERPUD1
TNFRSF1A	HIF1A
TNFRSF1B	HSPA1A
TRADD	HSPB1
TRAF6	HSPH1
	HTRA2
	HYOU1
	ING2
	IVNS1ABP
	KDM1A
	LRRK2
	MAPK7
	MCL1
	MIF
	MMP9
	NDUFA13
	NDUFS3
	NFE2L2
	NOC2L
	NONO
	OPA1
	PARK7
	PARL
	PGAP2
	PINK1
	PPIF
	PTPN1
	PTTG1P
	RRM2B
	RRN3
	SIRT1
	SNAI2
	SOD2
	SRC
	SYVN1
	TAF9
	TAF9B
	TMBIM6
	TMEM161A
	TPT1
	TRAP1
	TRIAP1
	TRIM32
	TXNDC12
	USP47
	VDAC2
	WFS1
	XBP1
	ZNF385A

Supplemental Table 4. Whole-exome sequencing data and RNA-seq data derived from TCGA-DLBC

Sample ID	RNF31 expression (log2[fpkm+1])	RNF31 level	Number of non-synonymous mutations	Number of SNVs at C/G within WRCY/ RGYW motifs	Mutations related to AID	
					Number of SNVs at C:G pairs	Number of transition SNVs
TCGA_FA_8693	3.433192779	low	139	16	89	117
TCGA_FA_A4BB	3.378465047	low	60	7	63	62
TCGA_FA_A4XK	3.605882128	low	57	13	56	53
TCGA_FA_A6HN	3.923326525	high	147	38	156	135
TCGA_FA_A6HO	4.088918093	high	38	4	39	36
TCGA_FA_A7DS	3.749852318	low	66	17	72	63
TCGA_FA_A7Q1	3.407832607	low	115	17	122	108
TCGA_FA_A82F	3.525318585	low	126	19	124	104
TCGA_FA_A86F	4.025166318	high	63	9	56	49
TCGA_FF_8041	3.96908928	high	158	20	164	159
TCGA_FF_8042	4.335474524	high	222	20	191	172
TCGA_FF_8043	3.73604922	low	92	10	90	92
TCGA_FF_8046	3.734145124	low	67	11	60	57
TCGA_FF_8047	4.015725016	high	101	11	107	115
TCGA_FF_8061	3.260872087	low	138	15	112	125
TCGA_FF_8062	3.615960329	low	120	21	110	103
TCGA_FF_A7CQ	4.015156781	high	101	21	100	94
TCGA_FF_A7CR	3.828972878	high	143	32	140	128
TCGA_FF_A7CW	3.902906089	high	36	4	37	33
TCGA_FF_A7CX	3.824814506	high	98	11	99	91
TCGA_FM_8000	3.724454855	low	113	6	104	111
TCGA_G8_6324	4.024117965	high	1116	118	1373	1456
TCGA_G8_6325	3.793983219	high	436	47	509	515
TCGA_G8_6326	4.151311915	high	373	38	405	449
TCGA_G8_6906	3.925795544	high	469	52	534	521
TCGA_G8_6907	3.78420038	high	389	42	440	456
TCGA_G8_6909	3.788774811	high	677	84	667	651
TCGA_G8_6914	3.71859885	low	400	45	465	486
TCGA_GR_7351	3.738807949	low	583	76	567	569
TCGA_GR_7353	4.538902117	high	414	47	441	480
TCGA_GR_A4D4	3.755117882	low	76	5	55	44
TCGA_GR_A4D5	3.52981948	low	49	6	59	51
TCGA_GR_A4D6	4.039498559	high	28	2	31	31
TCGA_GR_A4D9	3.510295565	low	62	6	52	40
TCGA_GS_A9TQ	3.582656442	low	67	5	60	54
TCGA_GS_A9TT	3.478160411	low	131	21	136	118
TCGA_GS_A9TU	3.797060331	high	41	3	39	40
TCGA_GS_A9TV	4.358108537	high	55	4	33	43
TCGA_GS_A9TW	3.835903844	high	180	21	174	144
TCGA_GS_A9TX	3.727934043	low	20	1	14	16
TCGA_GS_A9TY	3.442669245	low	109	8	106	89
TCGA_GS_A9TZ	3.812335231	high	294	36	304	259
TCGA_GS_A9U3	3.739806669	low	62	5	61	60
TCGA_GS_A9U4	3.923842062	high	16	2	23	17
TCGA_RQ_A68N	4.078441915	high	155	19	161	145
TCGA_RQ_A6JB	3.577042044	low	58	3	46	44
TCGA_RQ_AAAT	3.691684788	low	111	19	108	99
TCGA_VB_A8QN	3.488698312	low	117	15	139	129

For each DLBCL patient sequenced, clinical features are shown.^{1,2} The "Mutations related to AID" section shows number of single nucleotide variations (SNVs) at C/G within WRCY/RGYW motifs, and at C:G pairs and number of transition mutations. Blank fields indicate that a measurement was not taken or was irrelevant to the patient.

1. Grossman RL, Heath AP, Ferretti V, et al. Toward a Shared Vision for Cancer Genomic Data. *N Engl J Med*. 2016;375(12):1109-1112.
2. Lohr JG, Stojanov P, Lawrence MS, et al. Discovery and prioritization of somatic mutations in diffuse large B-cell lymphoma (DLBCL) by whole-exome sequencing. *Proc Natl Acad Sci USA*. 2012;109(10):3879-3884.

Supplemental Table 5. Murine homologue of previously reported driver genes in human DLBCL

Actb	Bcor	Dazap1	Gna13	Itpkb	Nfkbie	Setd1b	Tnfaip3	Zeb2
Actg1	Btg1	Dtx1	Gnai2	Klf2	Notch2	Sgk1	Tnfrsf14	Zfp3611
Ankrd11	Btg2	Dusp2	Grhpr	Klhl14	Osbp110	Socs1	Tox	
Arid1a	Card11	Ebf1	Hist1h1b	Klhl6	Pax5	Spn	Triobp	
Arid1b	Ccnd3	Ep300	Hist1h1c	Kmt2d	Pde4dip	Stat3	Trp53	
B2m	Cd70	Ets1	Hist1h1d	Ltb	Pim1	Syne2	Ttn	
Bcl10	Cd79b	Etv6	Hist1h1e	Mef2b	Pim2	Tbl1xr1	Ube2a	
Bcl2	Cdkn2a	Ezh2	Irf2bp2	Mpeg1	Plec	Tet2	Vmp1	
Bcl6	Ciita	Fas	Irf4	Myc	Pou2f2	Tmem30a	Wdfy4	
Bcl7a	Crebbp	Foxo1	Irf8	Myd88	Prdm1	Tmsb4x	Zc3h12a	

Among 90 genes mutated with frequency greater than 5% in human DLBCL,¹ eight genes lacking a murine homologue were excluded. Genes non-synonymously mutated in lymphomas derived from CD19-cre-HOIP/MYD88LP mice are bold.

1. Schmitz R, Wright GW, Huang DW, et al. Genetics and Pathogenesis of Diffuse Large B-Cell Lymphoma. *N Engl J Med.* 2018;378(15):1396-1407.

Supplemental Table 6. Murine homologue of previously known and predicted hypermutated genes in human DLBCL

Actb	Cd74	Ets1	Hist1h2ab	Hist2h2ab	Itpkb	Ms4a1	Prrt2	Tcl1
Actg1	Cd83	Etv6	Hist1h2ao	Hist2h2ac	Klf2	Myc	Rcc1	Tmsb4x
Arid5b	Cdkn1b	Fam102a	Hist1h2bc	Hist2h2bb	Klhl14	Ncoa3	Rftn1	Tnf
Atxn2	Ciita	Fcgr4	Hist1h2be	Hist2h2be	Klhl21	Nol9	Rhoh	Tnfrsf14
Bach2	Cxcr4	Foxc1	Hist1h2bg	Hist2h3b	Limd2	Osbp10	Rnf144b	Ube2j1
Bcl2	Dmd	Foxo1	Hist1h2bk	Id3	Lrmp	Pax5	S1pr2	Ube3c
Bcl6	Dtx1	Gadd45b	Hist1h2bm	Igll1	Lst1	Pim1	Serpina9	Vmp1
Bcl7a	Dtx4	Grhpr	Hist1h3b	Il10ra	Lta	Pim2	Sgk1	Wee1
Birc3	Dusp2	H2afj	Hist1h3c	Il16	Ltb	Pou2af1	Socs1	Zfp36l1
Btg1	Egr1	Hist1h1b	Hist1h3h	Irf2bp2	Map3k3	Ppp1r9b	Spred2	Zfp36l2
Btg2	Ehd1	Hist1h1c	Hist1h4d	Irf4	Mcl1	Pramef25	St6gal1	Zfp608
Cd44	Eif4a2	Hist1h1e	Hist2h2aa2	Irf8	Mpeg1	Pramef8	Tas1r1	Zfp804a

Among the previously reported 126 genes,¹ 18 genes lacking a murine homologue were excluded.

Genes non-synonymously mutated in lymphomas derived from CD19-cre-HOIP/MYD88LP mice are bold.

1. Schmitz R, Wright GW, Huang DW, et al. Genetics and Pathogenesis of Diffuse Large B-Cell Lymphoma. *N Engl J Med.* 2018;378(15):1396-1407.

Supplemental Table 7. Previously reported AID target genes in mice

1810065E05Rik	Cd79a	Fas	Jchain	Pik3ap1	Rpl3	Tcf4
Aatk	Cd79b	Fchsd2	Junb	Pim1	Rpl32	Terc
Abl2	Cd83	Fen1	Kpna2	Plac8	Rpl35	Tet2
Ablim1	Cdk11b	Fli1	Kpnb1	Plcb2	Rpl4	Tex14
Acot7	Cdk4	Fnbp1	Lmo1	Pms2	Rpl41	Tfap4
Actb	Chd2	Foxo4	Lrmp	Pola1	Rplp0	Tfdp1
Ada	Chek1	Fth1	Lsp1	Pold1	Rps12	Tmsb4x
Adar	Ciita	Ftl1	Ltb	Pold4	Rps14	Tnf
Agk	Clk1	Gadd45b	Ly6e	Pou2af1	Rps5	Tnfaip3
Aicda	Cnbp	Gadd45g	Lyn	Pou2f1	Rps6	Top1
Akap8	Cox4i1	Galnt1	Man1a	Pou2f2	Rps9	Top2a
Apex1	Cox6a1	Gas5	Mcm2	Ppard	Rrm1	Topors
Apobec1	Cox8a	Gdi2	Mcm6	Ppia	Rrm2	Tra2b
Apoe	Cradd	Gna13	Mcm7	Ppp1r15b	Runx1t1	Ttf1
Atf5	Csk	Grap	Mdfi	Ppp1r16b	Safb	U2af2
Atp5b	Csnk1d	Gsta3	Mdh2	Prdx1	Vimp	Uba3
Atp5e	Cyth1	H2afx	Mef2b	Psmc3	Serinc3	Ubac2
Atp5o	Daxx	H3f3b	Mir142b	Ptbp2	Sf3b1	Ubb
B2m	Ddb2	Hdac1	Mlh3	Pten	Sh3bp5	Ube2b
Bad	Ddx20	Hdac9	Mlst8	Ptma	Sipa1	Ube2n
Bcl11a	Ddx5	Hdgf	Mrpl51	Ptprc	Sirt6	Ube4b
Bcl6	Dnmt1	Hells	Ms4a1	Rac1	Slbp	Ubox5
Bid	Dok1	Hist1h1a	Msh2	Rad23a	Slc30a6	Ubf
Blk	Dsg4	Hist1h1b	Msh5	Rad51	Snx5	Uhmk1
Bmp2k	Dusp6	Hnrnpa2b1	Msh6	Rad9a	Sod1	Vav1
Brca1	Dyrk3	Hnrnpf	Mtor	Ranbp1	Sp3	Vav2
Btg1	E2f1	Hsf4	Mtss1	Rbm15	Spib	Vcl
Btg2	E2f2	Hvcn1	Mybbp1a	Rbm19	Sra1	Vdac1
C2cd3	E4f1	Id3	Myc	Rbm39	Srsf10	Xbp1
Cacng4	Ebf1	Ikzf1	Mycbp2	Recql4	St6gal1	Zc3h15
Calm1	Eef1a1	Il21r	Ncl	Rel	Stau1	Zcchc7
Cat	Eif2a	Il4ra	Nfkb2	Rev3l	Stx3	
Ccne2	Eif3a	Illdr2	Ntan1	Rfc2	Sv2b	
Cd19	Eif3d	lpmk	Parp1	Rgs13	Swap70	
Cd22	Eif4a2	lpo7	Pax5	Rhoh	Syk	
Cd24a	Eif5a	lrf4	Pcna	Rims1	Taf4	
Cd37	Ell	lrf8	Pex13	Rnf2	Taf9	
Cd48	Erh	ltga4	Phip	Rpa1	Tapbp	
Cd53	Eri1	ltgal	Pias1	Rpia	Tcea1	
Cd74	Ets1	ltgb2	Pick1	Rpl29	Tcf3	

Among the previously reported 291 genes,¹ 20 genes duplicated or with no correspondence in the current database were excluded. Genes non-synonymously mutated in lymphomas derived from CD19-cre-HOIP/MYD88LP mice are bold.

1. Alvarez-Prado AF, Perez-Duran P, Perez-Garcia A, et al. A broad atlas of somatic hypermutation allows prediction of activation-induced deaminase targets. *J Exp Med.* 2018;215(3):761-771.

Supplemental Table 8. Enrichment of WRCY mutations in genes mutated in lymphomas derived from transgenic mice

Mouse genotype group	Gene	No. of SNVs at C in WRCY in the indicated gene	No. of WRCY motifs in the indicated gene	No. of all WRCY motifs in the whole exome	No. of samples in the indicated genotype group	No. of SNVs at C in total WRCY among the indicated genotype group	Rate of SNVs in WRCY motifs	p value (Binomial test)	Gene sets	
									Alvarez-Prado, 2018	Schmitz, 2018
CD19-cre-HOIP/MYD88LP	Irf2bp2	23	109	2254406	8	145	8.04E-06	1.52E-94	FALSE	TRUE
CD19-cre-HOIP/MYD88LP	Pim1	11	56	2254406	8	145	8.04E-06	1.35E-45	TRUE	TRUE
CD19-cre-HOIP/MYD88LP	Hist1h1e	8	54	2254406	8	145	8.04E-06	1.82E-32	FALSE	TRUE
CD19-cre-HOIP/MYD88LP	Klf2	7	55	2254406	8	145	8.04E-06	4.40E-28	FALSE	TRUE
CD19-cre-HOIP/MYD88LP	Bhlhe41	7	84	2254406	8	145	8.04E-06	9.83E-27	FALSE	FALSE
CD19-cre-HOIP/MYD88LP	Nfkbia	6	70	2254406	8	145	8.04E-06	3.54E-23	FALSE	FALSE
CD19-cre-HOIP/MYD88LP	H2-Ab1	5	47	2254406	8	145	8.04E-06	5.15E-20	FALSE	FALSE
CD19-cre-HOIP/MYD88LP	Fgl2	3	102	2254406	8	145	8.04E-06	8.92E-11	FALSE	FALSE
CD19-cre-HOIP/MYD88LP	Man1a	3	127	2254406	8	145	8.04E-06	1.73E-10	TRUE	FALSE
CD19-cre-HOIP/MYD88LP	Tap1	3	167	2254406	8	145	8.04E-06	3.96E-10	FALSE	FALSE
CD19-cre-HOIP/MYD88LP	Cd83	2	47	2254406	8	145	8.04E-06	6.99E-08	TRUE	TRUE
CD19-cre-HOIP/MYD88LP	Hes5	2	49	2254406	8	145	8.04E-06	7.60E-08	FALSE	FALSE
CD19-cre-HOIP/MYD88LP	Mcl1	2	51	2254406	8	145	8.04E-06	8.24E-08	FALSE	TRUE
CD19-cre-HOIP/MYD88LP	Socs3	2	53	2254406	8	145	8.04E-06	8.90E-08	FALSE	FALSE
CD19-cre-HOIP/MYD88LP	Hist1h1b	2	59	2254406	8	145	8.04E-06	1.11E-07	TRUE	TRUE
CD19-cre-HOIP/MYD88LP	Eef1a1	2	75	2254406	8	145	8.04E-06	1.79E-07	TRUE	FALSE
CD19-cre-HOIP/MYD88LP	Dusp2	2	86	2254406	8	145	8.04E-06	2.36E-07	FALSE	TRUE
CD19-cre-HOIP/MYD88LP	Gm21948	2	87	2254406	8	145	8.04E-06	2.42E-07	FALSE	FALSE
CD19-cre-HOIP/MYD88LP	Myc	2	89	2254406	8	145	8.04E-06	2.53E-07	TRUE	TRUE
CD19-cre-HOIP/MYD88LP	Sgpp1	2	93	2254406	8	145	8.04E-06	2.76E-07	FALSE	FALSE
CD19-cre-HOIP/MYD88LP	Ehd1	2	116	2254406	8	145	8.04E-06	4.31E-07	FALSE	TRUE
CD19-cre-HOIP/MYD88LP	Sik1	2	176	2254406	8	145	8.04E-06	9.95E-07	FALSE	FALSE
CD19-cre-HOIP/MYD88LP	Tlr9	2	254	2254406	8	145	8.04E-06	2.07E-06	FALSE	FALSE
CD19-cre-MYD88LP	Irf2bp2	5	109	2254406	4	15	1.66E-06	1.49E-21	FALSE	TRUE

The “**No. of SNVs at C in WRCY in the indicated gene**” shows total number of SNVs at C/G within WRCY/RGYW motifs observed in the indicated genes among all the lymphomas derived from the indicated genotype group. The “**No. of SNVs at C in WRCY in the indicated gene**” shows the total number of WRCY/RGYW motifs in the indicated gene. The “**No. of all WRCY motifs in the whole exome**” shows total number of WRCY/RGYW motifs in the whole exome. The “**No. of samples in the indicated genotype group**” shows the number of samples in the indicated genotype (8 CD19-cre-HOIP/MYD88LP, 4 CD9-cre-MYD88LP). The “**No. of SNVs at C in total WRCY among the indicated genotype group**” shows the total number of SNVs at C/G within WRCY/RGYW motifs observed in lymphomas derived from the indicated genotype (145 CD19-cre-HOIP/MYD88LP, 15 CD9-cre-MYD88LP). The “**Rate of SNVs in WRCY motifs**” were calculated as follows: Rate of SNVs in WRCY motifs = [No. of SNVs at C in total WRCY among the indicated genotype group/ (No. of all WRCY motifs in the whole exome × No. of samples in the indicated genotype group)]. The “**Gene set**” section shows whether the indicated gene is included in each gene set (yes = “TRUE”, no = “FALSE”).

Supplemental Table 9. Analysis of somatic mutations in clonal IgH rearrangements of DLBCL-like lymphomas derived from transgenic mice

Tumor ID	Genotype	IGHV usage	No. of nucleotides analyzed	No. of mutations	Frequency of mutations (%)
786	CD19-cre-HOIP/MYD88LP	IGHV1-39*01	267	8	3.00
950	CD19-cre-HOIP/MYD88LP	IGHV1-72*01	192	23	11.98
1032	CD19-cre-HOIP/MYD88LP	IGHV1-81*01	233	1	0.43
1074	CD19-cre-HOIP/MYD88LP	IGHV1-55*01	195	3	1.54
1083	CD19-cre-HOIP/MYD88LP	IGHV1-63*01	248	1	0.40
1084	CD19-cre-HOIP/MYD88LP	IGHV1-80*01	195	3	1.54
1182	CD19-cre-HOIP/MYD88LP	IGHV1-87*01	184	40	21.74
1236	CD19-cre-MYD88LP	IGHV2-2*01	221	0	0.00
1237	CD19-cre-MYD88LP	IGHV1-59*01	196	0	0.00
1289	CD19-cre-MYD88LP	IGHV1-87*01	205	9	4.39
1385	CD19-cre-MYD88LP	IGHV1-69*02	198	2	1.01

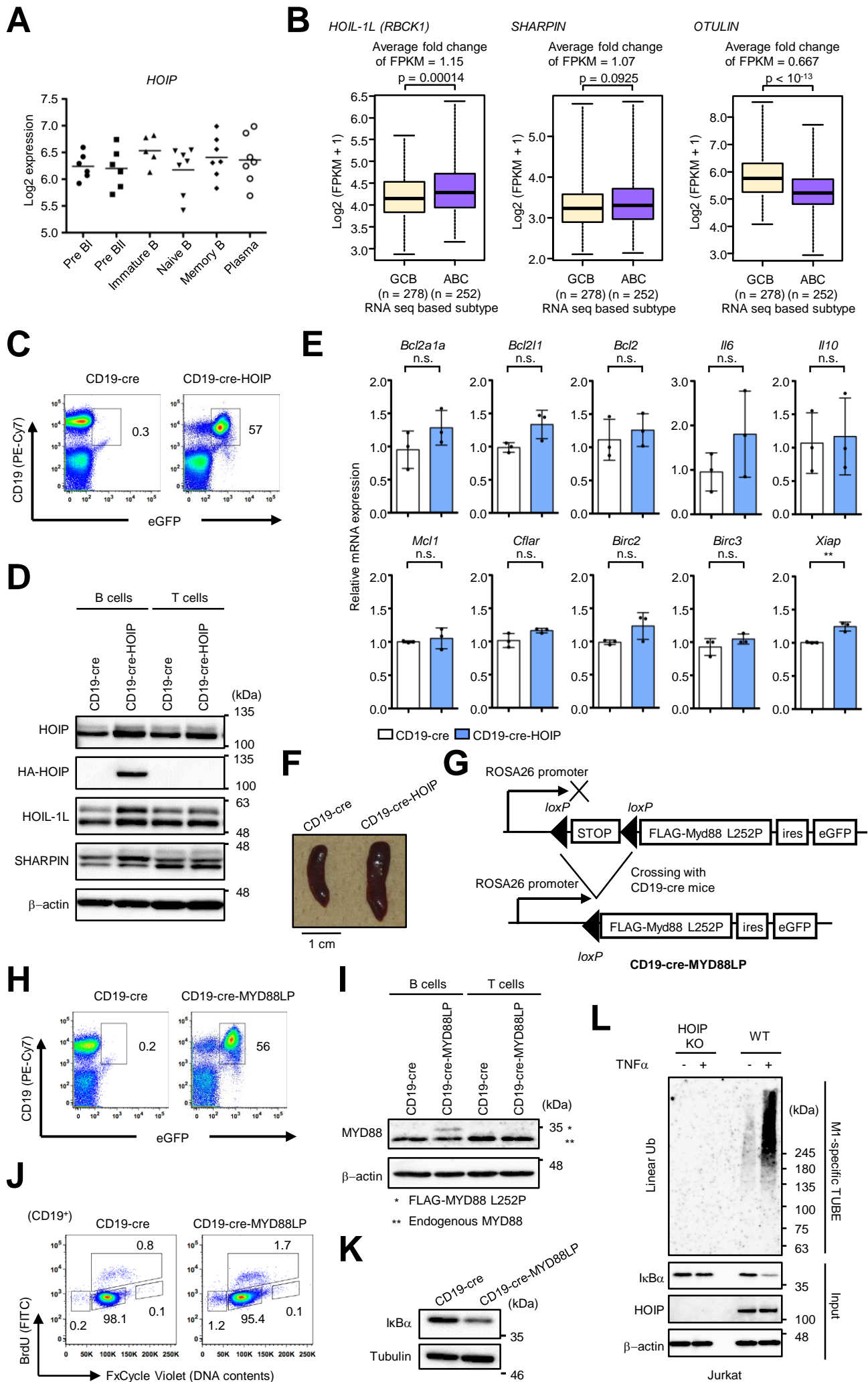
Supplemental Table 10. Primers for testing clonality of IgH V(D)J

Primer	Sequence (5'-3')
VH-specific primers 1	
36-60	CCTGGCCTCGTGAAACCTTCTCAG
81X	GGAGGCTTAGTGCAGCCTAGAGAG
J558	CTTCAGTGAAGATATCCTGCAAGG
Q52	CCCAGGTGCAGCTGAAGCAGTCAG
VH-specific primers 2	
36-60	GTCTCTCAGGCGCGCCGTCACTGG
81X	TCCCTGAGGCGCGCCTGTGAATCC
J558	GGCTTCTGGCGCGCCATTTACTGG
Q52	AGCCTGTCCATCACCTGCACAGTC
JH universal primer	GAAAACTCCATAACAAAGG
JH-specific primers	
JH1	AGCTTCTGCAGCATGCAGAGTGTG
JH2	GGCCAGGATCCCTATAAATCTCTG
JH3	ACAAAGGGGTTGAATCTTGATTCC
JH4	AAAATAAAGACCTGGAGAGGC

Supplemental Table 11. Primer sequences used for real-time PCR

	Forward primer sequence (5' – 3')	Reverse primer sequence (5' – 3')
Mouse		
<i>Aicda</i>	TCTGCTACGTGGTGAAGAGGAG	CCAGTCTGAGATGTAGCGTAGG
<i>Bcl2</i>	CCTGTGGATGACTGAGTACCTG	AGCCAGGAGAAATCAAACAGAGG
<i>Bcl2l1</i>	GCCACCTATCTGAATGACCACC	AGGAACCAGCGGTTGAAGCGC
<i>Bcl2a1a</i>	TCCACAAGAGCAGATTGCCCTG	GCCAGCCAGATTTGGGTTCAAAC
<i>Birc2</i>	GATACGGATGAAGGGTCAGGAG	GGGTCAGCATTTTCTTCTCCTGG
<i>Birc3</i>	GGACATTAGGAGTCTTCCCACAG	GAACACGATGGATACCTCTCGG
<i>Cflar</i>	GCTCTACAGAGTGAGGCGGTTT	CACCAATCTCCATCAGCAGGAC
<i>Il6</i>	TACCACTTCACAAGTCGGAGGC	CTGCAAGTGCATCATCGTTGTTC
<i>Il10</i>	CGGGAAGACAATAACTGCACCC	CGGTTAGCAGTATGTTGTCCAGC
<i>Mcl1</i>	AGCTTCATCGAACCATTAGCAGAA	CCTTCTAGGTCCTGTACGTGGA
<i>Myc</i>	TCGCTGCTGTCCTCCGAGTCC	GGTTTGCCTCTTCTCCACAGAC
<i>Nfkbia</i>	GCCAGGAATTGCTGAGGCACTT	GTCTGCGTCAAGACTGCTACAC
<i>Nfkbid</i>	GTGGAGGATCTGTTGAACCTGG	TCTCTGGCTTCCAGGTCAACCT
<i>Tnfaip3</i>	AGCAAGTGCAGGAAAGCTGGCT	GCTTTCGCAGAGGCAGTAACAG
<i>Xiap</i>	GGCAGAATATGAAGCACGGATCG	CACTTGGCTTCCAATCCGTGAG
<i>β-Actin</i>	CATTGCTGACAGGATGCAGAAGG	TGCTGGAAGGTGGACAGTGAGG
Human		
<i>BCL2</i>	ATCGCCCTGTGGATGACTGAGT	GCCAGGAGAAATCAAACAGAGGC
<i>BCL2L1</i>	GCCACTTACCTGAATGACCACC	AACCAGCGGTTGAAGCGTTCCT
<i>BIRC2</i>	CAGACACATGCAGCTCGAATGAG	CACCTCAAGCCACCATCACAAAC
<i>BIRC3</i>	GCTTTTGCTGTGATGGTGGACTC	CTTGACGGATGAACTCCTGTCC
<i>HOIP</i>	CTGGATCGTCATGGCAACCTTG	ACATCACCTCCGTGCTGGAACA
<i>HOIL1L</i>	TGACAACACCTACTCGTGCTCG	CACTGCGGTTTTTCAGCAATGGAG
<i>MCL1</i>	CCAAGAAAGCTGCATCGAACCAT	CAGCACATTCTGATGCCACCT
<i>NFKBIA</i>	TCCACTCCATCCTGAAGGCTAC	CAAGGACACCAAAGCTCCACG
<i>SHARPIN</i>	TGGCTGTGAGATGTGTAGCACC	CCTGGAGATGTCGGACTTGTGA
<i>XIAP</i>	TGGCAGATTATGAAGCACGGATC	AGTTAGCCCTCCTCCACAGTGA
<i>β-ACTIN</i>	CACCATTGGCAATGAGCGGTTC	AGGTCTTTGCGGATGTCCACGT

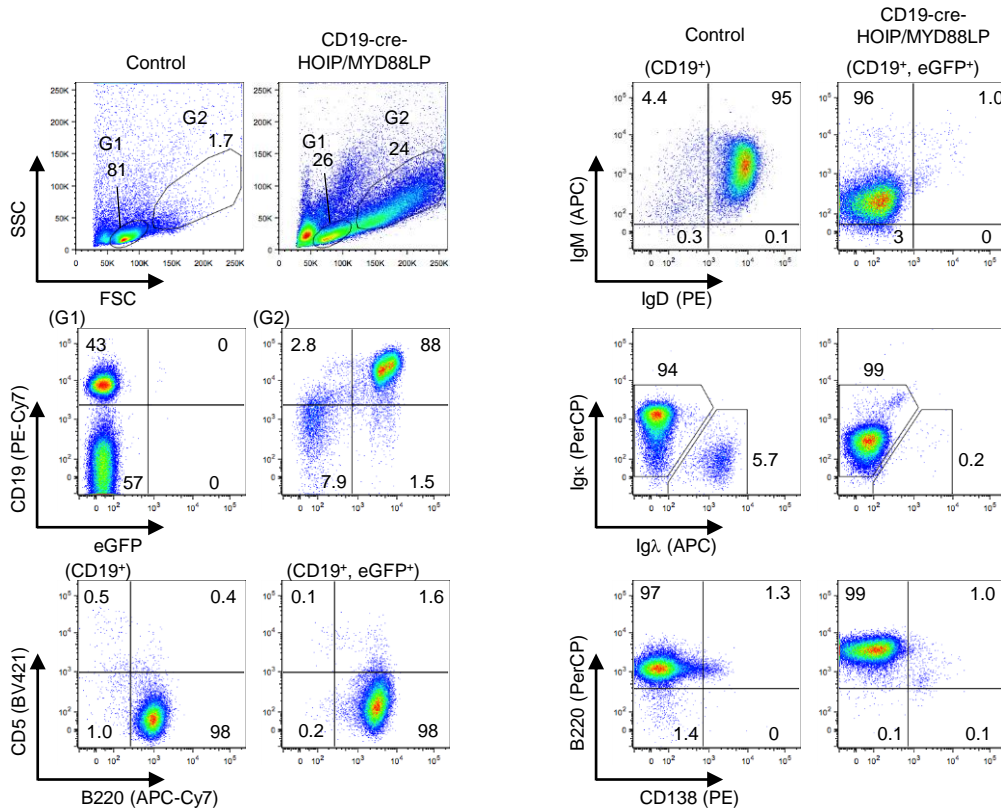
Supplemental Figure 1



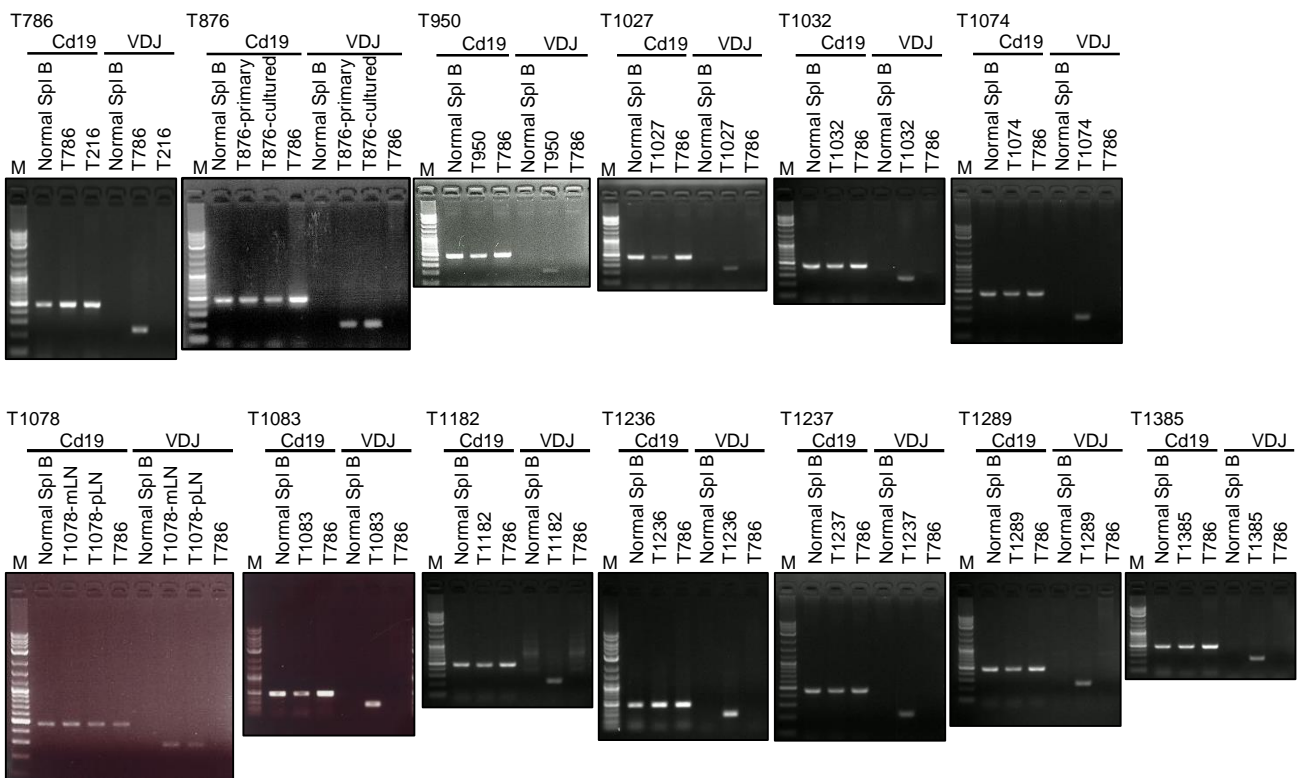
Supplemental Figure 1. Generation of a mouse strain expressing HOIP or MYD88 L252P specifically in B cells. (A) Expression profiles of *HOIP* in B-cell subsets in human bone marrow. (B) Association of *HOIL-1L* (*RBCK1*), *SHARPIN*, and *OTULIN* expression with cell-of-origin in human DLBCL. Boxes represent the median and the first and third quartiles, and whiskers represent the minimum and maximum of all data points. (C) B cell-specific expression of eGFP reporters in splenocytes from CD19-cre-HOIP mice. (D) B cell-specific expression of HOIP was confirmed by immunoblot analysis using MACS-purified splenic B or T cells. Expression of HOIL-1L and SHARPIN was also specifically elevated in B cells. β -actin was used as a loading control. (E) Transcript levels of NF- κ B target genes in unstimulated splenic B cells from mice (10 weeks old), normalized against *Actb* mRNA; n = 3 per genotype. Data are means \pm SD. (F) Macroscopic appearance of spleens in 14-month-old CD19-cre-HOIP mice. (G) Schematic representation of conditional expression of MYD88 L252P (the mouse equivalent of the human L265P mutation) in a Cre recombinase-dependent manner. (H) B cell-specific expression of eGFP reporters in splenocytes from CD19-cre-MYD88LP mice. (I) B cell-specific expression of transgenic MYD88 was confirmed by immunoblot analysis using MACS-purified splenic B or T cells. β -actin was used as a loading control. (J) *In vivo* BrdU analyses of splenic B cells. BrdU was administered by bolus intraperitoneal injection (50 mg/kg) 1.5 hours before dissection. (K) Immunoblots of MACS-purified splenic B cells from control and CD19-cre-MYD88LP transgenic mice (10 weeks old). (L) Cell lysates of HOIP KO or wild type Jurkat cells with or without TNF α stimulation were subjected to Halo-tagged linear ubiquitin-specific tandem ubiquitin binding entity (M1-specific TUBE) binding and Halo Tag based purification, and analyzed by immunoblotting. (E) ** p < 0.01. (B and E), two-tailed unpaired Student's *t*-test.

Supplemental Figure 2

A

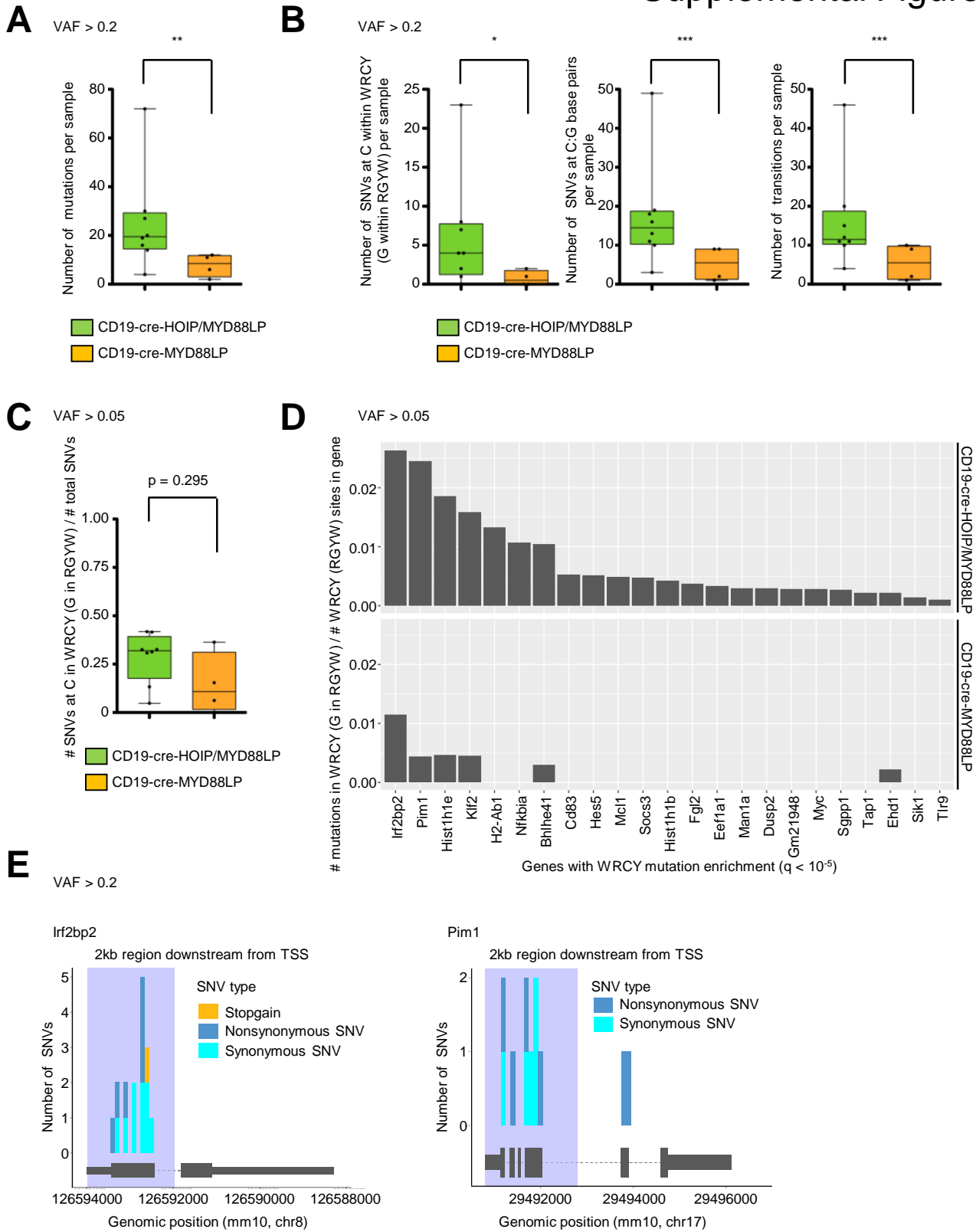


B



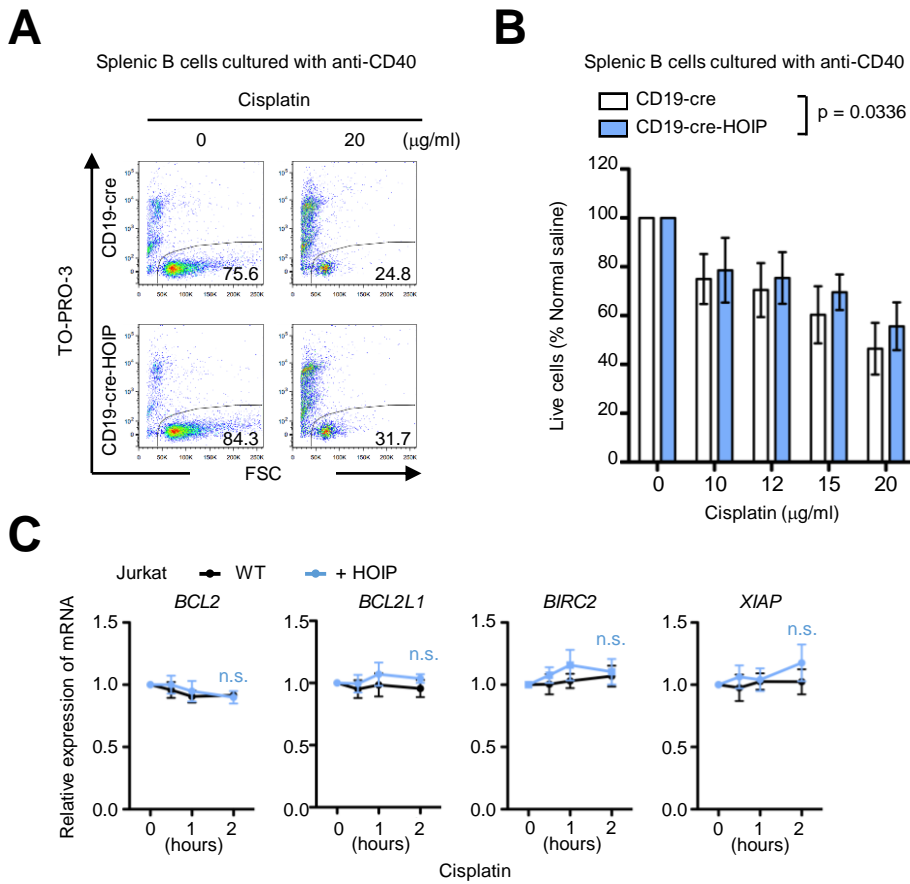
Supplemental Figure 2. Surface immunophenotypes of lymphomas derived from transgenic mice and clonality analysis of the tumors. (A) Representative data of FACS analysis for surface immunophenotypes of lymphoma cells. Large cells (G2) in tumor-affected organs were positive for eGFP, and eGFP-positive cells were analyzed for surface antigens. (B) Analyses for clonality of 13 cases (except for T1084, which is shown in Figure 1I).

Supplemental Figure 3



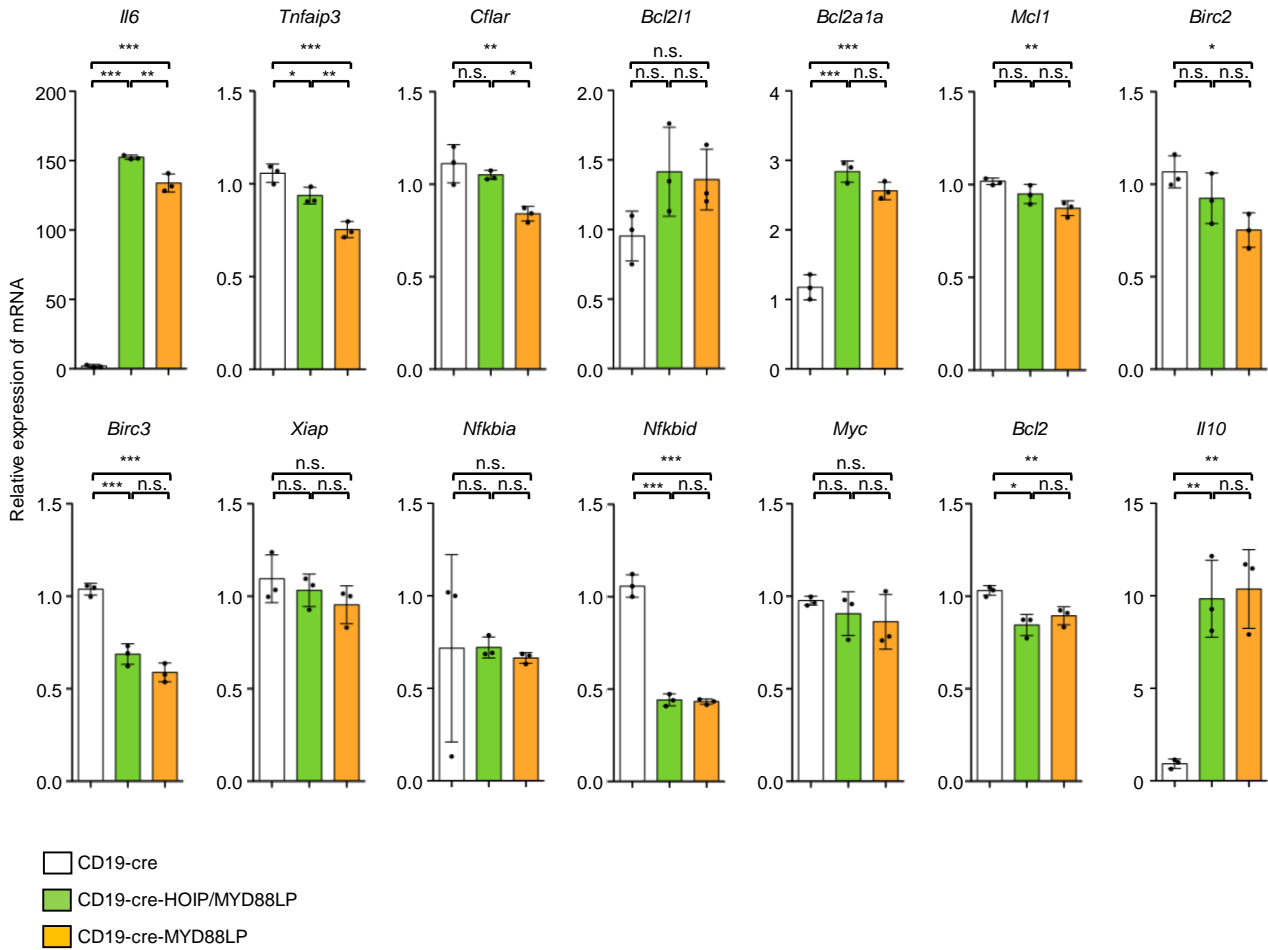
Supplemental Figure 3. LUBAC facilitates aberrant somatic hypermutations mediated by AID. (A, B, and E) Mutations with variant allele frequency (VAF) > 0.2 in tumor samples were selected and analyzed. (A) Numbers of mutations in each tumor sample. (B) Numbers of SNVs at C/G within the WRCY/RGYW motifs (left), and numbers of C:G (center) and transition mutations (right) in each tumor sample. (C-D) Mutations with VAF > 0.05 in tumor samples were analyzed. (C) Proportion of SNVs at C/G within the WRCY/RGYW motifs to total SNVs in each tumor samples. (D) Ratio of the number of SNVs at C/G within the WRCY/RGYW motifs to the number of WRCY/RGYW motifs in indicated genes among tumors derived from CD19-cre-HOIP/MYD88LP mice (upper panel) and CD19-cre-MYD88LP mice (lower panel). (E) Mutation distribution in targeted genes observed in lymphoma cells derived from eight CD19-cre-HOIP/MYD88LP mice. Shadows indicate the 2 kb region downstream of the transcription start site (TSS). (A, B, and C) Boxes represent the median and the first and third quartiles, and whiskers represent the minimum and maximum of all data points. * $p < 0.05$, ** $p < 0.01$, *** $p < 0.001$. Brunner–Munzel test.

Supplemental Figure 4



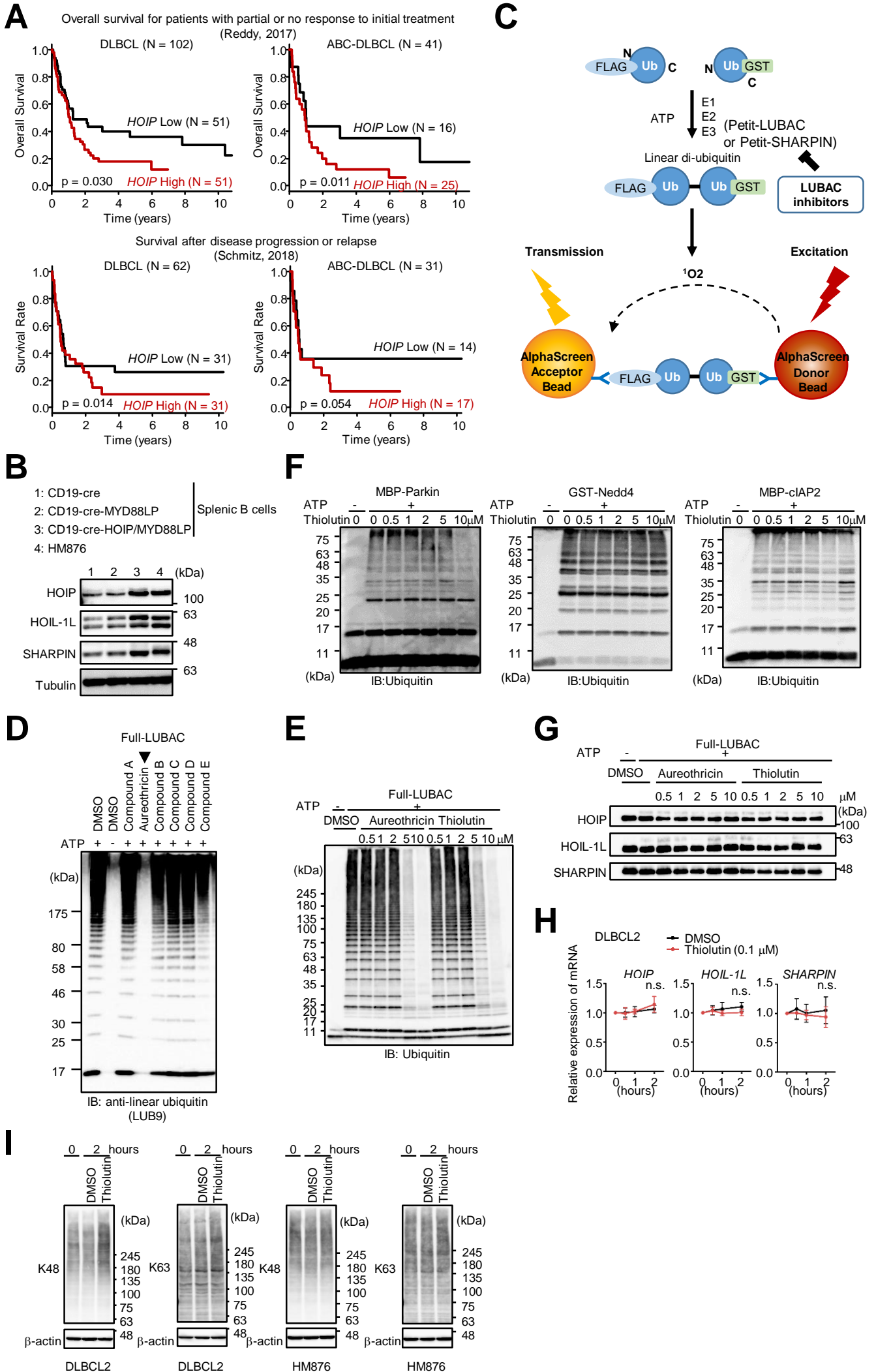
Supplemental Figure 4. Augmented LUBAC activity overcomes cell death induced by DNA damage thereby accelerating accumulation of somatic mutations. (A) Live cells were analyzed by FACS using TO-PRO-3 staining. Mouse splenic B cells derived from indicated genotypes were cultured with anti-CD40 antibody (10 $\mu\text{g/ml}$) for 24 hours and then were treated with or without cisplatin for 24 hours. (B) Percentage of live cells (\pm SD); $n = 6$ per group in three independent experiments. (C) Jurkat cells were treated with 3 $\mu\text{g/ml}$ cisplatin for the indicated periods, followed by quantitative RT-PCR, normalized against *ACTB* mRNA; $n = 3$ per genotype. Data are means \pm SD. (B and C) two-way ANOVA test.

Supplemental Figure 5



Supplemental Figure 5. Enforced LUBAC expression augments expression of NF- κ B target genes. Transcript levels of NF- κ B target genes in MACS-purified unstimulated splenic B cells from CD19-cre, CD19-cre-HOIP/MYD88LP, and CD19-cre-MYD88LP mice (10 weeks old), normalized against *Actb* mRNA; n = 3 per genotype. Data are means \pm SD. * p < 0.05, ** p < 0.01, *** p < 0.001 (one-way ANOVA with Turkey's post hoc tests).

Supplemental Figure 6



Supplemental Figure 6. LUBAC is an effective target for the treatment of DLBCL. (A) Overall survival of DLBCL cases following diagnosis who did not achieve complete response to initial therapy (Upper panels). Survival rate of DLBCL cases after disease progression or relapse (lower panels). If two Kaplan-Meier curves crossed early (≤ 18 months), differences between survival functions were examined by the log-rank test based on observations after the crossing point. (B) Immunoblot analyses were performed using lysates from splenic B cells of the indicated mouse genotypes and HM876 cells. (C) A schematic diagram of the AlphaScreen-based HTS system. Linear di-ubiquitin is formed in an enzymatic process that utilizes FLAG-Ub and Ub-GST, and Petit-LUBAC or Petit-SHARPIN as the E3 ubiquitin ligase enzyme, as well as E1, E2, and ATP. Anti-GST donor and anti-FLAG acceptor beads simultaneously capture linear di-ubiquitin. Proximity of acceptor and donor beads, induced by the production of linear di-ubiquitin, generates a luminescent signal upon irradiation at 680 nm. LUBAC inhibitors block formation of linear di-ubiquitin, thereby decreasing signal intensity. (D) *In vitro* ubiquitination assay confirmed that aureothricin (arrowhead) inhibited linear polyubiquitination mediated by LUBAC. Samples were probed with anti-linear ubiquitin antibody (LUB9). (E) *In vitro* Ubiquitination assay of LUBAC. Samples were probed with anti-ubiquitin antibody (P4D1). (F) *In vitro* ubiquitination assay of other types of E3 ligases, such as Parkin (left panel), Nedd4 (center panel), and cIAP2 (right panel). (G) *In vitro* Ubiquitination assay of LUBAC. Samples were probed with anti-HOIP, anti-HOIL-1L, and anti-SHARPIN antibody. (H) DLBCL2 cells were treated with or without thiolutin (0.1 μ M) for the indicated periods, followed by quantitative RT-PCR, normalized against *ACTB* mRNA in three independent experiments. (I) Cell lysates of DLBCL2 and HM876 treated with or without thiolutin (0.1 μ M) for 2 hours were analyzed by immunoblotting. Samples were probed with anti-K48 specific antibody (leftmost panel for DLBCL2, and middle right panel for HM876) or K63 specific antibody (middle left panel for DLBCL2, and rightmost panel for HM876). (A), log-rank test; (H) two-way ANOVA test.